(1)

THE PULSE RESPONSE OF ELECTRETS TO ENERGETIC IONS

DISSERTATION

Stephen R. Berggren
Major, USAF

AFIT/DS/ENP/88-1

DEPARTMENT OF THE AIR FORCE

AIR UNIVERSITY

AIR FORCE INSTITUTE OF TECHNOLOGY

Wright-Patterson Air Force Base, Ohio

AFIT/DS/ENP/88-1

THE PULSE RESPONSE OF ELECTRETS TO ENERGETIC IONS

DISSERTATION

Stephen R. Berggren
Major, USAF

AFIT/DS/ENP/88-1

AFIT/DS/ENP/88-1

THE PULSE RESPONSE OF ELECTRETS TO ENERGETIC IONS

DISSERTATION

Presented to the Faculty of the School of Engineering

of the Air Force Institute of Technology

Air University

In Partial Fulfillment of the

Requirements for the Degree of

Doctor of Philosophy

Stephen R. Berggren

Major, USAF

September 1988

AFIT/DS/ENP/88-1

THE PULSE RESPONSE OF ELECTRETS TO ENERGETIC IONS

Stephen R. Berggren

Major, USAF

Approved:

George John, Chairman — 5 Oct 1988

Theodore E. Luke — 5 Oct 1988

Denis E. Beller, Major USAF — 5 Oct 1988

Matthew Kabrisky — 5 Oct 1988

Charles J. Bridgman — 5 Oct 88

Accepted:

J. S. Przemieniecki 5 Oct. 88

J. S. Przemieniecki
Dean, School of Engineering

Dedication

To the memory of my father,

Dr. Frans R. Berggren, DC

who introduced me to the joy of learning how things work.

This dissertation reports on my investigation into how electrets respond to energetic ions. Other researchers have worked extensively with radiation effects on electrets, but have focused on the cumulative dissipation of the charge. My work emphasizes the electret's pulse response to an individual radiation event.

The investigation was motivated by a desire to develop a recording neutron dosimeter. I originally suspected, supported by calculations, that a fission fragment would produce a very strong signal when interacting with an elecret. I hoped to use this phenomenon to design a dosimeter functionally similar to the fission track etch dosimeter, but having real-time electronic readout. Such a device would be a significant improvement over current neutron dosimetry devices. Although this device proved too elusive, other original and functional designs for radiation monitors were realized. In addition, I have achieved a somewhat deeper insight into how ions interact with electrets.

Whatever success I have had is in a great part due to the help and support of others. My research director, Professor George John, provided advice, assistance, and most of all encouragement in my darkest hours. Bob Hendricks and the other lab technicians were a constant source of help with the laboratory experiments. Jack Tiffany and his merry band of fabricators in the AFIT Model Shop turned my bizzare drawings into working research instruments. I thank them all.

Finally, I must thank the one person most responsible for my initiating this endeavor; my sister, [redacted] without whose sibling rivalry this research would not have been necessary.

Stephen R. Berggren

Table of Contents

List of Figures

List of Figures, continued

List of Tables

ABSTRACT

The purpose of this study was to investigate how electrets respond to energetic ion irradiation. When an energetic ion interacts with an electret, a dielectric material containing a quasi-permanent electrostatic polarity, both electrical signals and luminescence signals result. The energetic ions used in the study were alpha particles and fission fragments. The electrets used were corona-charged and electron-beam charged polyfluoroethylene propylene. Both direct interaction (with the electret material itself) and indirect interaction (with the air above the electret) were studied.

The electret's pulse electrical response was measured at surface and near-surface electrodes using a charge-sensitive amplification system and a multichannel analyzer. Alpha particles were found to produce an electrical pulse response by indirect interaction. In a 0.2 cm air space, alpha particles produce a signal of about 10^{-15} coulombs. Fission fragments produce an electrical response by both indirect and direct interaction. The indirect interaction signal is about 10^{-14} coulombs while the direct interaction signal is barely above background noise at 10^{-16} coulombs. Further, the direct response occurs only in freshly electron-beam charged electrets and decays away over several hours. A model for the interaction of ions with electron-beam charged electrets is proposed which explains many of the characteristics of the direct interaction signal.

The pulse luminescence response of electrets was measured using a photomultiplier-amplifier-multichannel analyzer system. Luminescence was found to occur from the direct interaction of both alpha particles and fission fragments with electron-beam charged electrets. This response also decays away over several hours. The mechanism generating the luminescence was not determined but the data suggest that electron-hole recombination is responsible.

Because the direct response to energetic ions was found to be transient, it may mot be useful in radiation detection. The pulse response to the indirect

interaction of alpha particles is useful. An environmental radon monitor and a thermal neutron detector using this phenomenon were successfully tested.

THE PULSE RESPONSE OF ELECTRETS TO ENERGETIC IONS

I - Introduction

The proposal that an electret, a material that maintains a quasi-permanent electrostatic polarity, was possible was first made by Michael Faraday in 1839. Early electrets, made of waxes and resins, could not maintain polarities high enough to make them more than physics curiosities. Recently, however, thin film polymer electrets have become available that maintain very strong electric fields. Such electrets are finding many novel applications, including radiation detection.

The current state of research has produced electrets with remarkable electrostatic characteristics. Polymer-foil electrets have been produced with internal fields that approach the dielectric breakdown strength of the material itself. This is the practical limit of an electret's internal field. Surface potentials in excess of 3000 volts are readily achieved and maintained. Under careful storage, the half life of the electret's charge has been measured at greater than 100 years. These electrets are so stable that the charge layer itself is not believed to migrate appreciably. These characteristics make electrets useful in a wide range of applications.

Electrets are rapidly finding their way into new devices for radiation detection and monitoring. In most of these devices, they provide the electric field for an ionization chamber dosimeter. When an electret is used in such a dosimeter, the loss of equivalent surface charge of the electret is monitored as a measure of total dose. None of the applications attempt to detect and record an individual radiation event.

This research has shown that one type of radiation, energetic ions, produces a detectable signal from the interaction of an individual particle with an electret. Energetic ions, such as alpha particles and fission fragments, have very high energies (2 -110 MeV) and deposit their energy along very short paths (a few cm in

air, a few μm in solids). If the path is through the field of a charged polyfluoroethylene propylene (FEP) electret, the resulting disturbance produces a detectable signal. Both electrical signals and photon emissions resulting from ion interaction with electrets were detected. Determining the characteristics of an electret's response to individual energetic ions and identifying the mechanisms that produce it were the objectives of this research.

This research may have practical application to the measurement of some forms of radiation. A self-powered, passive radon monitor of a unique design was developed and tested. Preliminary tests were also made on a self-powered thermal neutron detector.

This research investigated how alpha particles and fission fragments induce electrical signals and luminescence in an electret. The specific work was divided into three areas of experimentation; the electrical response to alpha particles, the electrical response to fission fragments, and the luminescence response to both alpha particles and fission fragments. This report is organized to present these areas as three separate, but interrelated topics.

The dissertation first presents background material on the two principal subjects; electrets and energetic ions. Then Chapter III discusses how the electrets used in this research were produced, handled and stored. Chapter IV presents the investigation of alpha particle interaction with electrets, specifically the indirect interaction of alpha particles with the air above the electret. Chapter V is concerned with fission fragment interaction with electrets. It discusses both indirect interaction and direct interaction with the electret material itself. Chapter VI discusses the luminescence of electron-beam charged FEP in response to both alpha particles and fission fragments. Chapter VII presents conclusions and recomendations for further investigation.

II - Background

Introduction

The two principal subjects of this research are electrets and energetic ions. This chapter discusses some of the principles by which they operate. These principles form the bases for the development of theory, for the design of experiments and for the analyses of the experimental data.

Electrets

An electret is a dielectric material having a quasi-permanent electrostatic polarity. The term "quasi-permanent" means that spontaneous charge decay is not usually a factor over the time span of an experiment. Unless the electret has electrodes on both surfaces, its electrostatic polarity creates an external electric field. It is this quasi-permanent, external electric field that makes electrets so useful in a wide variety of applications. These applications include acoustic and mechanical transducers,(28) electrophotography,(31:165-166) dust filters,(6) and radiation dosimeters.(18)

Types of Electrets. Electrets may be classified based on any of several characteristics, including method of manufacture, material of construction, and source of the polarization. The last method is the most appropriate for a basic discussion of electret principles. The source of electret polarization may be either internal polarization of an electrically neutral material or polarization by the introduction of a net charge from an external source. Under some circumstances, polarization is the result of a combination of internal and external effects. Figure 2-1 shows the charge and field distributions of various electret types.

Two examples of internal polarization are dipole orientation and charge separation. Electrets formed by dipole orientation consist of molecules with a

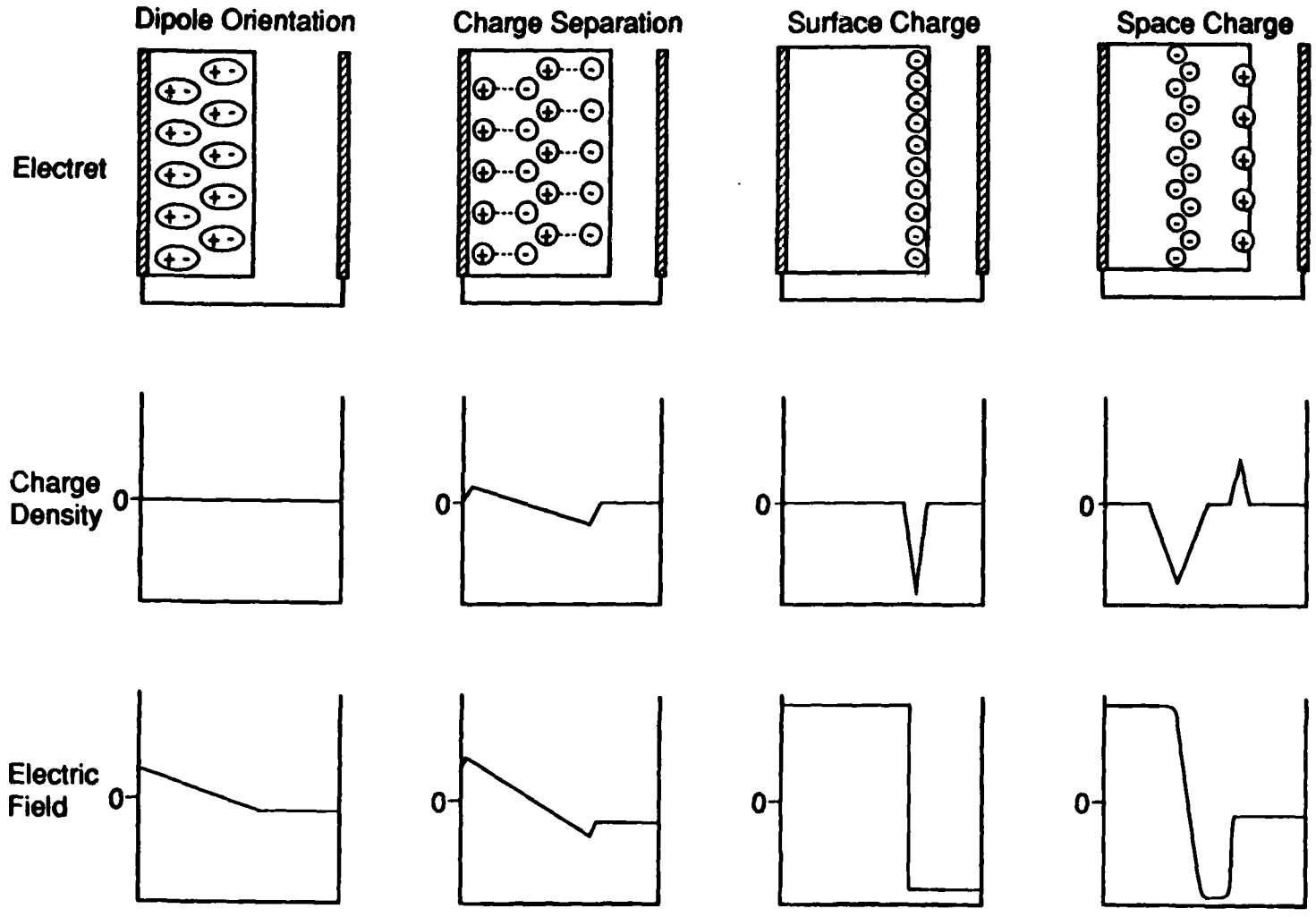

Figure 2-1. The Charge and Field Distributions of Various Electret Types

strong dipolar structure. Because the orientation of the molecules is usually random, the pristine material contains no gross polarization. When the molecules are placed in a generally uniform orientation, each makes a small contribution to the polarity of the material. The result is a material with a net polarization, an electret. The uniform orientation is usually accomplished by melting the material to allow rotation of the individual molecules, placing the molten material in an electric field to orient the molecules, and cooling the material to freeze in their orientation. This type of electret is called a thermoelectret.

The field of a thermoelectret is opposite that of the electric field applied in manufacture. However, over time such an electret can collect free charges on its surfaces or dissociate charge pairs within itself.(14:96-100) These charges often eliminate, and then reverse, the net electric field of the material to produce an electret having a polarity identical to the applied field. These electrets are called heteroelectrets and homoelectrets, respectively.

Internal polarization may also be accomplished by separation of disassociated charge pairs. If the electret material is placed in an electric field and electron-ion pairs are generated (e.g. by gamma irradiation), the charge pairs will separate and then become trapped. This causes a net polarization similar to that in dipole orientation. The electric field may even be omitted if the gamma irradiation is directional rather than isotropic. A Compton scattered electron generally follows the path of the ionizing photon leaving the positive ion behind. This will induce the charge separation and polarization without an externally applied field.(25:36-37) Electrets produced solely by the effect of ionizing radiation are called radioelectrets.

The electret types discussed above are polarized but have no net charge. Polarization can also be produced by the introduction and trapping of charges in the electret. Some dielectric materials, particularly polymers, contain trap sites that can immobilize charge carriers. If the charge carriers are trapped closer to one surface, there is a potential difference between the two surfaces and the material becomes an electret. Both surface-charged and space-charged electrets use this principle.

Surface-charged electrets are dielectrics that have positive ions or electrons trapped on their surface. Corona charging, for example, involves using corona discharge to produce charge carriers in air.(23:3397-3398;24:643-644) An electric field is applied to drive the charges to the surface of a dielectric foil. The charges collect until they fully compensate the applied electric field. When the applied field is removed, the opposing external field of the trapped charges remains. Alternate methods of generating a surface charge include controlled electric breakdown of the material(30) and the use of a charged, liquid-contact electrode.(5)

A space charge can be produced by bombarding an electret material with a beam of electrons.(26;27) The electrons penetrate the material before stopping and becoming trapped. The depth of penetration is determined by the energy of the electrons. If the electrons are essentially monoenergetic and monodirectional, the charge is deposited in a fairly thin layer within the material. Coulombic forces will then cause a slow dispersion of the charge region.

One important characteristic of electron-beam charging is the creation of a layer of increased conductivity between the front surface and the charge layer.(13) The conductivity is called radiation-induced conductivity (RIC). The radiation dose from the electron beam increases the number of charge carrier pairs in this region by ionization and excitation of the valence electrons of the material. After a few seconds of irradiation, the conductivity stabilizes as recombination rates increase to match charge-carrier pair production. The conductivity, G, of this region is a power function of the dose rate, ϕ (8:2849)

$$G = 2 \times 10^{-16} \phi^{\delta} (ohm-cm)^{-1} \tag{2-1}$$

where $0.5 \leq \delta \leq 1.0$. Experimental measurements show that δ varies somewhat with dose rate. For dose rates of 10^{-2} to 10^{4} rads/sec, δ varies from 0.63 to 0.85 (8:2849) while for very high dose rates (pulsed electron beams) $\delta \approx 1.0$.(15:1012) After irradiation ceases, the induced conductivity slowly decays and is known as delayed radiation induced conductivity (DRIC). The decay of this delayed conductivity is described by (8:2843):

$$G = \frac{G_0}{1 + bt} \tag{2-2}$$

where G_0 is the conductivity at termination of irradiation, and t is the time since termination of irradiation. The value of b is experimentally determined to be about 1.0 sec^{-1}.(8:2849)

Uses of Electrets in Radiation Detection. Electrets are now being used in several radiation detection applications. Three methods are most commonly reported: use of the electrostatic field of the electret to replace a high voltage power supply, gross depolarization of the electret by direct radiation interaction, and the use of the electret field to collect dust particles for activity measurement.

The electrostatic field from an electret has been used to replace the high voltage power supply in ionization chamber dosimeters(3;4;20). One dosimeter even takes advantage of charge multiplication at the electret surface.(16) Use of electrets in dosimeters has the advantages of greater simplicity and the elimination of electronics. Generally, the designs are simply a gas chamber containing an electret. Ionizing radiation produces electron-ion pairs in the gas which are separated by the electret's electric field. The electret's electric field is reduced by collection of the opposing charge on its surface. Various means are used to measure the electric field of the electret. The reduction in the electric field is proportional to the radiation dose.

Other dosimeter designs measure the gross depolarization of an electret by direct radiation interaction.(18:173-176) The depolarization of these electrets can be measured by analysis of the field strength or by thermally stimulated current (TSC). TSC is an analytical method of determining polarization by slowly heating an electret while measuring the current between its surface electrodes. Such devices are suitable for kilogray dose measurements but are too insensitive for personnel dosimetry.

Electrets are also used as electrostatic particle traps for detection of radon progeny.(17) In this method, the electret is used as an electrostatic precipitator. An electret film is placed adjacent to a conventional counting device. The charged surface attracts and traps aerosols bearing radon progeny just as in an electrostatic precipitator. This provides the dust collection efficiency of electrostatic precipitation without the need for a high voltage power supply.

Electrical Characteristics of Electrets. From a practical standpoint, the most important properties of an electret are its charge, its rate of charge decay and the strengths of its electric fields. The amount of charge carried by an electret is generally described as an effective surface charge density in units of coulombs per square centimeter. The rate of charge decay is described by the time constant in an exponential decay equation. The strengths of the various electric fields and the electrets' surface potential can be determined from the charge density.

For electrets charged by a uniformly distributed electron beam, the charge density is the integral of the beam current, i_b. The charge density, σ, within the charge layer is:

$$\sigma = \frac{1}{A_b}\int_0^{t_c} i_b(t)\,dt \qquad (2\text{-}3)$$

where A_b is the cross-sectional area of the electron beam and t_c is the total time of charging. An experimentally-determined charging efficiency can also be applied to account for spontaneous discharges during the charging process.(14:226)

Electron-beam charging produces a charge layer distributed within the electret. The distribution of the charge may begin as a thin layer but disperses with time or annealing. The mechanism for the dispersion is thought to be the escape of electrons from shallow trap sites, field-driven transport through the media, and eventual retrapping at deeper trap sites.(27:120-122) Also, holes generated in the irradiated region are thought to migrate toward the charge layer and combine with trapped electrons, leaving their less-mobile negatively-charged partners behind.(13:4875) The effect is that dispersion in electron-beam charged electrets strongly favors the irradiated region. The mean depth of the charge layer has been determined experimentally and is shown in Figure 2-2.(27:113)

The space-charged electrets produced by electron-beam charging have strong internal fields produced by the charge layer and the compensating charges on electrodes near its surfaces. Figure 2-3 is a diagram of a space-charged electret with a thin charge layer and shorted parallel electrodes near its surfaces. The assumption of a thin charge layer makes possible the analysis of electrets by the 'Box

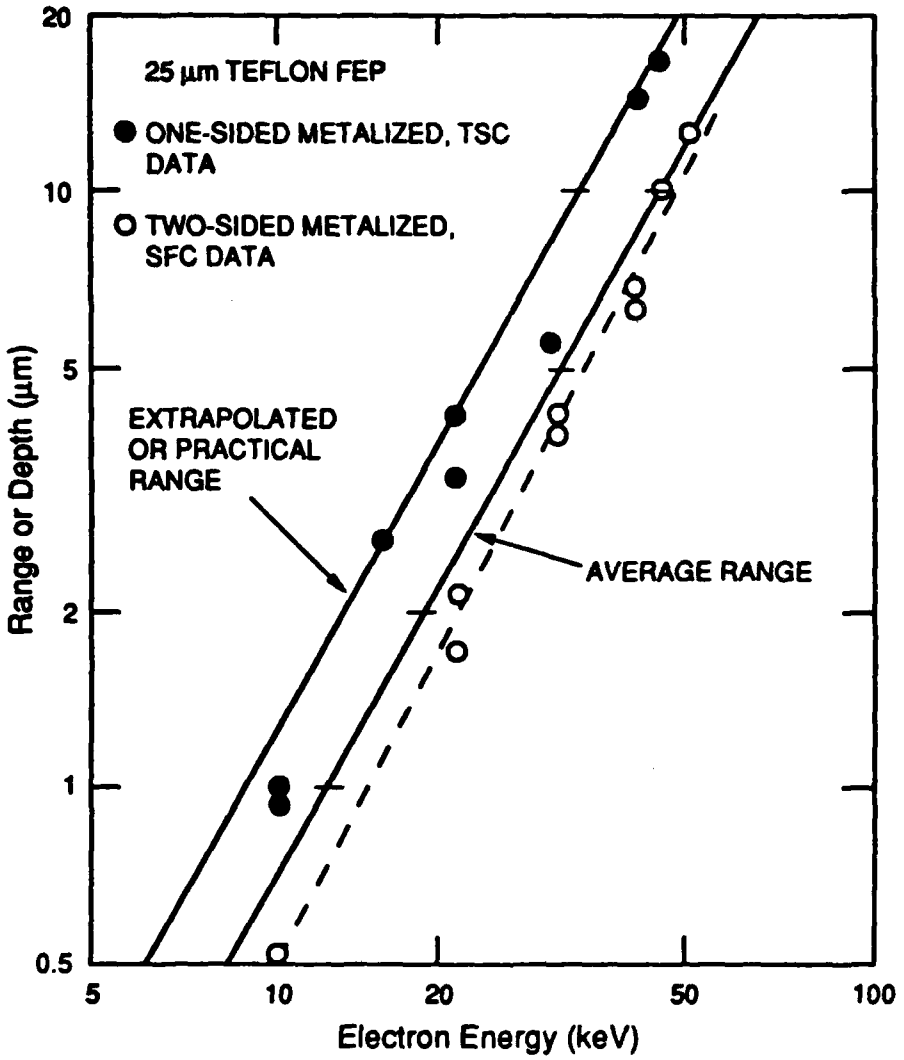

Figure 2-2. Mean Charge Depth on One-Sided and Two-Sided Metalized 25 μm FEP Film as a Function of Electron Beam Energy (27:113)

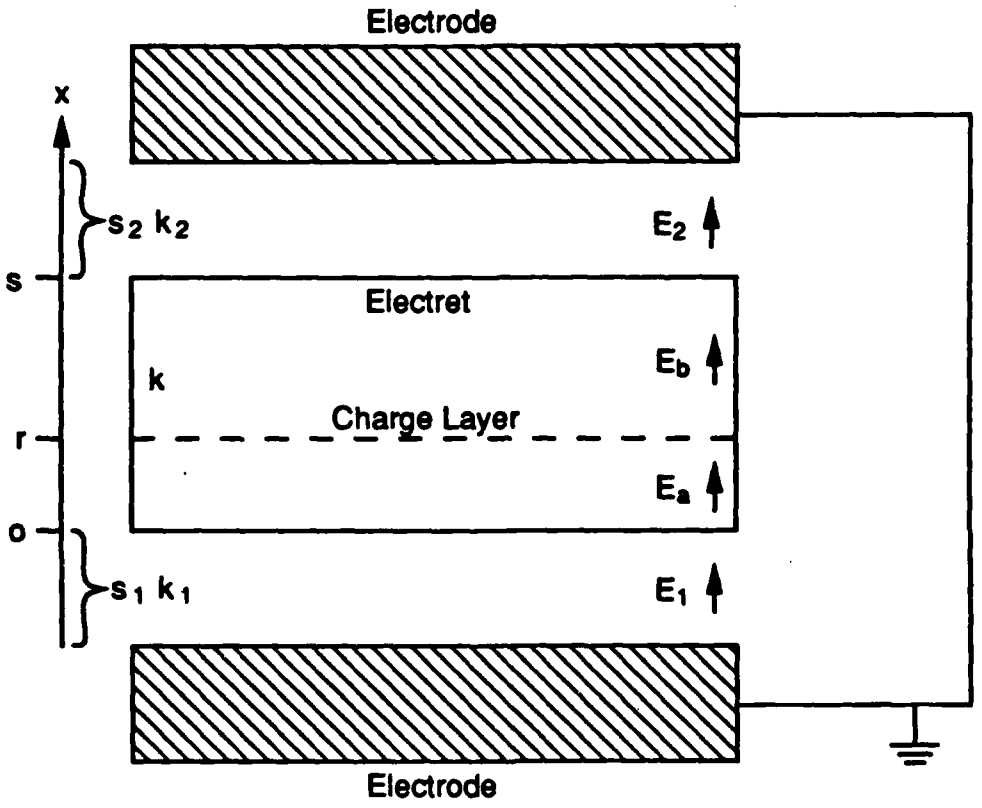

Figure 2-3. Diagram of a Space Charged Electret

Model.'(12) In this model the electric fields, E_1 and E_a, may be determined from:(25:14-15)

$$s_k E_1 = -\frac{\sigma}{k\epsilon_0 k_1 k_2}\left(k_2 (s-r) + k s_2 \right) \tag{2-4}$$

$$s_k E_a = -\frac{\sigma}{k^2\epsilon_0 k_2}\left(k_2 (s-r) + k s_2 \right) \tag{2-5}$$

with:

$$s_k = \frac{s_1}{k_1} + \frac{s}{k} + \frac{s_2}{k_2} \tag{2-6}$$

where ϵ_0 is the dielectric constant, r is the charge depth, and s and k represent various distances and dielectric coefficients shown in Figure 2-3. Corresponding equations may be written to determine the electric fields E_2 and E_b. In the case where the electrodes are in contact with the electret, ($s_1 = s_2 = 0$), then:

$$E_a = \frac{-\sigma}{k\epsilon_0}\left(1 - \frac{r}{s}\right) \tag{2-7}$$

$$E_b = \frac{-\sigma}{k\epsilon_0}\left(\frac{r}{s}\right) \tag{2-8}$$

For a charge distributed through the electret, Equations 2-7 and 2-8 become integrals over the thickness of the electret. For these equations a volumetric charge density describes the distribution of charge in the charge region. The relationship between the volumetric charge density, ρ, and the charge density is:

$$\sigma = \int_0^s \rho(x)\, dx \tag{2-9}$$

It now becomes useful to define the effective surface charge density, $\hat{\sigma}$, as the integral over the first moment of the charge density

$$\hat{\sigma} = \frac{1}{s}\int_0^s (s-x)\rho(x)\, dx \tag{2-10}$$

The effective surface charge density is the projected contribution of every portion of the charge layer to an equivalent surface charge. If the electret is surface

charged, $\hat{\sigma} = \sigma$, of course. The surface potential of an electret with a space-charge distribution and an attached back electrode can be determined from $\hat{\sigma}$. If one electrode is attached ($s_2 = 0$) and the other electrode is distant ($s_1 >> s$), the potential, V, between the front surface and the back electrode is approximately:

$$V = \frac{s\hat{\sigma}}{k\epsilon_0} \tag{2-11}$$

This equation is useful because an electrometer can readily measure the surface potential of an electret. From the surface potential we can derive the effective surface charge density. The internal charge density can then be determined if the box model is used and the depth of the charge layer is known.

An electret slowly loses its effective surface charge through dissipation of the charge region and collection of compensating charges at its surface. The charge decay of FEP electrets occurs in two stages. An early, comparatively-rapid charge decay is attributed to the escape of electrons from shallow traps.(27:120-122) Once the early decay is complete, the electrets demonstrate a temperature-dependant charge decay of:(14:14)

$$\hat{\sigma} = \hat{\sigma}_0 \, e^{\frac{-t}{\tau(T)}} \tag{2-12}$$

where $\hat{\sigma}_0$ is the surface charge density at time $t = 0$. The value of τ at room temperature is too large to be directly determined by charge loss measurements. By extrapolation from higher temperature data, τ at $T = 25^{\circ} C$ is about 200 yrs.(25:69)

Dissipation of the charge region within the electret is determined by the mobilities of the positive and negative charge carriers. Charge mobility in FEP is described as a 'trap modulated' mobility.(32) FEP contains trap sites with activation energies of 1.8 eV for electrons and 0.7 and 1.0 eV for holes. The charge carriers 'hop' from trap site to trap site and spend most of their time in the trap. Thus, the number densities and activation energies of the trap sites determine charge mobilities. The number density of charge carriers and their mobilities determine the conduction discharge current. The trap-modulated mobility of electrons in FEP at room temperature is estimated at 5×10^{-17} cm^2 (volt-

sec)$^{-1}$,(8:2850) while hole mobility is 2×10^{-9} cm^2 (volt-sec)$^{-1}$.(7:556) This explains the remarkable charge retention properties of negatively charged FEP.

The ability of an electret to retain its effective surface charge depends strongly on the handling and storage it receives. The electret's electric field attracts charges of opposite sign to its surface, producing a compensating charge layer that masks the internal charge. For the large decay constants observed in FEP, the principal mechanism of discharge is believed to be charge-carrier pair production by ambient radiation in the air surrounding the electret.(1:424) Further, any conductor contacting the exposed surface allows a rapid transfer of compensating charge. Momentary contact with a fingertip is sufficient to destroy the surface charge at that point. For hydrophilic electret materials, even moisture from the air can create a conducting surface to transport a compensating charge. The optimum storage for polymer film electrets is in open circuit inside a small, sealed container of dry air.(1:430)

Energetic Ions

Energetic ions are atoms that carry both a net charge and a significant kinetic energy. The two types of energetic ions used in this research are alpha particles and fission fragments. Alpha particles carry a charge of +2 and energies in the range of about 1 to 8 MeV. Fission fragments carry an initial positive charge of 18 to 20 and energies in the range of 60 to 110 MeV. In spite of the energy and charge differences in the two, the way they interact with a surrounding medium is quite similar.

Ion Interaction with a Medium. As an ion traverses a medium, it deposits its energy principally through inelastic collisions with the valence electrons of the medium.(34:9) The energy deposition generates charge carrier pairs as well as electronic excitation and heat. The rate at which the ions deposit energy in the medium is called the stopping power, the amount of energy deposited per unit distance. The stopping power is a function of the composition of the medium and the mass, charge and kinetic energy of the particle. A semi-empirical formula by Montenegro et. al.(22) was used to calculate the stopping power for various ions in

air and FEP. The program implementing these calculations is listed in Appendix D. Figure 2-4 shows the stopping power of various fission fragments in FEP. Figure 2-5 shows the stopping power of a 4.2 MeV alpha particle in air. In spite of the obvious variations in the stopping power, an average stopping power may usually be used for a given ion interaction. The average stopping power, $\bar{S}$, is defined as:

$$\bar{S} = \frac{1}{L}\int_0^L S(x)\,dx = \frac{\Delta E}{L} \tag{2-13}$$

where L is the track length and ΔE is the energy lost along that track. Treating stopping power as a constant greatly simplifies the calculation of other characteristics of ion interaction.

Part of the energy deposited in the medium is used in the production of charge carrier pairs. The average amount of energy, W, required to produce one charge carrier pair is called the W-value. The W-value is fairly constant for a given radiation type in a given medium. For alpha particles in air, W is 35.2 eV.(19:152) The W-value for FEP is not known. A W of 1000 eV for FEP is taken as an upper limit.(8:2850) A related value, reported for an electron beam in polystyrene, is 120 eV.(21:1006)

In the absence of an electric field, the charge-carrier pairs will recombine. However, in a sufficiently strong electric field the charge-carrier pairs are separated and collected on the electrodes. The total charge collected, Q, is:

$$Q = \frac{Le\bar{S}}{W} \tag{2-14}$$

where e is the charge on the electron. This equation is correct only if the electric field is strong enough to prevent any recombination. A large value of S combined with a small value of W produces a high charge pair density in the medium. This condition makes recombination more likely and higher field strengths are required to collect all of the charge pairs. The very high stopping powers associated with fission fragments makes recombination very likely and Equation 2-14 less useful.

The maximum measurable charge from the interaction of an energetic ion with a medium is:

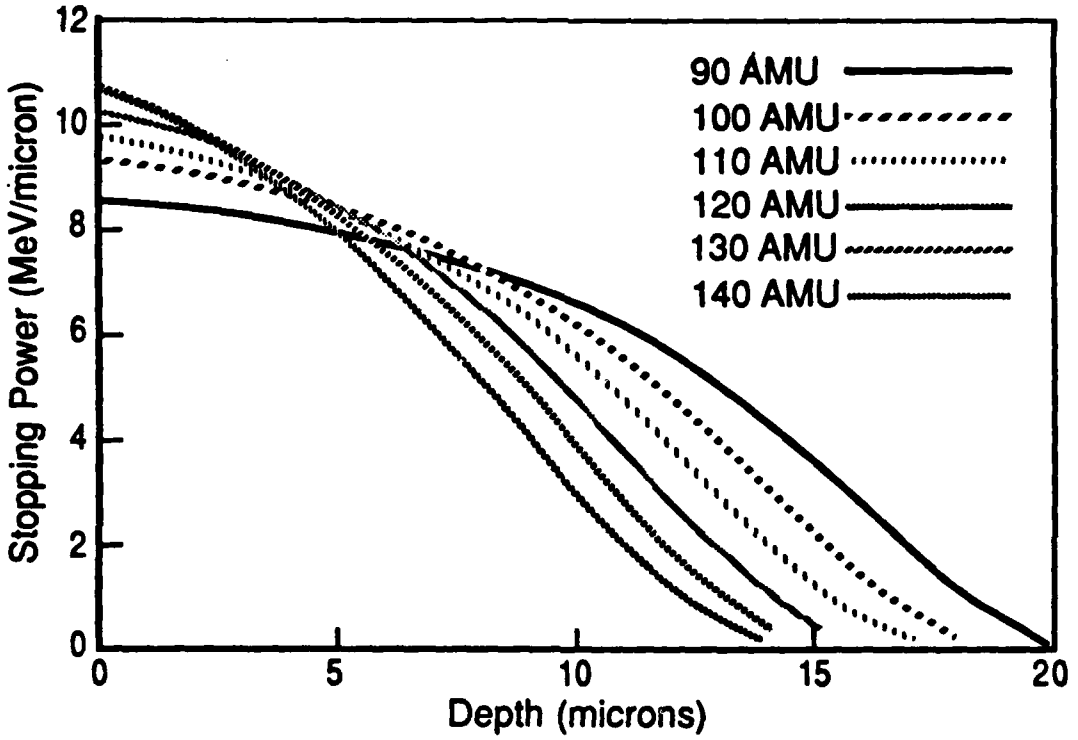

Figure 2-4. Stopping Power for Fission Fragments in FEP

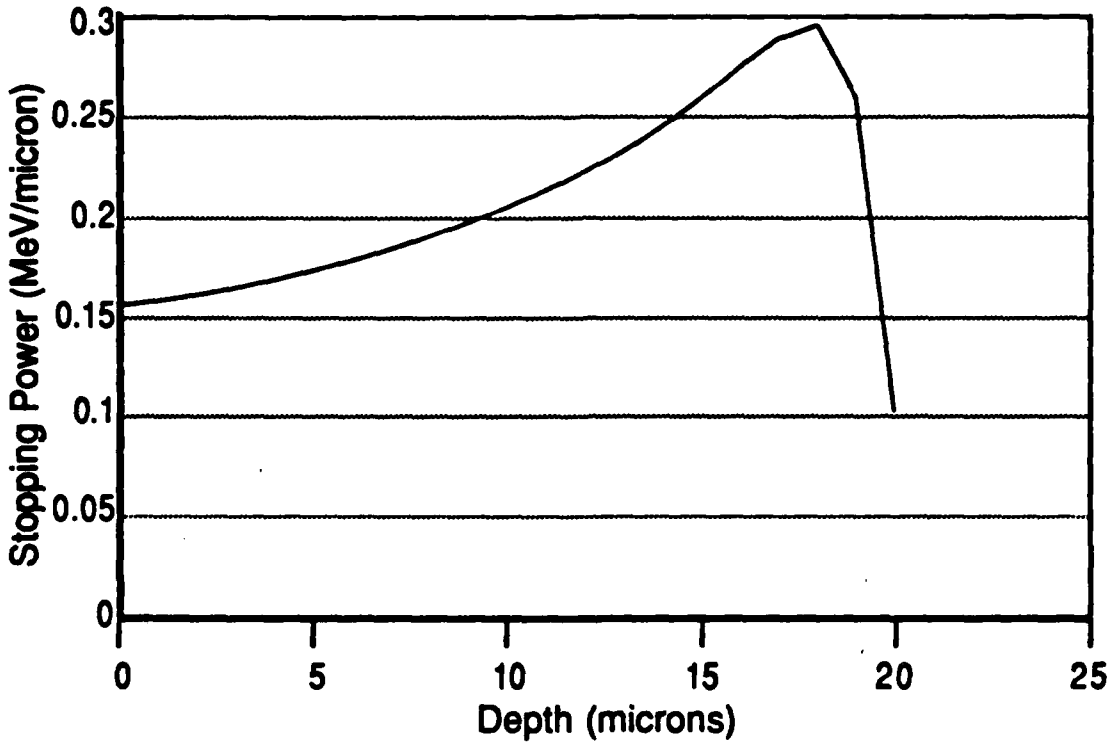

Figure 2-5. Stopping Power for 4.2 MeV Alpha Particle in FEP

$$Q = \frac{E_i e}{W} \tag{2-15}$$

where E_i is the energy of the energetic ion. This maximum occurs under 3 conditions: 1) the dimensions of the medium is larger than the maximum range of the ion, 2) the particle loses no energy to self-absorption in the source and 3) no recombination of charge carriers occurs. Condition 1 is met when the smallest dimension of the medium is larger than the track length. Condition 2 is essentially met if the source of the energetic ions is a very thin film or a small particle. Condition 3 is difficult to achieve in a volume large enough to meet condition 1. Recombination is expected to play a significant role where a large volume medium is used. However, in the absence of an effective means of determining recombination rates, Equation 2-15 will be used for a theoretical treatment of a large volume detector.

Equation 2-14 and 2-15 assume that the separated charge-carrier pairs drift until they reach an electrode. If the charges drift only a portion of the electrode spacing, they will not make a full contribution to the effective charge. From Equation 2-14 and the derivation in Appendix B, the effective charge, Q_e, of the signal is:

$$Q_e = \frac{Le\bar{S}R}{WD} \tag{2-16}$$

where R/D is the fraction of the electrode spacing traveled.

Alpha Particles. An alpha particle is a ^{4}He nucleus consisting of 2 protons and 2 neutrons. Alpha particles are emitted spontaneously from certain radionuclides or may be produced by nuclear reactions. An example of a spontaneous source is:

$$^{235}U \rightarrow {}^{231}Th + {}^{4}He + 4.85\ MeV$$

while an example of a nuclear reaction is:

$$^{10}B + n \rightarrow {}^{6}Li + {}^{4}He + 2.79\ MeV$$

For spontaneous alpha emissions, the activity of the source, A, (the rate of emission of alpha particles) is:

$$A = \frac{dN}{dt} = 0.693\frac{N}{H} \tag{2-17}$$

where N is the number of source atoms and H is the half life of the isotope. For neutron induced emissions:

$$A = N\sigma_f F \tag{2-18}$$

where σ_f is the cross section for neutron absorptions resulting in an alpha emission and F is the neutron flux. The alpha particle emitters of interest to this research are listed in Table 2-1. Where more than one energy is listed, the radionuclide decays to different energy states of the product, resulting in different kinetic energies of the alpha particles.

Table 2-1: Characteristics of Alpha Emitters

Isotope	Half Life	Energy(MeV)	Cross Section(Barns)
Boron-10	stable	2.31,2.79	4017[1]
Radon-222	3.825 days	5.49	-
Polonium-218	3.05 min	6.00	-
Polonium-214	164 μsec	7.68	-
Uranium-235	7.1×10^8 years	4.40,4.58	580[2]

1 Thermal neutron - alpha reaction

2 Thermal neutron - fission reaction

Fission Fragments. Fission fragments are energetic atomic nuclei resulting from the nuclear decomposition of a fissionable isotope, e.g. ^{235}Uranium. When the nucleus of a ^{235}U atom absorbs a neutron, it becomes unstable and may disassemble into two smaller nuclei with an accompanying energy release of about 207 MeV. About 167 MeV appears as kinetic energy in the two nuclei with the remaining energy appearing as kinetic energy of emitted neutrons.

The fission of ^{235}U by thermal neutrons produces a distinctively bimodal distribution of nuclear masses and nuclides. Figure 2-6 shows the distribution of fission fragment masses from the thermal neutron induced fission of ^{235}U.

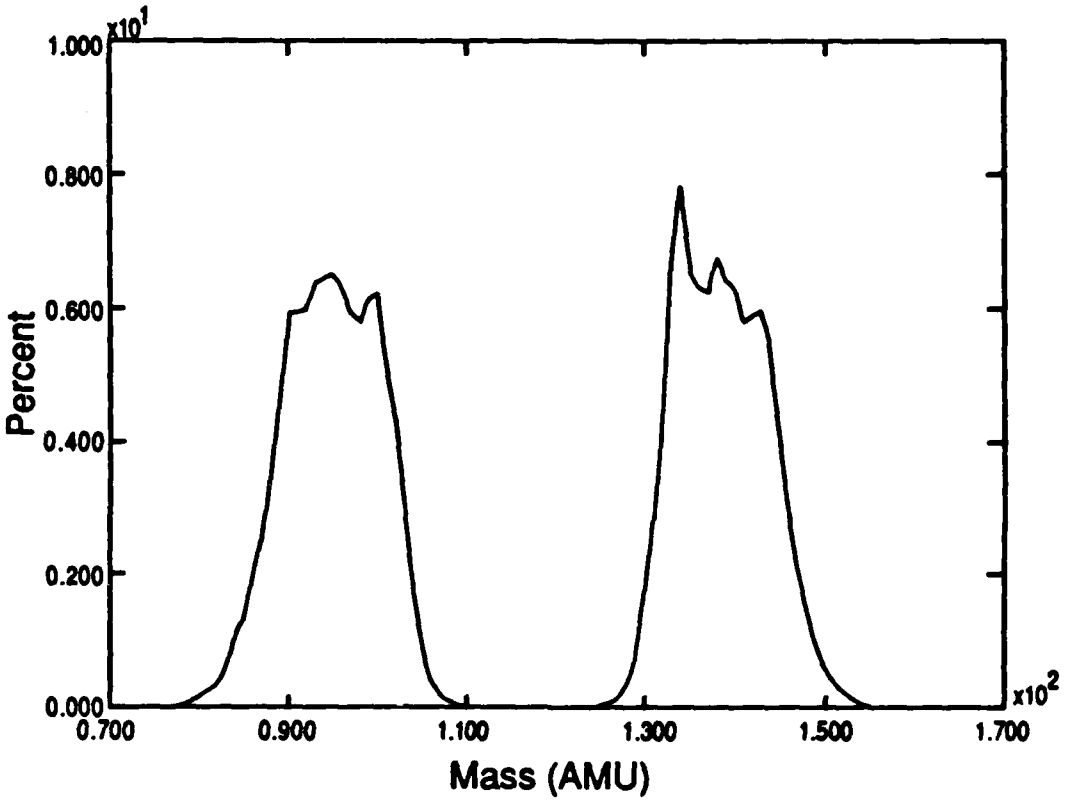

Figure 2-6. Mass Distribution of Fission Fragments from Thermal-Neutron Fissioned Uranium-235

Conservation of energy and momentum require that the fission kinetic energy be distributed between the two nuclei thus:

$$E_{ff} = E_{total}\left(1 - \frac{M_{ff}}{M_{total}}\right) \tag{2-19}$$

where M_{ff} and E_{ff} are the mass and kinetic energy of the fragment, M_{total} is the mass of the original nucleus, and E_{total} is the total kinetic energy available. The direction of travel is random although fission fragment pairs are oppositely directed. Fission fragments are produced as ions with an initial positive charge of 18 to 20.(19:13)

The stopping powers of various fission fragments in FEP are shown in Figure 2-4. These stopping powers were used to determine the total track length, L, by a numerical integration of the equation:

$$L = \int_{E_{ff}}^{0} \frac{de}{S(e)} \tag{2-20}$$

where E_{ff} is the fission fragment energy. The results for various fission fragments are shown in Figure 2-7.

The depth of penetration of fission fragments is as important as their track lengths. Since both the energy and direction of a fission fragment are represented as distributions, the depth of penetration is also a distribution. A Pascal program was written to determine this distribution by numerical approximation. The program selected the energy and direction of a large number of representative fission fragments based on a sequence of quasi-random numbers. The depth of penetration of each fission fragment was then calculated using the methods described above. The distribution in these values was then determined. This distribution is shown in Figure 2-8.

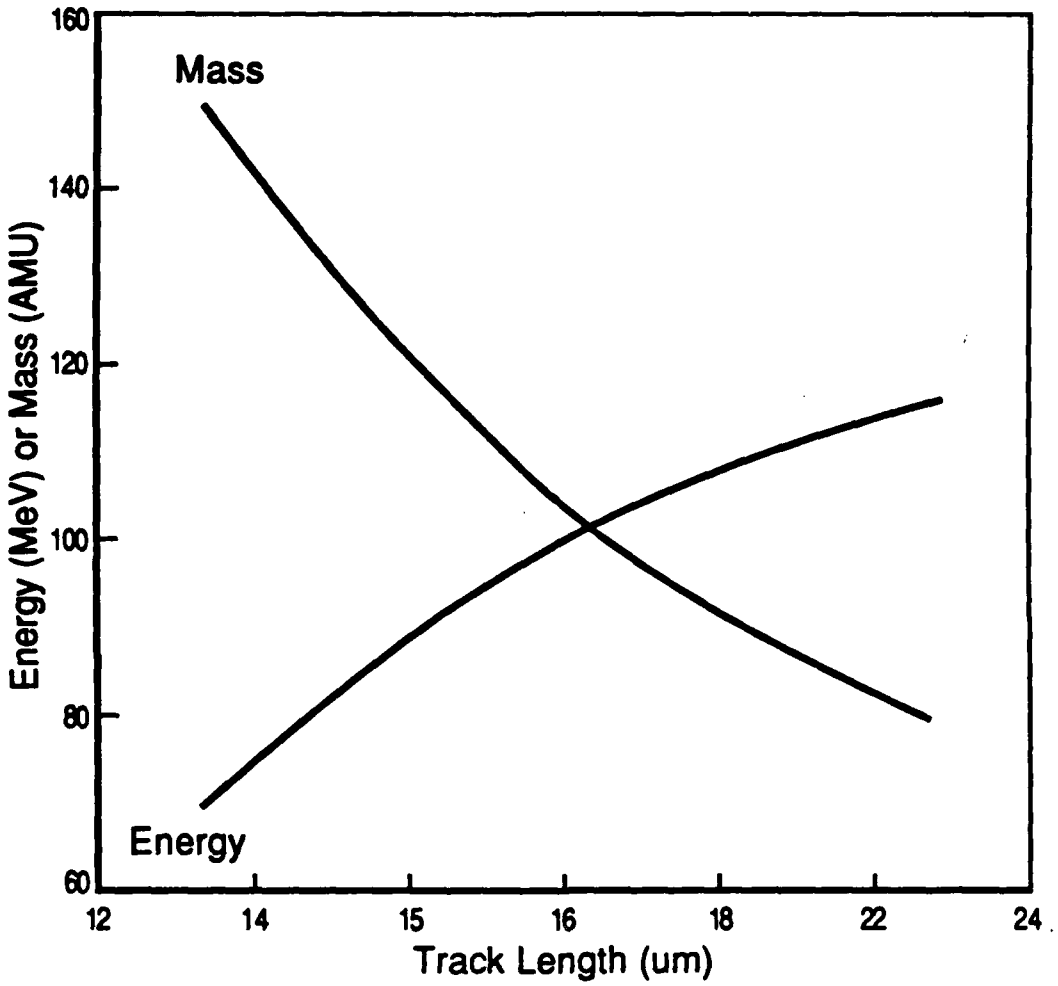

Figure 2-7. Track Length of Fission Fragments in FEP

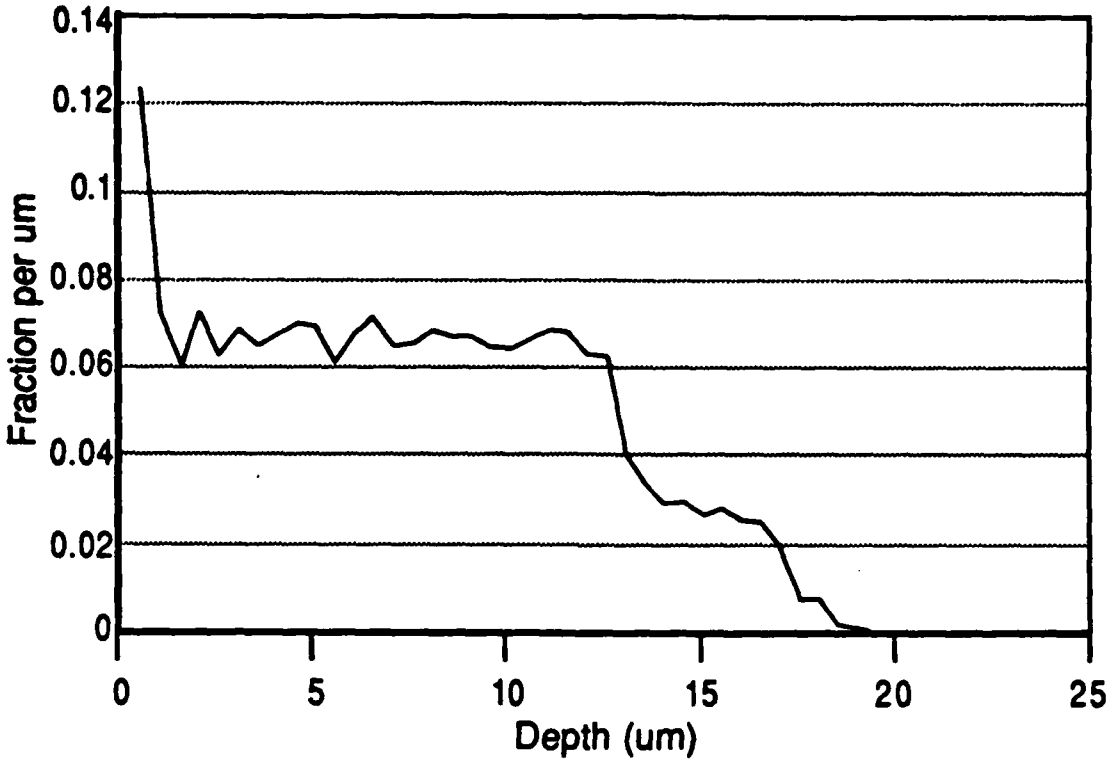

Figure 2-8. The Distribution in Depth of Penetration of Fission Fragments in FEP

III - Production of Electrets

Introduction

The methods used to produce, measure, handle and store electrets play a very important role in how the electrets respond in experiments. This chapter discusses those methods. It also presents the results of experiments used to evaluate the charge densities, charge uniformities, and storage lifetimes of the electrets that were produced.

The chapter is organized to parallel the process of making and using electrets. First, it discusses the process of selecting and mounting the electret material. Then it presents the various methods used to charge the electret material. Next, it describes the method used to measure the charge densities and charge uniformities achieved by the charging techniques. Finally, it discusses the storage and handling procedures used and present data on long-term charge stability under these storage conditions.

Selection and Handling of Electret Materials

The properties required of an electret material depend on the type of electret being produced. All electret materials must be dielectric in order to support an electric field. Thermoelectrets require a strongly dipolar molecule which can be oriented by an electric field and then 'locked' in position. Surface-charged and space-charged electrets must contain trap sites in which the charge carriers can reside. The number and depth of these trap sites determine the strength and stability of the electret.

The first electrets produced were thermoelectrets made from a mixture of carnauba wax, beeswax and white resin. Preliminary tests showed that these electrets did not respond to ion interaction. Externally charged polymer foils, which would support stronger electric fields, then became the focus of electret production

efforts. Externally charged electrets were made from several candidate materials, including polytetrafluoroethylene (Teflon - TFE), polyfluoroethylene propylene (Teflon - FEP), and polyethylene terephthalate (Mylar - PET). All are commonly used in electret research.

Of the externally charged electret materials, FEP demonstrated the best charge stability and handling characteristics. Samples of FEP, aluminized on one side, were obtained from Sheldahl Corporation while unaluminized samples were obtained from DuPont Corporation. Some experiments were conducted using several different thicknesses of FEP. For 3 reasons the 25.4 μm (1 mil) film was used most commonly; 1) it is readily available, 2) there is a large amount of data available on its characteristics as an electret, and 3) it is near the minimum thickness that will completely absorb fission fragments and alpha particles. The characteristics of FEP foils are available in the manufacturer's product brochure.(33)

Two methods were devised to handle the polymer film electrets. For most applications, the foils were simply attached to a stainless steel planchet by various means. When access to both sides of the foil was required, a ring clamp device was used. Figure 3-1 shows the details of both mounting methods.

Two types of adhesive were used to attach foil to the back of a planchet. A commercial conductive adhesive, ECCOBond 59-C, was first used. Its method of application, similar to a contact cement, was simple and avoided contamination of the exposed surface. A catalyzing agent could be added to promote full hardening beneath the foil. However, the hydrocarbon solvents used in the adhesive made it unsuitable for use in a vacuum system. Still, many of the corona charged electrets used for long-term charge retention studies and for indirect ion interaction experiments were constructed using this adhesive. The most suitable adhesive for electrets used in vacuum systems was found to be conductive epoxy. The silver-loaded resin was mixed with hardener and applied as a small lump in the center of the planchet. When the planchet was then pressed against the aluminized surface of the foil, the epoxy spread into an even coating. This process minimized air bubbles between the foil and the planchet. When the epoxy had cured, the excess foil was trimmed from the edges of the planchet. The resulting electrets could be

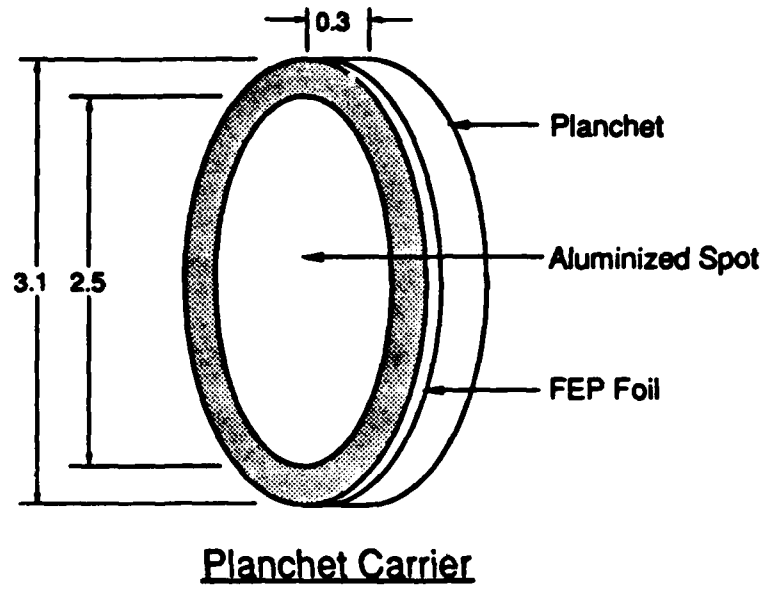

Planchet Carrier

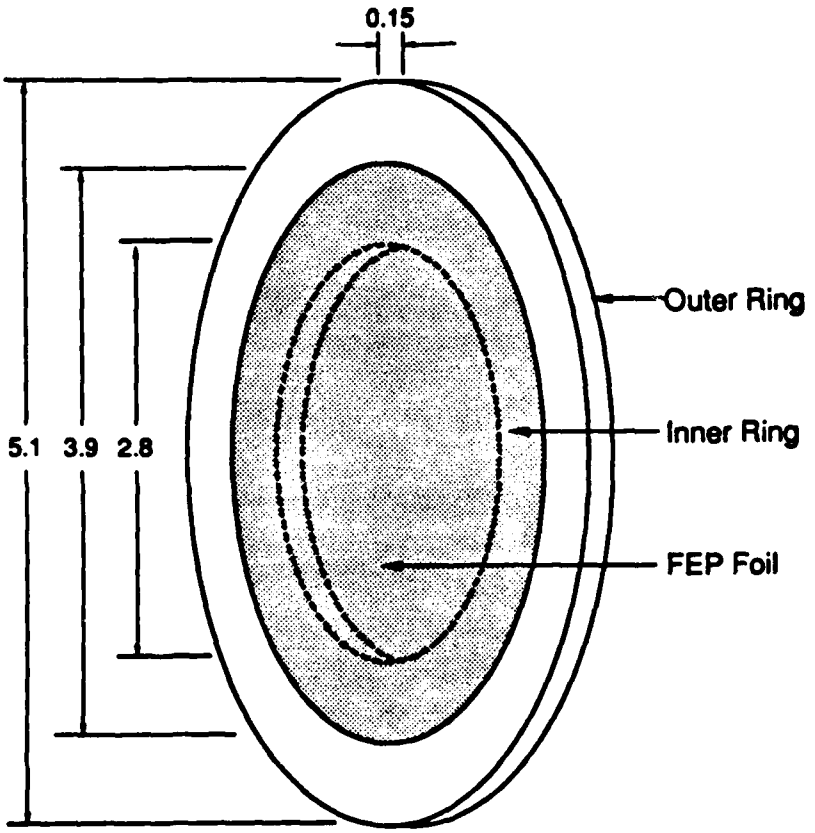

Ring Carrier

Figure 3-1. FEP Foil Mounting Methods, Dimensions in cm

used in vacuum systems to 10^{-7} Torr and annealed at 100^{o} C without adverse effects.

The direct ion interaction experiments required an electret with a front electrode attached. For these electrets, a 2.5 cm spot on the front surface was covered with a vapor-deposited layer of aluminum. The electret was first mounted in a plate which masked the outer edge, leaving an exposed spot at the center. The electret was then placed in a vapor deposition system and exposed to a stream of aluminum vapor until the aluminum deposit was about 1000 angstrom.

When access to the back side of the electret was required or when the foil was to be removed from the carrier after charging, a ring carrier was used. This consists of two concentric, nested rings of plexiglass. The outer ring diameter is 5.1 cm, while the inner ring diameter is 3.9 cm. The inner diameter of the inner ring is 2.8 cm. The electret foil was stretched over the inner ring with the aluminized surface facing out. It was then clamped in place using the outer ring and any excess foil was trimmed. The foil could then be charged through the hole in the inner ring. All of the electret luminescence experiments were conducted using this mounting technique. For study of the electronic response, the stretched foil was generally too sensitive to vibration.

Electret Charging

Three methods were used to charge polymer foils; breakdown charging, corona charging and electron-beam charging. Breakdown charging and corona charging produced surface-charged electrets, with corona charging producing a more uniform distribution of surface charge. However, neither type of surface-charged electret proved satisfactory for fission-fragment direct-interaction experiments. The detector system had to be evacuated to prevent air ionization by alpha emissions from the uranium. Such ionization produced signals which completely masked the fission fragment signal. When a surface-charged electret was placed in a vacuum, Paschen discharge occurred as the air pressure fell. This produced compensating charges on the electret surface, limiting their effective surface charge to about 350 volts, the Paschen limit. Even external biasing to protect the electret's field during evacuation could not prevent discharge. Space-charge

electrets were used for these experiments because surface compensation leaves their very strong internal fields intact. A modified electron-beam system was used to produce space-charged electrets.

Breakdown Charging. Charging by controlled breakdown fields was investigated first because it was reported to produce high surface-charge densities.(30) In this process a layer of polymer foil and a 0.12-cm layer of glass was placed between electrodes biased to +/- 15 kV. The induced field exceeds the breakdown strength of the foil but not of the glass. Current leakage through the glass provides charges which collect on the surface of the foil. When the bias is removed, the charges are trapped at the surface. After about 10 minutes, the electrodes were shorted and the foil immediately recovered. This process minimizes the loss of surface charge through breakdown in air. By this method, FEP foils were produced with surface potentials greater than 3400 volts (the limit of our charge measurement device). However, the uniformity of the charge was very poor; some regions were charged to only 20 percent of the maximum.

Corona Charging. The corona discharge method was investigated because of its simplicity and its potential to produce greater charge uniformity.(23;24) In this method, a 10-15 kV negative bias was applied to a corona pin mounted about 4 cm above the foil. The back of the foil was grounded. The electric field at the pin point ionizes the air and produces a shower of negative ions. The electric field drives the ions to the foil. The air ions that strike the foil deposit electrons which then become immobilized in surface traps. Initial charging is very rapid, but charging slows as the foil develops its own electric field which repels the ions. Charging to about 3000 V required only about 1 minute. The uniformity of the charging is not especially good as the electric field driving the air ions is not uniform.

Charge uniformity and full control of the surface potential was achieved by installing a biased grid between the corona pin and the foil. A negative bias of 1 to 3 kV was used. The grid produces an initially uniform field above the foil. Air ions penetrate the grid and are carried to the foil surface where their electrons are trapped. As one portion of the foil charges, the field between the grid and the foil becomes distorted to direct the air ions to the less charged areas. Charging stops

when the surface potential of the electret matches the potential of the grid. About 30 minutes of charging would produce electrets uniformly charged to the grid potential. One problem with the system was that the copper grid was rapidly corroded by the air ions. The grid was cleaned periodically by dipping in a weak hydrochloric acid bath.

Electron-Beam Charging. The electrets used for studies of direct interaction by fission fragments were produced by electron-beam charging. The electron beam system used was part of a custom-built x-ray spectroscopy system. The system consisted of a biased electron emission filament, electrostatic focusing rings and a target carousel as shown in Figure 3-2. Samples were clamped into the carousel mount using three hex screws. A copper guard ring contacted the outer edge of the front surface to serve as a grounded guard ring. Filament current and focusing voltage were provided by a battery-rheostat-meter system that was isolated and maintained at the filament bias. Filament bias was provided by a high voltage power supply and monitored on an electrostatic voltmeter. The system was originally intended to provide a finely focused, high current electron beam for x-ray generation. Use of this system for the production of electrets required a uniformly dispersed electron beam of lower but more consistent current. To accomplish this, the polarity of the focusing rings was reversed to provide controlled dispersion rather than focusing. In addition, rotary beam deflection was provided by an external rotating magnetic field generated by a magnetic stirrer.

The uniformity of the electron beam was tested using a 'reverse' Faraday cup. An aluminum disk containing a 1.27-cm diameter hole was placed on the carousel. Electrons striking the disk produced a measurable current while those passing through the hole struck the grounded plate behind. The reduction in the measured current as the hole traversed the beam yielded the beam current density. The current density distribution for various configurations was measured to find the optimum conditions of 60 volts on the focusing ring and the stirring motor at 9 cm from the beam path. Direct observation of the beam pattern using a fluorescent screen showed a generally dispersed pattern with several bright spots revolving around the center. A more quantitative check on the uniformity of the beam was performed by charging an uncoated FEP electret to about 2×10^{-8} coul/cm^2 (200 volts). At this charge density Paschen discharge does not occur. The

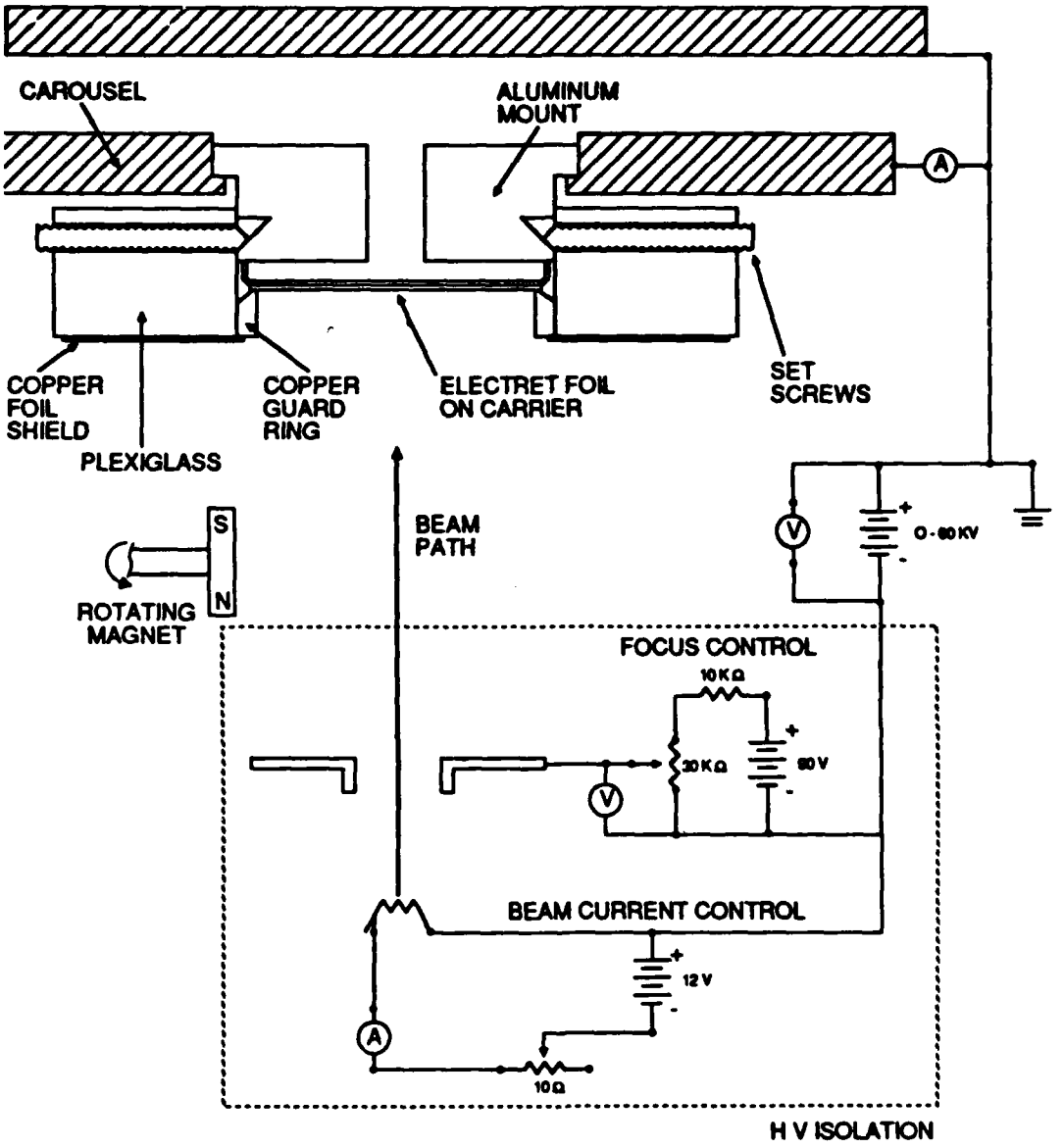

Figure 3-2. Electron Beam Charging System

resulting charge distribution is shown in Table 3-1. As can be seen, there is significant nonuniformity in the beam not identified by the more gross measurements using the reverse Faraday cup. This nonuniformity presents a major problem in understanding the results of the direct interaction experiments but could not be avoided using this system.

Table 3-1: Relative Charge Distribution in a 25.4 μm FEP Foil E-Beam Charged at 40 kV.

Y \ X	-11	-7	-3	1	5	9
10	14	76	67	36	11	4
6	78	100	91	51	38	15
2	72	44	71	77	37	22
-2	75	51	90	83	24	19
-6	75	84	87	54	20	20
-10	13	47	42	29	28	23

Percent of maximum charge measured
from electret center (mm)

FEP electret samples were charged using the electron beam system at energies from 10 to 50 kV, beam current densities from 10^{-11} to 10^{-8} amps/cm^2, and charging times from 30 sec to 2 hrs. Charging time was controlled by rotating the carousel to place the sample in the electron beam. After charging, samples were left under vacuum for at least 20 minutes to minimize discharge due to RIC.

Determination of Charge Density

As shown in Chapter 2, most of the electrical characteristics of an electret depend upon its charge density. Volumetric charge densities resulting from electron-beam charging are very difficult to measure directly. The integral of the volumetric charge density may be determined from the beam current density. The effective surface charge density of either a surface-charged or space-charged electret is relatively easy to determine from measurement of the surface potential.

The charge densities achieved by electron beam charging could not be measured directly. Paschen discharge introduced compensating charges to the front surface when the sample was removed from the system vacuum. However, during charging the sample's back electrode current was monitored while the front surface was left floating. The grounded guard ring prevented surface leakage to the back electrode. The current to the back electrode was monitored using a picoammeter and recorded on a strip chart recorder. Integration of the current using Equation 2-3 yielded an estimate of the charge density.

A strip chart recording of the back electrode current showed a general pattern of charging, spontaneous discharge to either the front or back electrode, and finally full breakdown discharge indicating charge saturation. Figure 3-3 shows a typical history of the charging process. Charging at less than 35 kV produced mostly spontaneous discharge to the front surface (down spikes) while above 35 kV some discharge occurred to the back surface (up spikes). As shown in Figure 2-2, this beam energy corresponds to an electron range of half the thickness of a 25.4 μm FEP foil. The accumulated charge density at which the full breakdown occurs corresponds to an internal electric field which approaches the dielectric strength of FEP as calculated using Equation 2-7. Figure 3-4 shows the charge densities achieved in FEP foils as a function of beam current density. Current densities above 2×10^{-9} Amps/cm^2 yielded lower charge densities, presumably because of increased RIC in the irradiated region. Current densities below about 2×10^{-10} Amps/cm^2 produced no full breakdown. This is probably because sufficient charge could be dispelled in an individual spike to allow a period of recharging. At such low charging rates it was very difficult to maintain steady beam currents for the hours needed to charge saturate the electret.

A Monroe 440 Isoprobe electrostatic voltmeter was used to measure an electret's effective surface charge density. The voltmeter uses a noncontacting, vibrating reed probe to determine the electric potential of a surface in a range of +/- 3000 V. The effective surface charge density could then be determined using Equation 2-4. Electrets were placed in a mounting bracket attached to a grounded X-Y translation stage. The voltmeter probe was mounted over the bracket. The entire assembly was built into a plexiglass box to minimize dust contamination. For repeatability in sample placement, the mounting bracket

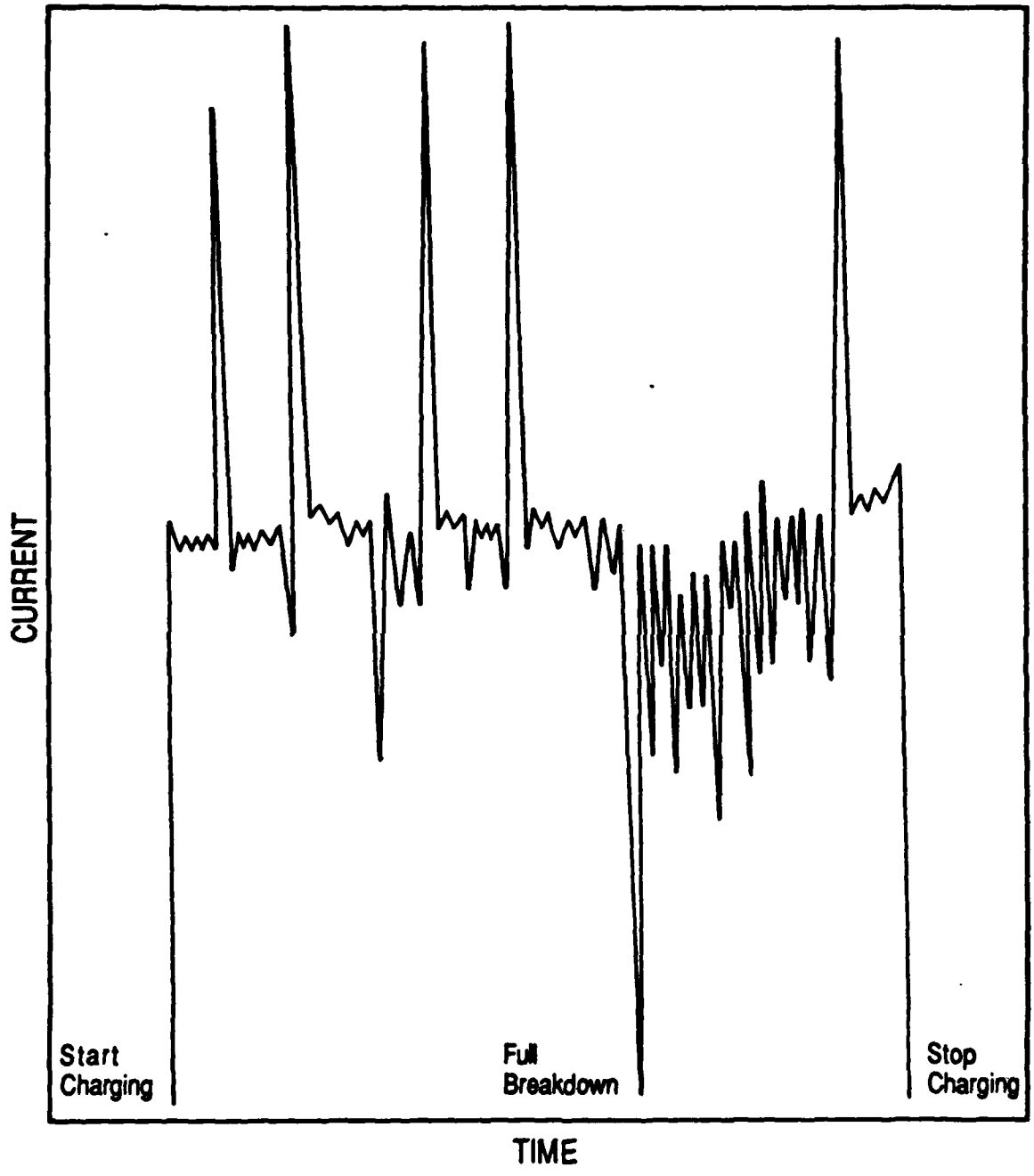

Figure 3-3. Typical Charging History for FEP Charged with 40 kV Electron Beam

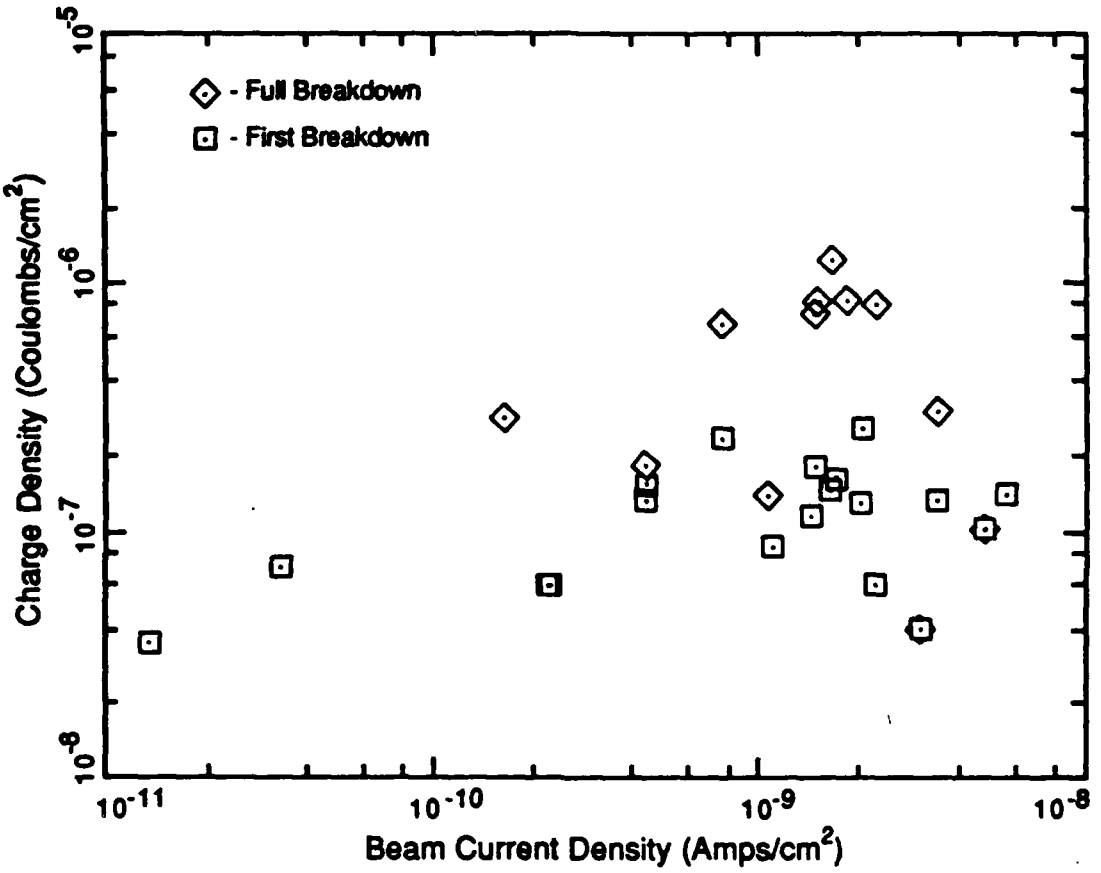

Figure 3-4. Charge Densities Achieved in FEP using a 35-40 kV Electron Beam

contained a circular depression of the diameter of the carrier planchets. A reference mark on the planchet could then be aligned to a mark on the bracket. The system is estimated to have an x-y spatial reproducibility of +/- 0.05 cm. For electrets without a front electrode, the surface potential was measured at points in a 6 x 7 grid of 0.4 cm spacing. For electrets with a front electrode, the charge on the electrode itself was measured.

Handling and Storage of Electrets

Proper handling and storage of electrets is critical to long-term charge retention and to reproducibility of charge release experiments. Exposure to moisture, uncontrolled heating, or contact with the surface rapidly degrades the effective surface charge density of an electret.

Electrets were stored in 8 cm diameter by 2.8 cm steel ointment cans. The cans had slip-on steel tops which, although not airtight, provided good isolation of the electrets from ambient air. A sample used for a long-term charge storage test was stored with its mounting planchet in electrical contact with the can. Other planchet-mounted samples were not stored in electrical contact with the can. Their planchets were attached to the bottom of the can by strips of double-sided adhesive tape. A sample on a ring carrier was simply laid in its can with its charged surface facing upward.

Thermal annealing of an electret is a method of producing more stable electrets.(9) It works by promoting charge transport from shallow traps to deeper, more permanent traps. It also reduces DRIC in electron-beam charged electrets. A thermostatically controlled oven was used to thermally anneal samples. Annealing was accomplished by placing the samples, either in their metal storage containers or in a covered glass petri dish, inside the oven at 100° C for various periods. Annealing at 150° C was tried, but gas bubbles formed under the FEP foil, possibly due to outgassing of the adhesive.

Annealed samples lost at least 50 percent of their original charge over a 12 hour period at 100° C. More importantly, their response to direct ion interaction essentially disappeared. Because of this, electrets used in ion interaction experiments were not thermally annealed after charging. Electrets were annealed as

part of a process for discharging and reusing electret samples.

The large number of experiments conducted made one-time use of the electrets impractical. A charge release technique was used to restore samples to their pristine charge state for reuse.(35) In the process samples were gamma irradiated for 2 hours at 14.2 rads/hr using an isotropic ^{60}Cobalt source. They were then annealed at 100° C for at least 10 hours. After undergoing this process, an electret had a uniformly zero effective surface charge. No variation in experiment results are attributed to this process, even though it was repeated 6 times on some electrets.

Seven FEP electrets were tested for their long-term charge retention properties. Planchet-mounted samples were corona charged and stored in ointment cans. Their patterns of surface charge were periodically tested using the electrostatic voltmeter. Figure 3-5 shows the pattern of long-term decay in a typical FEP electret foil. Occasional measurements indicate a point's charge increasing with time instead of decreasing. This is attributed to a slight misalignment of the sample and a steep charge gradient at that point. Generally, the patterns show that charge retention is good, although somewhat nonuniform. It should be noted that these samples were handled weekly for measurement of their effective surface charge, in a somewhat humid environment. The nonuniformity, particularly about the edges of the sample, is likely the result of casual contact during handling. In one sample, accidental contact with the surface resulted in an immediate 30 percent charge loss at that point and a more rapid charge decay thereafter.

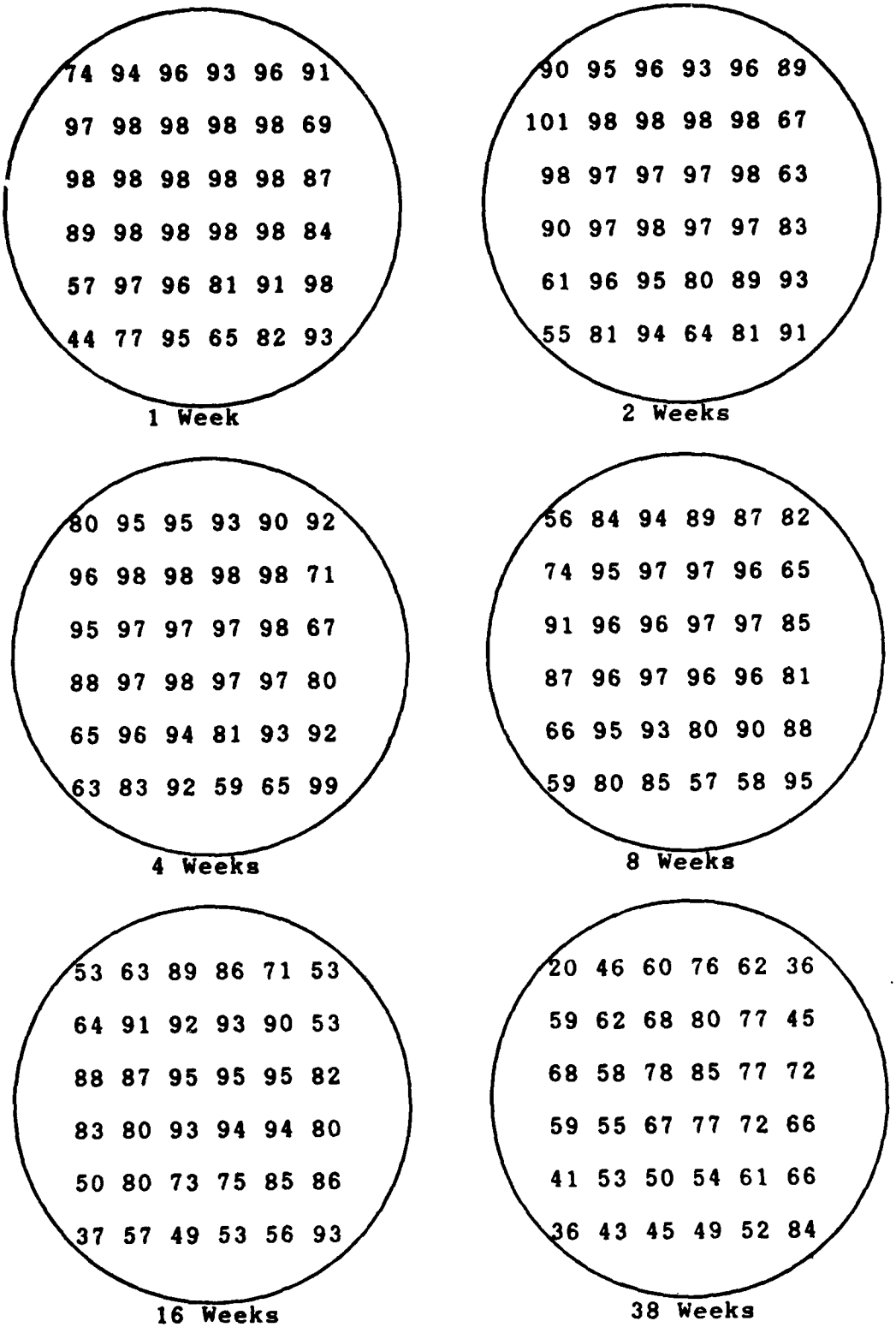

Figure 3-5. Charge Decay Pattern in 25.4 um FEP Corona-Charged to -1.5×10^{-7} coul/cm^2. Values are Percent of Initial Charge at 0.4 cm Spacing

IV - Electric Response to Alpha Particles

Introduction

As shown in Chapter II, alpha particles produce charge-carrier pairs when interacting with a medium. If the charges are in the electric field of an electret, they drift, producing an electric signal. The mechanism is the same as that found in an ionization chamber detector. The interaction may occur directly, within the electret material itself, or indirectly, in the air above the electret's surface. Because of charge recombination, alpha particles interacting directly with the electret material are not expected to produce a significant signal. However, interaction in the air above an electret will produce a sizeable electric signal. The characteristics of the signal are determined by the alpha particle's energy and the characteristics of the medium, including its shape. A small volume of medium will not absorb all of the alpha particle's energy.

This chapter reports on an investigation of alpha particle interaction in an air volume above an electret and the electrical signal produced by the interaction. Both small air volumes and large air volumes were investigated. Each type of volume produces a distinctive signal and each is the basis of an experimental radiation detector.

Theory

For radiation detection the most important characteristics of alpha particle interaction are how large the signal is and how the signal changes with time. Except in large volumes of medium, alpha particle interaction produces a distribution in signal size determined principally by the size and geometry of the medium volume. The total charge in the signal, Q, is related to the dissipation of the effective surface charge in the electret and the decay in the electret's electric field.

Signal Size. An alpha particle interacts with an electret to produce a flow of charge carriers and either to reduce the electret's surface charge or to increase its surface compensating charge. The charge carrier flow, a current, is the electrical signal. The size of the signal is the total charge contained in the current. Equation 2-14 relates this charge to the length of the alpha particle path through the medium. When the volume of the medium is small, some or all of the alpha particles have paths smaller than the maximum track length. When the volume of the medium is large, essentially all of the alpha particles have track lengths equal to their maximum. The equation for the signal size is then simplified to Equation 2-15. Both of these equations ignore charge recombination.

In a small volume of medium at least one dimension is less than the track length. For alpha particles crossing this dimension, only a portion of the particle's energy is deposited in the medium. The direction of particle travel and the exact geometry of the medium enter into the determination of the collected charge, Q. Let us assume a cylindrical chamber of height T, less than the alpha track length and of arbitrarily large diameter. At the top of the chamber is an electret inducing an electric field. A thin film of alpha emitter is uniformly distributed on the bottom. For this geometry, Q is:

$$Q = \frac{\bar{S}Te}{W\cos(\theta)} \tag{4-1}$$

with the constraint:

$$\frac{\bar{S}Te}{W} \leq Q \leq \frac{E_\alpha e}{W}$$

where θ is the angle of alpha emission from surface normal. Since the number of alpha emissions is distributed on θ as the sine from 0 to π radians,(spherical distribution) Q is also a distribution. The minimum constraint in the distribution represents alpha particles emitted normal to the surface. The maximum constraint represents the case where all the alpha particle's energy is deposited in the medium.

Direct interaction of an alpha particle with the field region of the electret must be considered to occur in a small volume of medium. The charge depth is usually less than half the maximum track length. From Equation 4-1 it is clear

that the interaction of the alpha particle with the electret itself will not produce a strong electrical signal. If there is no recombination and 1 keV is required per charge carrier pair produced, the maximum charge resulting from a 5 MeV alpha is only 8×10^{-16} coul. Further, only those alpha particles striking at a very shallow angle would produce this size signal. But if the interaction occurs in an air gap between the electret and an electrode, a much larger signal results. The maximum signal becomes 2.5×10^{-14} coul and, if the air gap is 3.5 cm or more, all of the alpha particles will produce this signal. The electrical response of electrets to alpha particles is greatest, and most detectable, if the particle generates charge carrier pairs in an air gap above the electret.

In a medium where the diameter, $2R$, is also less than the alpha track length, both the position and direction of the particle track become important factors in determining the charge collected. Analysis of the distribution is unwieldy, but an average value may be estimated. The average charge, $\bar{Q}$, collected from a small, cylindrical medium above a uniformly distributed source is:

$$\bar{Q} = \frac{\bar{S}e}{W}\left[T \ln\left(\sqrt{(0.85R)^2 + T^2}\right) + 0.85R \tan^{-1}\left[\frac{T}{0.85R}\right]\right] \qquad (4\text{-}2)$$

as derived in Appendix A.

Electret Charge Dissipation. A dissipation of the effective surface charge of an electret occurs with every ion interaction in the air above it. The charge carriers collected on the surface of the electret either neutralize or compensate the electret charge. We can use Equation 2-4 and Equation 4-1 or 4-2 to determine how alpha interactions neutralize the effective surface charge of the biasing electret. For the electret-alpha source system described above, the average current, i, generated by alpha particle interaction is:

$$i = \frac{\bar{Q}A}{2} \qquad (4\text{-}3)$$

The activity, A, of the source is divided by 2 because only half of the alpha particles are directed outward from a thin film alpha source. To fully neutralize the electret, we must apply to the surface a charge equal to the total effective surface charge. A circular electret of radius R has a total effective surface charge, Q_e, of:

$$Q_s = \delta\pi R^2 \tag{4-4}$$

If charge collection efficiency does not change as the electric field is reduced, (not true for low field strengths) the number of alpha events required to neutralize the electret, N_n, is:

$$N_n = \frac{Q_s}{\overline{Q}} = \frac{\delta\pi R^2}{\overline{Q}} \tag{4-5}$$

and the time required, t_n, is:

$$t_n = \frac{\delta 2\pi R^2}{\overline{Q}A} \tag{4-6}$$

Equations 4-5 and 4-6 represent minimum values because $\overline{Q}$ assumes that recombination does not occur. As the electric field of the electret is reduced by dissipation of the effective surface charge, collection of charge carriers must eventually become less efficient. The charge dissipation of the electret should be essentially linear until the electret's field is too weak to prevent additional recombination of the charge carrier pairs.

Experimental Procedure

Two detection systems were devised to record the electronic response of electrets to alpha particles. In one, the medium consisted of a small air gap between an electret and an electrode. The characteristics of signals from this configuration allowed the use of conventional pulse measurement electronics. In the other, an electret biased a larger volume of air in a cylindrical container. The slower, broader pulses emitted using this configuration were filtered out by conventional charge measurement electronics. A simple system was devised to count these pulses. Using these systems, alpha particle interactions in small and large air spaces above the electret were detected.

Attempts to detect the direct interaction of alpha particles with an electret were unsuccessful. Some increase in the recorded noise levels may have been attributable to alpha interaction, but this was not quantifiable.

Small Volume Interaction. For studying alpha particle interaction in a small air volume, a detection system was assembled to measure the movement of

compensating charge on electrodes adjacent to an electret. A charged electret on a planchet was placed in a Teflon TFE holder with a uranium-coated copper disk. A 0.2-cm gap was left between the electret and the disk. Spacer rings beneath the copper disk could be used to increase this spacing. The holder was enclosed in an aluminum container which acted as both a faraday cage and a vacuum vessel. The detector could be evacuated to 50 μm Hg with a forepump. A charge-measuring system was attached to the copper disk and the planchet was grounded.

The charge-measuring system consisted of a charge-sensitive amplification system, a multichannel analyzer and a data recording system. Signals from the detector first enter an Ortec 142B charge-sensitive preamplifier. Output from the preamplifier is transmitted through a Canberra 2020 linear amplifier and an Ortec 542 pulse stretcher to a Nuclear Data 100 multichannel analyzer. Data collected by the multichannel analyzer is then transmitted via a custom RS-232 serial interface box to a Zenith Z-100 microcomputer for storage on floppy disk. Output from the preamplifier is also transmitted through a custom wideband amplifier having a gain of 1000 to a Tektronix 465M oscilloscope for visual analysis of the output signal. Finally, charge calibration of the entire system is accomplished with an Ortec 419 precision tail pulse generator connected to the test input of the preamplifier. Figure 4-1 is a diagram of the entire detector system. This system records the total charge contained in an electrical pulse and tracks the number distribution by charge in a series of pulses. The result is a charge distribution spectrum of the interaction pulses. Such equipment is commonly used to determine the energy distribution of radiation sources. As currently configured, the system is capable of reliably detecting effective charge events greater than 3×10^{-16} coul.

Large Volume Interaction. For study of alpha particle interaction in a large air volume, a corona-charged FEP foil attached to a copper disk was placed on an insulating support and installed in a metal can. Early tests used an ointment can of the type used for electret storage and a 2.8-cm diameter foil. For later test, a stainless steel can of 11.4-cm diameter by 4.4 cm was used with a 7.6-cm diameter FEP foil. Figure 4-2 shows the large volume detector as configured to detect atmospheric radon. The copper disk was attached to a

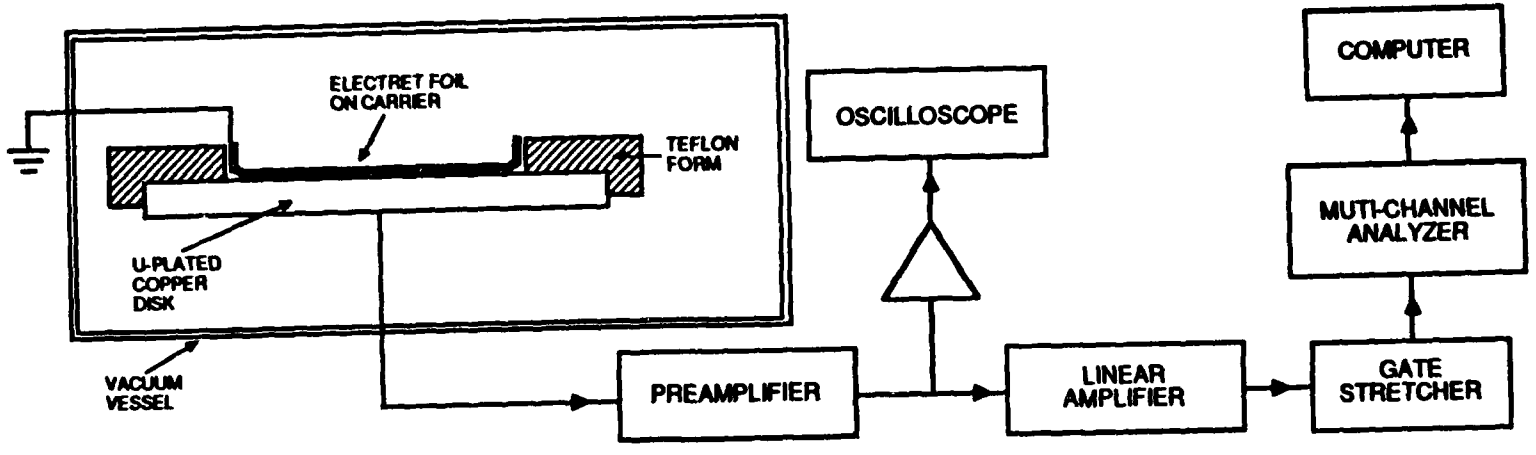

Figure 4-1. Detection System used to Study Electret Response to Alpha Particle Interaction in Small Air Volumes

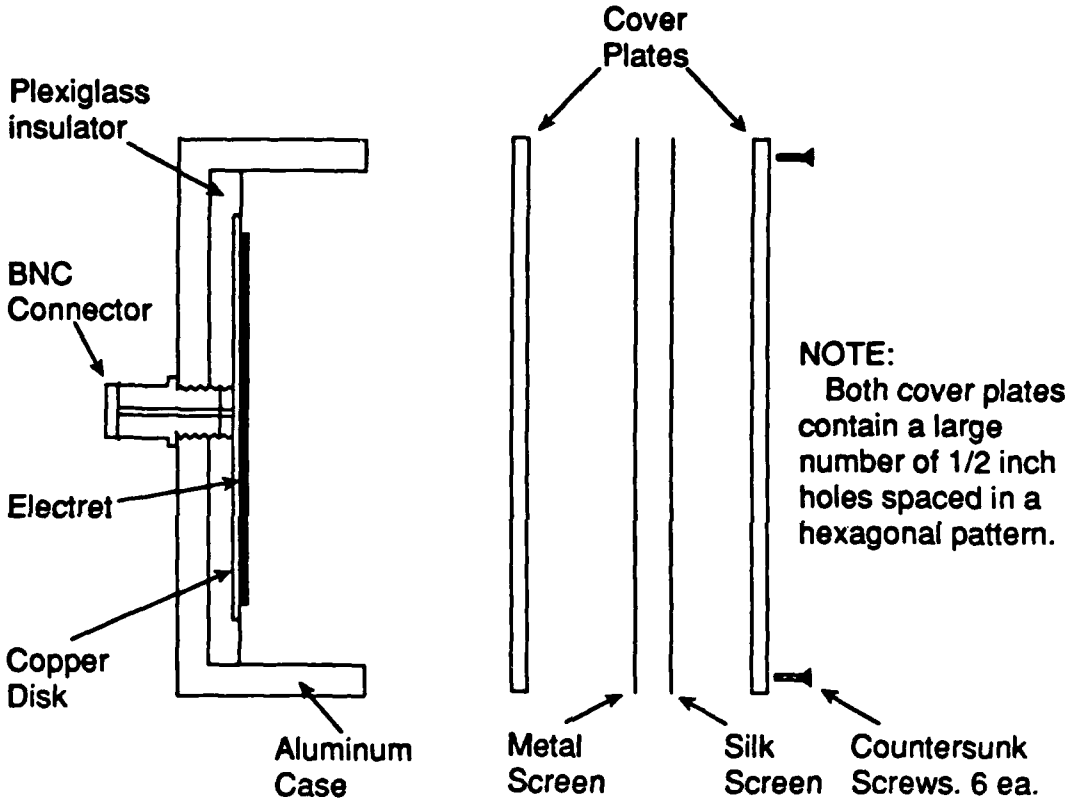

Figure 4-2. Detector used to Study Electret Response to Alpha Particle Interaction in Large Air Volumes

system consisting of a charge sensitive preamplifier (an Ortec-142B), a custom broadband amplifier and an oscilloscope (a Tektronix 465M). A multichannel analyzer could not be used because the slow rising pulses were filtered out by noise filters on the linear amplifier. However, the pulses could be observed on the oscilloscope and counted using the sweep trigger to drive a multichannel scaler (a Nuclear Data μMCA).

Results

Alpha interaction in the air above a charged electret yields a significant electrical response. The response signal in the small air volume was somewhat different from the response signal in the large volume. In the small air volume, the event was also shown to discharge the electret, eventually reducing and eliminating the signal.

Small Volume Interaction. When an FEP electret, corona charged to 1.5×10^{-7} coul/cm^2, was placed in the detector system with a uranium-coated disk, pulses up to about 7.3×10^{-15} coul were detected. The signal disappeared as the air gap was evacuated and returned on repressurization. The charge distribution in the pulses for three air gap thicknesses is shown in Figure 4-3. Note that the signal minimum is smaller for the smaller air gap. The smaller air gap also registered significantly more counts, particularly at the lowest charge.

Alpha particles of about 2 MeV were also detected using the small-volume detector. The uranium-coated disk used in the above experiment was replaced with a copper disk coated with amorphous boron powder containing 19 percent ^{10}B. A 0.2-cm air gap was used. When the system was exposed to a flux of thermal neutrons inside a neutron pile, pulses attributed to the neutron-alpha reaction were observed. When the system was outside the pile, only occasional pulses were seen. These signals are attributed to the much lower, but still measurable, neutron flux escaping the pile. The charge distribution of the signal is shown in Figure 4-4. Note the broad peak corresponding to the minimum charge interaction of an alpha particle emitted normal to the surface. The broadness of the peak and the pulses observed at lower energies are probably the result of significant self-absorption in the boron powder.

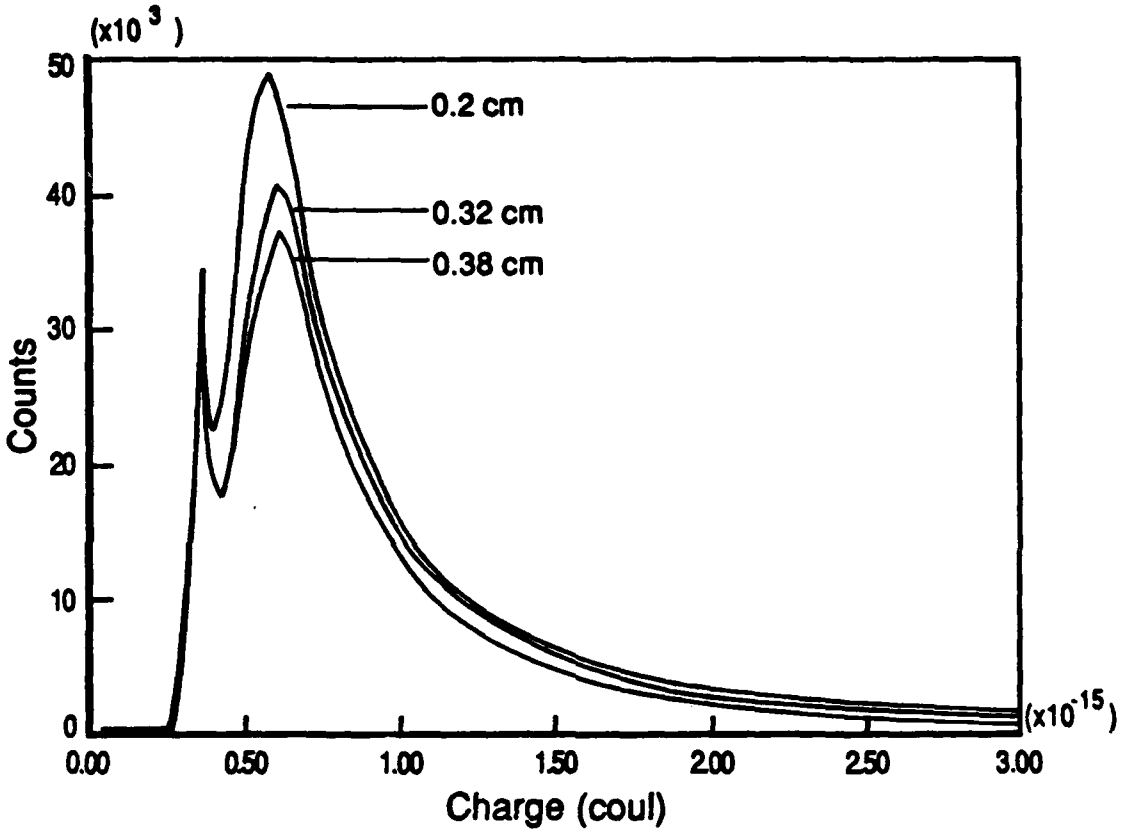

Figure 4-3. Charge Distribution of ^{235}U Alpha Particles Interacting in Various Air Gaps above Corona Charged FEP

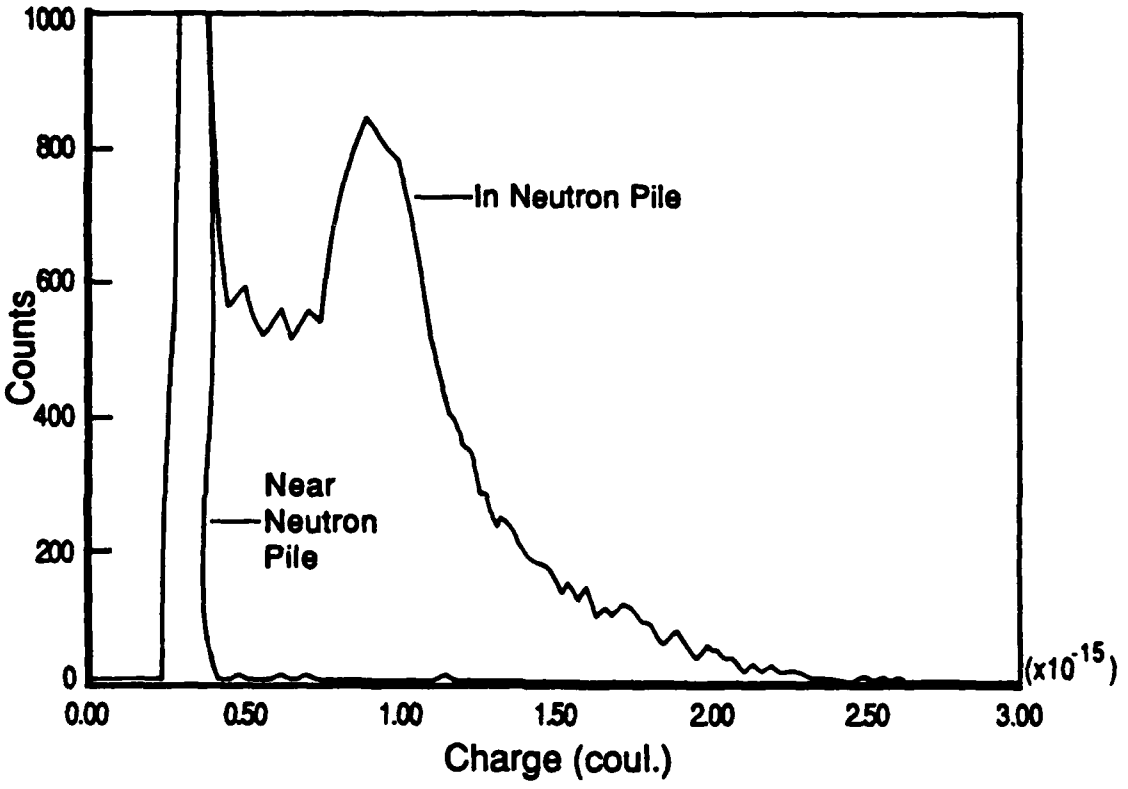

Figure 4-4. Charge Distribution of Alpha Particles from the N-Alpha Reaction of ^{10}B Interacting of a 0.2 cm Air Gap above Corona-charged FEP

Large Volume Interaction. The large volume detector also responded to alpha interaction, but with a somewhat different signal. A small ^{235}U alpha particle source, attached to a wooden dowel, was placed in the center of the detector. Alpha interactions were clearly seen as broad, irregular pulses having a rise time of about 0.5 msec and a decay time of about 2 msec. When the source was moved off center, the response continued but the pulses were smaller and somewhat more rounded. The efficiency of the detector also changed as the source was moved toward the edge of the chamber. Figure 4-5 shows the efficiency as a function of radial position of the source. Clearly the lower electric field and the loss of signal from alpha particles striking the wall degrade efficiency. With the sample removed, the pulses became much more infrequent and after several hours essentially stopped. This delayed signal is attributed to atmospheric radon and its progeny.

The charges collected by alpha interaction in a large volume were not of the size predicted by Equation 2-15. This is attributed to the very slow rise time of the signal entering the preamplifier. If a parallel plate geometry in the detector is assumed, the electric field was 130 volts/cm. In such a field both positive and negative charges would require about 0.1 sec to cross the detector.(19:155-156) Note that this is 50 times longer than the duration of the detected pulse. This is much too long to be efficiently integrated by the preamplifier. Under such conditions, the linear relationship between the height of the preamplifier output pulse and the total charge in the input pulse is lost.

A major problem with the large volume detector is its sensitivity to acoustic vibration. It responded to tapping with a signal of approximately the same size and shape as the alpha signals. It also responded to noise at a specific, fairly-narrow frequency range. Considering the similarities between this detector design and the design of an electret microphone, these are not surprising results. The establishment of an acoustic standing wave in the air chamber is probably responsible for the specific harmonic response.

Electret Charge Dissipation. The decay of the alpha signal was recorded using a recording picoammeter to determine the total current being released by alpha interaction. Figure 4-6 shows the total current released by alpha particle

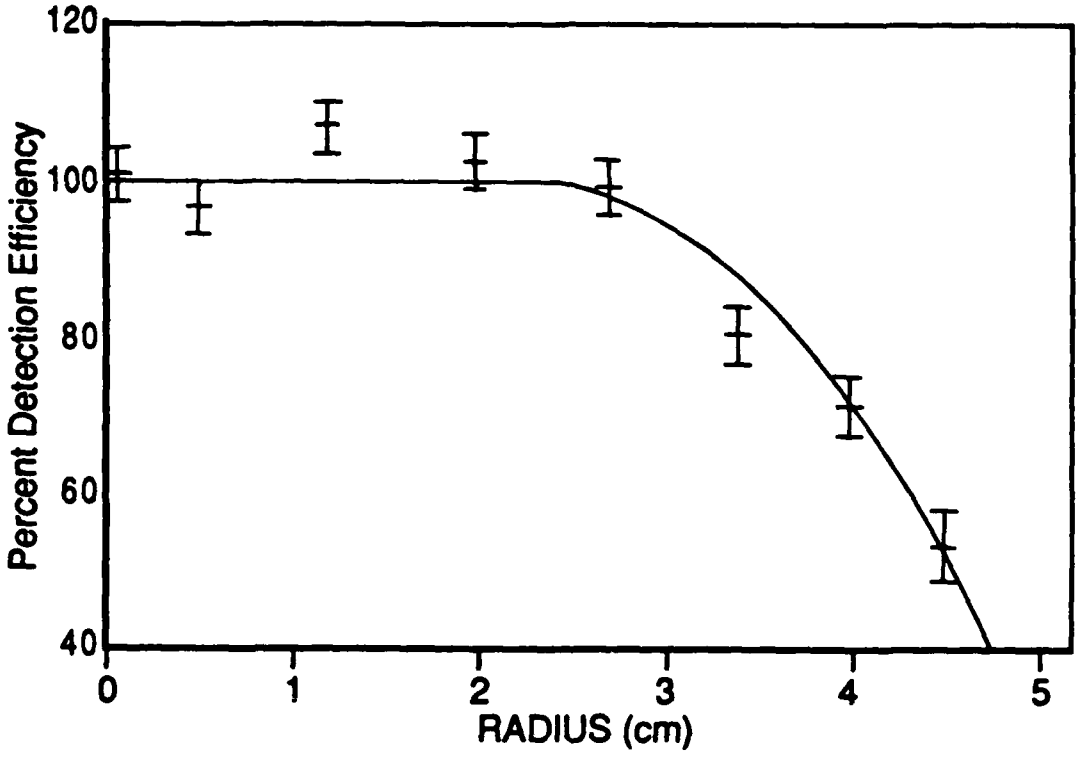

Figure 4-5. Alpha Particle Detection Efficiency of Large Volume Electret Detector

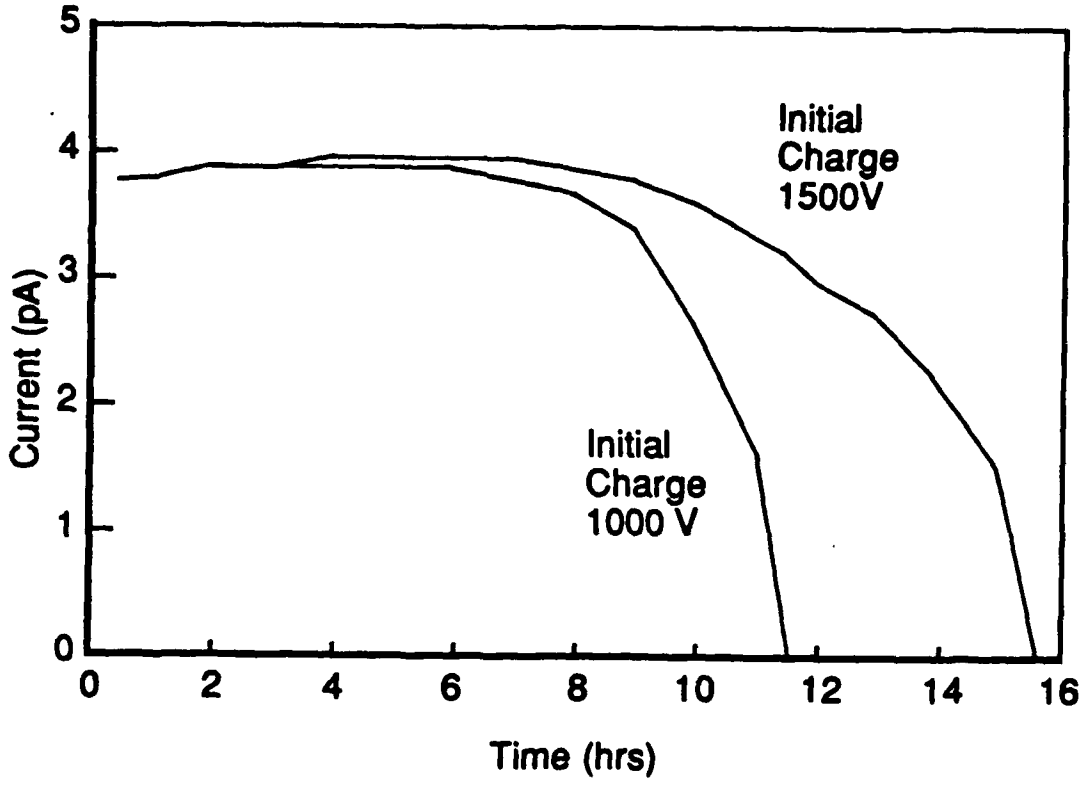

Figure 4-6. Charge Collection Current for 4.5 MeV Alpha Particles in a 2.8 cm Diameter by 0.2 cm Air Volume

interaction in a 0.2 cm air gap for two corona-charged electrets, one charged to 1000 volts and the other to 1500 volts. Note that despite the different initial surface charge and the continuous loss of surface charge, the current remains constant until the electret can no longer provide a field sufficient to prevent charge pair recombination. This shows that the detector began operating on the 'alpha plateau' where recombination is not significant and small variations in the electric field do not affect charge collection. The plateau current is defined by Equation 4-3. For the activity of the uranium sample used, 3.8×10^{3} decays per sec, and using Equation 4-2 for the average charge, the current should be 6.8×10^{-12} Amps compared with 3.8×10^{-12} Amps observed. The recorded current shows that charge collection efficiency is retained until the electret surface potential falls below about 300 volts.

Discussion

The two different volumes of medium studied produced strikingly different results. The small volume detector has a much stronger electric field. This minimized recombination and provided a sharply rising signal useful for electronic analysis. However, it sacrificed some of the alpha particle energy to interaction outside the active volume. Except for the effect of variations in stopping power with particle energy, the signals from the small volume detector were independent of the alpha particle energy. The large volume detector had a much lower electric field and its signal was more difficult to analyze.

The small volume detector provided a sharp, easily recorded signal in response to an alpha particle interaction. The size of the pulse was smaller than predicted by Equation 4-1. The net current output was also smaller than predicted by Equation 4-3. The shape of the pulse distribution is consistent with the expected distribution of a small volume detector.

Comparison of the data collected from a small volume medium relies on various means of estimating the average charge collected per alpha interaction, $\overline{Q}$. Several methods are available. First, the most direct approach is to use the data for the 0.2-cm air gap in Figure 4-3. The average charge collected is simply the sum of the charge in all of the counts divided by the number of counts. Second,

use the plateau current in Figure 4-6 with Equation 4-3. Third, use decay times in Figure 4-6 to estimate the average charge. Note that the 500 volt difference in initial charge resulted in a 4.7-hr difference in the time to complete charge decay giving a voltage loss rate. Using the time derivative of Equation 2-11:

$$\frac{dV}{dt} = \frac{\bar{S}}{k\epsilon_0}\frac{d(\hat{\sigma})}{dt} \tag{4-7}$$

this value can be converted to a rate of effective charge density loss. Now Equation 4-6 can be rearranged

$$\bar{Q} = \frac{\hat{\sigma}}{t_n}\frac{2\pi R^2}{A} \tag{4-8}$$

and the ratio converted to a rate

$$\bar{Q} = \frac{d(\hat{\sigma})}{dt}\frac{2\pi R^2}{A} \tag{4-9}$$

to find the average charge. Finally, a theoretical approach may be used as represented by Equation 4-2. Table 4-1 lists the average charge as determined by each of these methods.

Table 4-1: Estimates of the Average Charge Collected from a 4.5 MeV Alpha Particle in a 0.2 cm Air Space

Method	Equation	Value (Coul)
Charge Distribution	—	1.1×10^{-15}
Average Current	4-3	2.1×10^{-15}
Current Decay	4-9	8.3×10^{-15}
Theory	4-2	3.7×10^{-15}

As can be seen, all estimates of the average charge collected are within an order of magnitude of each other, with the theoretical value very near the center. This is not especially good correspondence. Of these values, the charge distribution value is the most disappointing. It should be a direct measurement of Q. The current decay method is the least precise because it relies on uniform charge collection at low field strengths.

The large volume detector demonstrated its ability to respond to alpha particles. However, the signal quality was poor and the response to acoustic noise was significant. The size and shape of this detector is clearly not optimized for detection of alpha particles. A smaller chamber would improve the signal size and shape at the cost of some loss of efficiency. Further, the preamplifier was designed to measure fast rising signals in a large capacitance detector. A great improvement in signal quality may be realized through the use of a preamplifier optimized to the detector.

Applications

The small volume detector does not appear to have application to the direct detection of alpha emitters. Alpha particles do not have the range to penetrate a thick shell to reach the ionizing medium while a thin window would introduce acoustic response as window vibrations would change the detector capacitance. However, the design may have a significant application as a thermal neutron detector. Thermal neutrons will readily penetrate an aluminum shell and the neutron-induced alpha emission of ^{10}B will generate alpha emissions within the detector. Figure 4-7 is a diagram of a simple thermal-neutron detector using the response of an electret to alpha particles. It consists of an aluminum shell containing a charged electret attached to an electrode and mounted on an insulator. Across an air gap from the electret is a layer of ^{10}B. Alternatively, the air could be replaced with argon which ionizes more readily to produce a larger signal, or with $^{10}B\ F_3$ which would increase the detector's sensitivity. Signals from the electrode are detected by a charge-sensitive amplification system and accumulated in a pulse counter/ratemeter.

The use of a boron loaded ionization chamber to detect thermal neutrons is not new. However, current designs need a high voltage power supply to provide the electric field. The use of an electret obviates that need and the power requirement it entails. Low-power amplifier and counting circuitry would make this design a dosimeter-sized neutron monitor with real-time readout.

The large volume detector has been tested as an environmental radon monitor. Radon is a naturally-occurring radioactive gas which can accumulate in

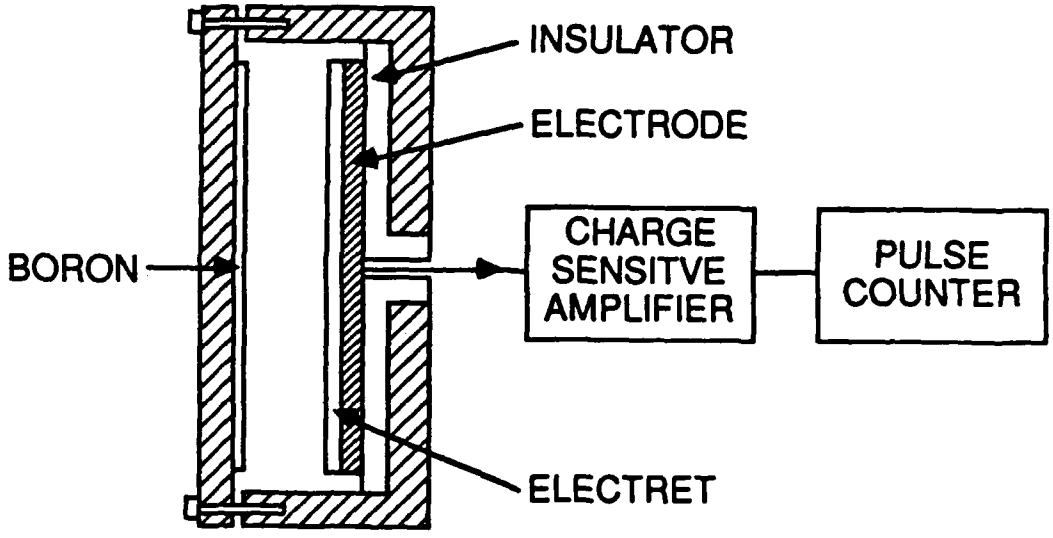

Figure 4-7. Design for an Electret Thermal Neutron Detector

mines, caves and poorly ventilated buildings. It has been associated with an increased risk of lung cancer. ^{222}Radon and two of its fast-decaying progeny, ^{214}polonium and ^{218}polonium, are alpha emitters as shown in Table 2-1.

The radon detector is essentially the device used in the large volume interaction studies. One end of the chamber was modified to admit radon from the environment. The detector is shown in Figure 4-2. The end opposite the electret consists of two plates containing 37 holes of 1.27-cm diameter. Between the plates are a copper screen and a silk screen. The copper screen shields the internal electric field while the silk screen excludes dust. The electrode connects to the same electronic system used in the large volume alpha particle interaction studies.

The detector operates by allowing radon gas to diffuse into the detector chamber through filtered openings. Inside, the radon decays by emitting an alpha particle which is detected. The charged decay products drift to the surface of the electret where they also decay with the emission of two additional alpha particles. On average, one of these additional alpha particles is directed away from the surface and detected. Thus, for each radon atom entering the chamber, two alpha interactions with air are detected.

The detector was calibrated and tested by operating it in parallel with a Pylon PRD-1 passive environmental radon monitor. Figure 4-8 shows the result of 8 days of operation. The diurnal variations in the radon concentrations are characteristic of radon buildup and dispersion. Note that both detectors recorded essentially identical results for the first three days. On the fourth day a rainstorm occurred causing a precipitous drop in radon concentrations as tracked by both detectors. The electret detector, however, did not fully recover its sensitivity. This is likely due to the effect of high humidity on the electret charge. The electret detector still tracked radon concentration variations, but at a reduced efficiency.

Calibration of the radon detector indicated that 0.79 +/- 0.08 counts per minute would be recorded at a radon concentration of 1 picocurie per liter. Since the detector volume is 0.21 liters, 1 picocurie per liter should theoretically result in 0.93 alpha interactions per minute (at 2 per ^{222}radon disintegration). This is a detection efficiency of 85 percent which is consistent with the radial efficiency

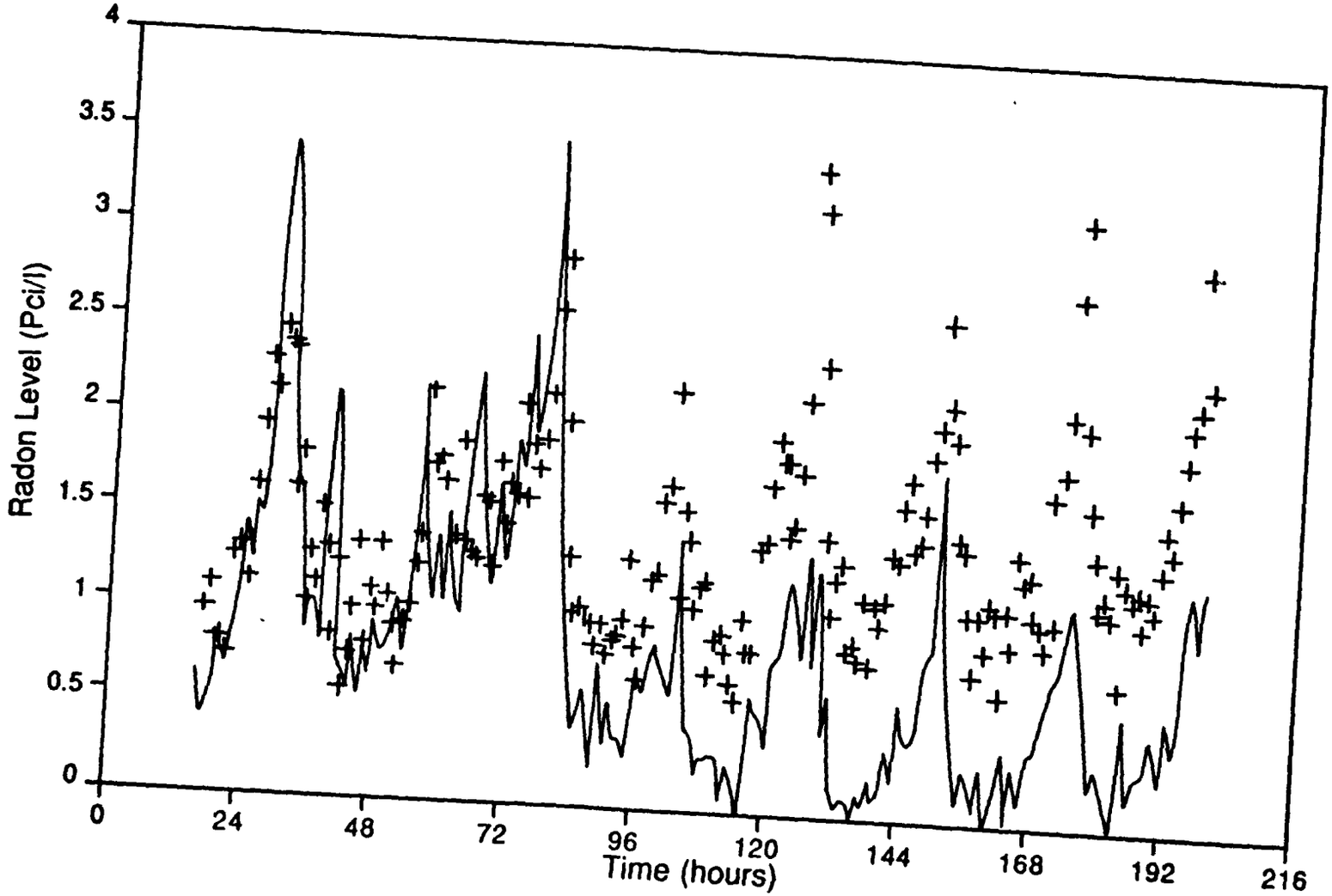

Figure 4-8. Radon Levels in Building 470, - is Electret Radon Detector, + is Commercial Detector

shown in Figure 4-5. The area-weighted integral of the efficiencies shown in this figure is about 77 percent. The slightly higher observed efficiency may be attributed to some radon progeny decaying before they reach the electret surface. In this case, slightly more than 2 alpha interactions per radon disintegration would be observed.

V - Electric Response to Fission Fragments

Introduction

Fission fragments produce electrical responses in an electret. Interaction in the air above the electret produces a large response by generating charge-carrier pairs which are collected by the electret. Interaction with the electret material itself also produces a detectable response but the signal is smaller both in size and number than simple calculations predict. The mechanism involved appears to be more complex than charge carrier pair production and collection. A mechanism is proposed which involves interaction with the charge layer itself to generate a signal having the observed characteristics. Several problems made analysis of the signal difficult.

Theory

The theory of indirect interaction of fission fragments with an electret is identical to that of indirect interaction by alpha particles. The signals from direct interaction cannot be explained by that theory. A theoretical treatment involving the intersection of the ion track with the charge layer appears to explain some aspects of the observed signal.

Indirect Interaction. Fission fragment interaction with a small air gap above an electret produces an electrical response by charge-carrier pair production and collection. The equation describing the charge collected is:

$$Q = \frac{\bar{S}Te}{W\cos(\theta)} \tag{4-1}$$

with the constraints:

$$\frac{\bar{S}Te}{W} \leq Q \leq \frac{E_{ff}e}{W} \tag{5-1}$$

which is identical to the equation for alpha particles except that the maximum

charge is related to the fission fragment energy, E_{ff}. However, with fission fragments E_{ff} may not be considered a constant. It is a distribution derived from the mass distribution shown in Figure 2-6. The value of $\bar{S}$ also varies with the mass and energy of the fission fragment. Recombination of charge-carrier pairs complicates the problem further. At the very high stopping powers of fission fragments, the charge-carrier pair concentration in the fission track is so dense that recombination becomes a very significant factor. The effect is that less charge is collected than predicted by Equation 4-1.

Direct Interaction. The electrical response of an electret to direct interaction with the electret material is detectable but does not follow the predictions of a simple charge-carrier production model. The charge intersection model is proposed to explain some of the characteristics of the fission event signal.

The charge-carrier production model is essentially identical to the model for indirect interaction. The interaction of fission fragments produces charge-carrier pairs which drift in an electric field to produce an electric signal. Equations 4-1 and 5-1 define the amount of charge in the signal. However, since the charge carriers attracted to the charge layer will not reach the back electrode, the correction factor for the effective charge must be used. A derivation of the correction factor is contained in Appendix B. Equation 4-1 is replaced by:

$$Q_e = \frac{\bar{S}er^2}{WDcos(\theta)} \tag{5-2}$$

The value used for W is the estimated maximum, 1000 eV per charge carrier pair produced.(8:2850)

An important prediction of the charge-carrier production model is the number of fission fragments that should produce a full signal. Since θ is distributed as the sine, the number of full energy signals, F, is:

$$F = \int_{\phi}^{\frac{\pi}{2}} sin(x)\, dx \tag{5-3}$$

$$F = cos(\phi) \tag{5-4}$$

with:

$$\phi = \cos^{-1}\left(\frac{s}{T}\right) \tag{5-5}$$

where D is now the depth of the charge layer. So:

$$F = \frac{s}{T} \tag{5-6}$$

For a 10 μm charge depth, about 50 percent of the fission events should produce a full signal. When the maximum value for W is used for an 80 MeV fission fragment and a 25.4 μm FEP foil, Equation 5-2 gives the resulting effective charge signal as 5×10^{-15} coul.

If the electric field in the electret is strong enough, no recombination will occur to reduce this signal. Equation 2-7 gives the electric field between the charge layer and the front surface of an electret. For a charge density of 10^{-7} Coul per cm^2 the electric field is about 3×10^5 volts/cm. The dielectric breakdown strength of FEP is about 2×10^6 volts/cm. At these field strengths recombination was not expected to be a major factor in reducing the electric signal. If no recombination occurs, the electric signal is not dependent on the electric field strength and thus is not dependent on the charge density.

The proposed alternate model of direct interaction of fission fragment with an electret is the charge intersection model. It assumes that the fission fragment track provides a conductive path into the charge region. The resulting distortion in the electric field releases trapped charges and funnels them to the electrode. The effect is as though the fission fragment intersected and collected trapped charges in an area about its path. It has been established that an ion track in electron-beam charged FEP will collect electrons from the charge layer.(2) A full derivation of the charge intersection model is contained in Appendix C. Appendix E contains a Pascal program which computes the distribution in the signal predicted by the model.

The fission fragment track may reasonably be expected to provide a conductive path. A gross estimate of the conductance of a fission fragment path is possible using a semiempirical equation for radiation-induced conductivity, Equation 2-1. This equation is for electron-beam irradiation at dose rates many orders of magnitude below that seen around a fission fragment track. Use of this equation

will establish a lower limit to the conductance of the path. The volume irradiated is assumed to be a cylindrical volume 20 μm long and of unknown radius. The irradiation time is assumed to be the fission fragment travel time: for a fission fragment energy of 80 MeV, this is about $3X10^{-12}$ sec. The stopping power, S, is assumed a constant 4 MeV/μm. From these values the conductance of the fission fragment track is estimated at $3X10^{-6}$ $Ohms^{-1}$. Although this seems small for normal applications, it is very large compared to the equivalent path in intrinsic teflon (on the order of 10^{-24} $Ohms^{-1}$) and is quite capable of conducting a useful signal. Ionization effects, not considered in the radiation-induced conductivity equation, should make the conductance significantly larger than shown, if only for a few microseconds.

The signal predicted by the charge intersection model is critically dependant on both the charge density and the depth distribution of the charge layer. In the ion interaction experiments neither was known with any accuracy and this severely handicapped the ability to make predictions using this model. One may, however, assume reasonable values of both to determine the signal distribution it predicts. With a charge density of $1X10^{-7}$ coul/cm^2 and a sawtooth depth distribution, the charge intersection model predicts signals distributed as shown in Figure 5-1. Note that the narrow charge distributions deep within the electret produce the strongest signals. However, they also produce the fewest signals. When the charge was distributed over 4 μm at an average depth of 12 μm, only 17 percent of the fission fragments produced a significant signal. Charge dispersion, particularly dispersion toward the front surface, drastically reduces the signal size while somewhat increasing the number of signals.

Experimental Procedure

The experimental device used to study the indirect interaction of fission fragments with charged FEP electrets was the same system used to study alpha particle interaction with a small volume medium. The device and associated electronics are shown in Figure 4-1. To study the direct interaction of fission fragments with the electret material, the device was modified slightly. First, the air gap was completely eliminated by vapor-depositing an aluminum electrode on the front surface of the electret, placing the electrode in direct contact with the uranium-

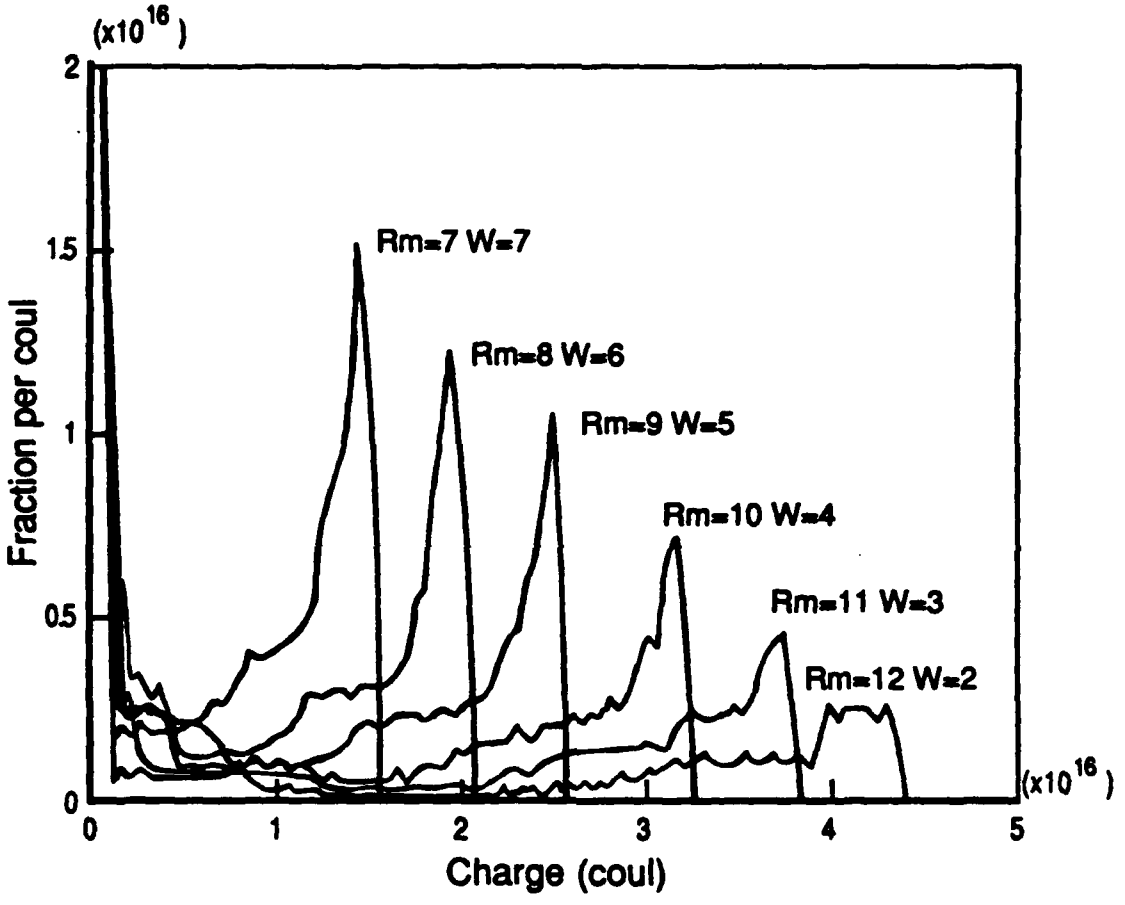

Figure 5-1. Signal Charge Distribution of Fission Fragment Interaction with 25.4 um Electron-Beam Charged FEP, as Predicted by the Charge Intersection Model. The Electret Charge is 10^{-7} coul/cm^2 having a Sawtooth Depth Distribution with Rm the Mean Depth and W the Full Width at Half Maximum

coated disk and evacuating the container to remove any residual air. Also, when a source of fission fragments was desired, the detector was placed in a thermal neutron pile to generate fission events within the uranium plating. In all other respects data collection was identical to that used in the studies of indirect alpha particle interaction using a small air volume.

Fission Fragment Source. The copper disk serving as one electrode was plated with uranium to provide a source of fission fragments. Early studies used natural and 30-percent enriched uranium. Later, uranium enriched to 97 percent ^{235}U was used. A plating solution was first produced by digesting uranium oxide powder in nitric acid, evaporating to near dryness, and redissolving in isopropyl alcohol. A small quantity of this solution was then pipetted into a plating cell consisting of a 2.8-cm diameter glass tube cemented to the center of the copper disk and filled with isopropyl alcohol. A copper electrode was suspended inside the cell 1 cm above the disk and positive biased to several hundred volts. The bias was adjusted to maintain a cell current of about 2 milliamps. After about 10 minutes plating was essentially complete. The copper disk was then recovered and the uranium concentration measured by both alpha counting in a 2π proportional counter and gamma counting using an intrinsic germanium detector. The process would plate about 3×10^{18} atoms of ^{235}U onto the disk. In the test position within the thermal neutron pile this would generate about 2.7 fissions per second.

Problems. There were several specific problems associated with the detection of direct fission fragment interaction with an electret. These included neutron interaction with the detection electronics, Paschen discharge of the electrets, and electron emissions accompanying the fission event.

In an early version of the preamplifier system, the first stage of a field effect transistor (FET) preamplifier was placed directly inside the detector to minimize capacitance noise. The signal was then conducted out of the pile via a coaxial cable for further amplification. The FET, however, proved sensitive to thermal neutrons, producing pulses having characteristics similar to the fission event pulse. A cadmium shield reduced but did not eliminate the signal. The system was replaced by a preamplifier mounted outside the pile and connected by a 1 meter

coaxial cable. This preamplifier also responded to thermal neutrons, but at acceptable noise levels. The neutron-FET noise was found to be a negative-going pulse while the fission fragment interaction produced a positive-going pulse.

Another source of noise was the fission event itself. When the uranium plate was negatively biased, a fission event was accompanied by a shower of electrons. The source of the electrons is believed to be either thermionic emission at the surface of the uranium plating or delta rays. A delta ray is an electron which has acquired significant kinetic energy from electronic interaction with an energetic ion and whose path roughly parallels the ion track. The signal could be eliminated by using only negatively biased electrets, which left the uranium plating at a positive bias.

Several other practical problems arose in the detection and measurement of the direct interaction signal. First, alpha particle and fission fragment interaction in even a tiny air space above the electret completely swamped the direct interaction signal. The detector must be evacuated. This creates the second problem. During evacuation, air pressure falls to a point where Paschen discharge ionizes the remaining air above the electret. This limits the electret surface potential to about 400 volts. The remaining potential is too small to allow observation of the direct interaction signal. Third, the electrodes must be placed as close to the electret surface as possible to produce a strong signal (see the derivation of the effective charge in Appendix B) but the increased capacitance induces additional noise in the preamplifier. Finally, at very close electrode spacing, tiny changes in the electrode spacing create significant noise.

These problems were solved by using electron-beam charged electrets with vapor-deposited aluminum electrodes on both surfaces. The surface electrodes eliminate any air gap and provide the closest possible electrode spacing. Electron-beam charging produced a charge layer deep within the foil, providing a strong internal field even though the surface electrodes carried a compensating charge that eliminated the external field. The 1000-angstrom aluminum coatings were essentially transparent to the fission fragments. This technique made possible the detection of the direct interaction signal.

Results

The interaction of a fission fragment with air above an electret produces a strong electrical signal. The direct interaction of a fission fragment with an electron-beam charged FEP electret also produces a detectable electrical signal. However, in direct interaction the fission event signal is produced by only a small percentage of the fission events and even this response decays with time. No signal is seen from uncharged electrets.

Indirect Interaction. To observe the interaction of fission fragments with a small air gap, the method used was identical to that used to observe alpha particle interaction. The only variation was that the detector was placed in the neutron pile. Figure 5-2 shows the distribution of the fission event signal using a 0.2 cm air gap. Note that the signal is about 13 times stronger than that produced by alpha particles as shown in Figure 4-3. The alpha particle signal is still present, of course, but appears only slightly above the lower level discriminator. This indicates that, ignoring problems with recombination, the stopping power of fission fragments in air is 13 times the stopping power of 4.5 MeV alpha particles, or about 18 MeV per cm.

Direct Interaction. In direct interaction experiments, the fission fragment was found to produce a conductive path through FEP. An electret having an aluminized front surface was charged with the front surface floating. The front surface retained a potential of about 200 volts. This was covered with a layer of aluminum-backed 12.7 μm FEP foil and placed in the detection system. Fission fragments penetrating the front foil produced very large multiple pulse signals. This phenomenon disappeared after about 3 minutes. The fission fragment track through the front foil provided a temporary conductive path to discharge the aluminum on the front surface of the electret. The signal disappeared when the aluminum lost its charge. This demonstrates that the fission fragment track through FEP is a temporary conductive path capable of transporting a significant signal.

Fission fragments interacting with an electron-beam charged FEP electret induce charge carrier transport. This is detectable as an effective charge appearing at the surface electrodes. Figure 5-3 shows the distribution in the effective charge

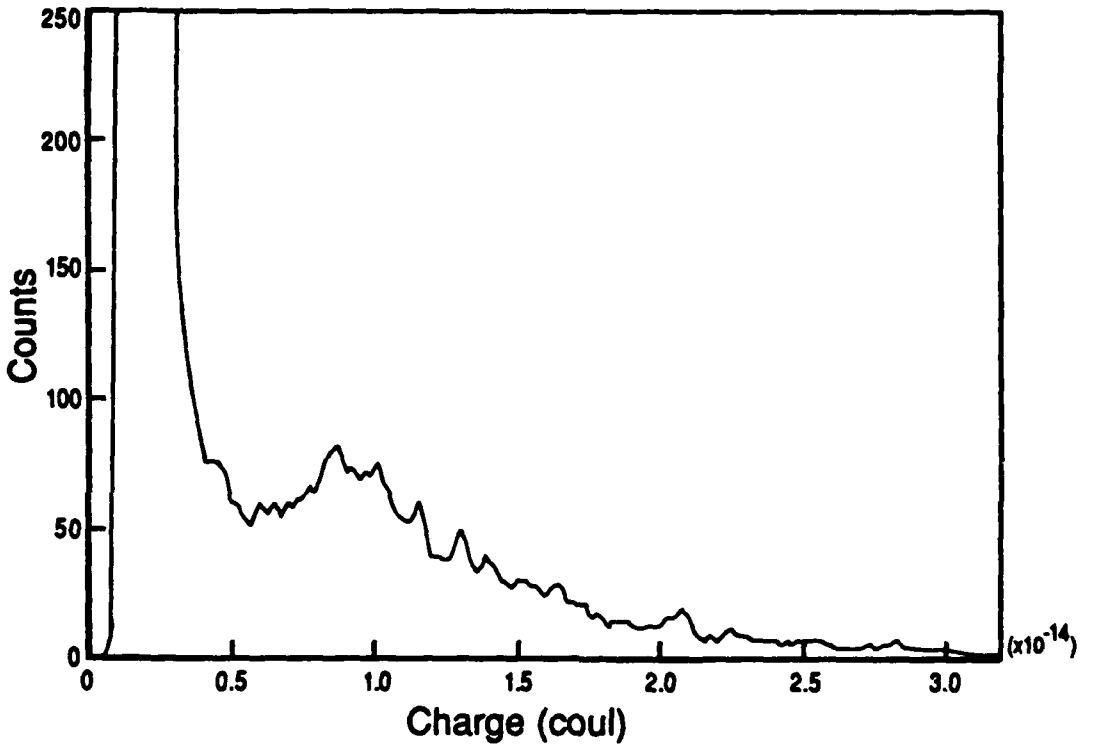

Figure 5-2. The Charge Distribution from Fission Fragment Interaction in a 0.2 cm Air Gap above Electron-beam Charged FEP

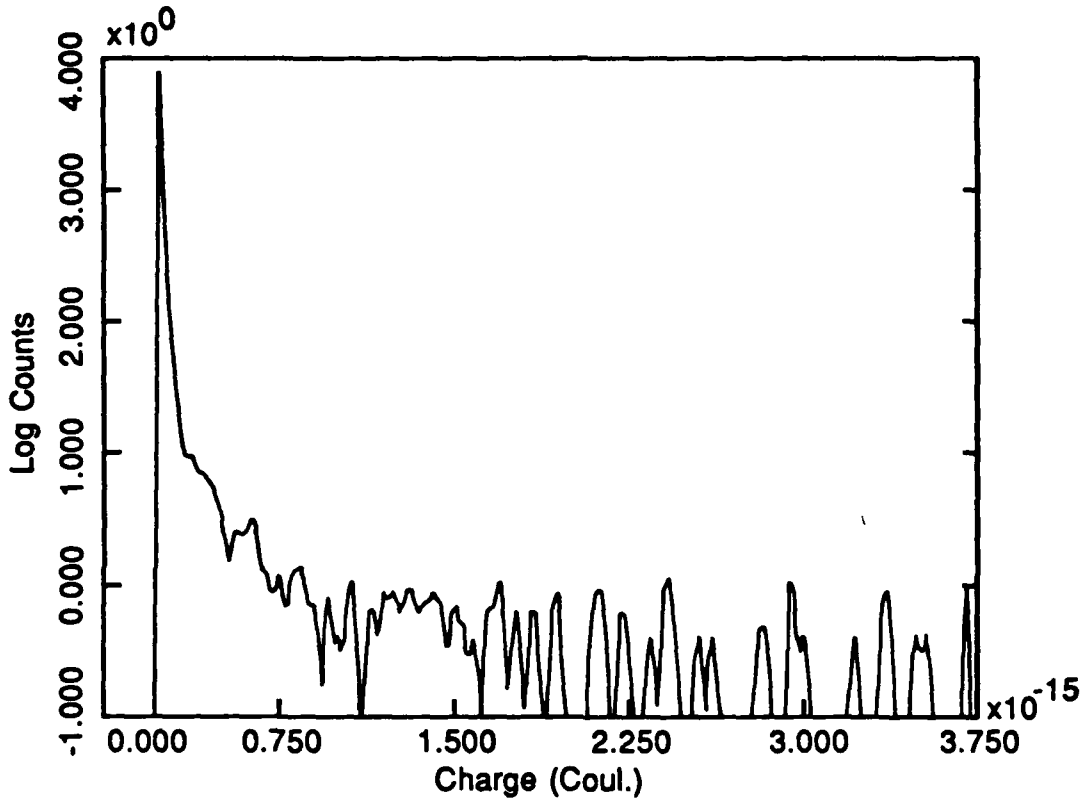

Figure 5-3. The Charge Distribution of the Fission Event Signal in Electron-beam Charged FEP

from the fission event signal in an electret charged to 1×10^{-7} coul/cm^2 at 40 keV. It is important to note that less than 1 percent of the expected fission events appear as counts in this distribution, taken over a 3 hour period. Note also that there is no apparent structure or clear maximum signal. Much of the signal is of low charge, blending into the noise level at about 3×10^{-16} coul.

The fission fragment signal decays with time. Over a period of days, the number of pulses recorded above background decreases. Figure 5-4 shows how the number of pulses having an effective charge greater than 3×10^{-16} coul decreases over a 25 hour period. An exponential fit to this data gives a decay constant of about 10.5 hours. This data provides some quantification to the observed phenomenon that the electrets no longer respond significantly to fission fragments after a few days. An interesting aspect to this data is the initially low count rate which increases abruptly. This characteristic is seen in much of the other long-term counting data but remains unexplained. The unusually high count rates at about 17 hours is believed due to mechanical noise.

Uncharged FEP does not produce the fission event signal even when externally biased. An uncharged FEP foil was placed in the detector and a - 1000 volt bias provided by an external high voltage power supply. No fission event signal was seen when the detector was placed in the neutron pile.

Discussion

Because of the nonuniform charge distribution in the electrets, and the transient nature of the fission event signal, very few hard conclusions may be drawn concerning the fission event signal. What is clear is that it does not follow a simple ion chamber model. The suggested charge intersection model appears to explain some of the results.

According to the charge carrier production model, about 50 percent of the fission events should produce 5×10^{-15} coul signals. This is clearly not observed. Both the number and size of the signals are at least an order of magnitude lower. But the fundamental characteristics of ion interaction with matter make it difficult to reject the idea that charge-carrier pairs are being produced and collected. It seems likely that in spite of the strong electric field recombination plays

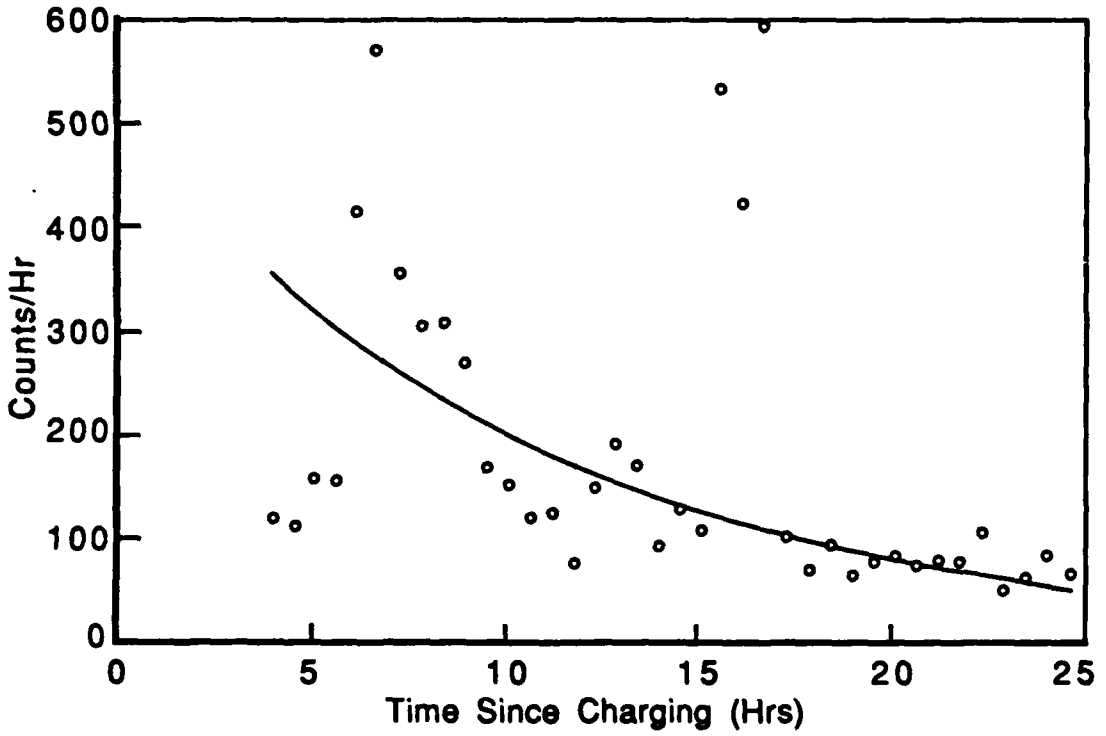

Figure 5-4. The Time Decay of the Fission Event Signal in Electron-beam Charged FEP, Line is Exponential Least Squares Fit

a very large part in the fission fragment interaction process. The extremely large stopping power of fission fragments in FEP indicates that a very high charge pair density is involved. The high charge pair density makes recombination much more likely. The signal, resulting from charge carriers that avoid recombination, may be lost in the electronic noise. This would explain the absence of these signals and the absence of signals in the biased but uncharged FEP. It would not explain the number and charge distribution of the observed signals.

The charge intersection model predicts that only a small number of fission events will produce a detectable signal. It further predicts that signals of the size observed would be produced at the charge densities and charge depths achieved in the electrets used. However, the characteristic signal distribution predicted by the model was not observed. This may be due to the very poor spatial uniformity in the charge densities achieved in the electrets. As shown in Table 3-1, charge densities varied by about 50 percent over the surface of the electret. Since the charge intersection model predicts a nearly cubic dependance on the charge density, this variation would have a profound effect on the distribution of the observed signal.

The variance in the fission event signal with time is also explainable using the charge intersection model. Migration of the charge layer reduces both the peak charge density and the average depth. As shown in Figure 5-1 these are predicted to reduce the size of the fission event signal but to increase the number of signals. Initially the very deep and narrow charge layer produces a few very strong signals. The number increases as the charge layer spreads toward the front surface and more fission fragments reach its depth. As the charge layer spreads further, the signal size falls below the noise level and the number of recorded signals diminishes. It is probably stretching the charge intersection model beyond its limits to suggest that this fully explains the time characteristics of the fission event signal. It does not explain the relatively sharp increase in the count rate a few hours after charging.

It should not be construed that the charge intersection model is proposed as the precise mechanism producing the fission event signal. There is simply insufficient evidence to reach that conclusion. No doubt other factors are involved. What is suggested is that a model which involves direct interaction

with the charge layer provides a better explanation of the phenomenon than simple charge carrier production and collection. A more accurate model must await experiments with electrets whose charge distribution is precisely known. The process would be further simplified through the use of monodirectional, monoenergetic ions such as those from a particle accelerator.

Applications

An original motivation for this investigation was the possibility of designing a thermal neutron detector that employed the fission event signal from direct interaction with an electret. Unfortunately, the observed signals are much smaller and fewer than originally expected. They are far too small and too few to make such a device practical. Acoustic and electronic noise would overwhelm the signal. Further, the fairly rapid decay in the signal would make calibration impossible.

The charge intersection model does offer some hope that the signal strength can be improved. The charge densities achieved in these experiments were 5-10 times less than the theoretical maximum for FEP. Since the model predicts a cubic dependance on charge density, a signal 100-1000 times stronger than observed may be a possibility. There may also be more subtle ways of incorporating the uranium in the FEP that would significantly improve sensitivity. A practical neutron detector that uses this phenomenon must await further research.

VI - Pulsed Luminescence in FEP

Introduction

The discharge of an electron-beam charged FEP electret is accompanied by an emission of light. The thermal luminescence spectrum of this material shows a striking similarity to its thermally stimulated current spectrum. The source of the luminescence is unknown but may be caused by electron-hole recombination.

Interaction by both alpha particles and fission fragments stimulates photon emission. However, over a period of several hours the electrets become insensitive to ion interaction.

Theory

Luminescence from electron-beam charged FEP has been observed by other researchers.(27:115) They saw flashes of light as an electret was brought up to atmospheric pressure after charging. The source of the phenomenon remains unknown.(36) An analysis of the energies associated with various processes in the electret, and the associated wavelengths, should be useful in determining the source of the luminescence.

Luminescence occurs when an electron falls from a high energy state to a lower energy, releasing the energy difference as a photon. The energy, E, of the photon is related to its wavelength, λ, by Planck's constant, h, and the speed of light, c:

$$E = \frac{hc}{\lambda} \tag{6-1}$$

Thus, the wavelength of the emitted light is determined by the amount of energy in the photon. The energy is provided by the energy drop the electron experiences. The electron's energy is distributed between the photon and internal kinetic processes. Thus λ is the shortest frequency photon that can be emitted by

an electron energy loss of E.

Inside an electret, two types of electron energy losses are possible sources of the luminescence; trapping and recombination. A 'hole', an unfilled electron position in the valence band of the medium, will also experience these types of energy losses. The clear energy differences between trapping and recombination may distinguish between the two as possible sources of the observed luminescence.

In trapping, the electron enters a localized region of lower electrical potential from which it cannot escape without an energy input. Such traps are caused by electronegative impurities, atomic vacancies in the medium's molecular structure, or distortions in the medium's molecular structure.(14:10) It is these traps which make surface and volume charged electrets possible by capturing injected electrons. When an electron drifting in the conduction band enters a trap, it loses energy, some of which may be emitted as a photon. The remaining energy goes into thermal processes. Thus, the minimum possible wavelength of the photon corresponds to the depth of the trap. In FEP, trap depths are about 1.8 eV for electrons and 0.7 and 1.0 eV for holes. These energies correspond to wavelengths of 690, 1770 and 1240 nm, respectively.

Recombination occurs when an electron encounters a hole. Unlike the trap, where the electron retains its identity and charge, recombination results in the elimination of both the free electron and the hole. The electron falls from the conduction band to the valance band so the energy involved is the band gap of the medium, 4 - 6 eV.(14:9) This corresponds to a minimum wavelength of 310 - 206 nm.

Detection of any internal photon emission requires that the medium be transparent and the detector sensitive at the emission wavelength. The photo transmittance of FEP is about 94 percent at wavelengths from 350 up to 3500 nm.(33:15) Further, the visible spectrum is about 400 to 700 nm and the phototube used in the pulse detection experiments operates efficiently from about 320 to 650 nm. None of the trapping processes would produce photons detectable by eye or by the phototube. Only the photon emissions from recombination should be detectable.

Experimental Procedure

Luminescence in electron-beam charged FEP was demonstrated using both thermal stimulation and stimulation by energetic ions. In every case uncharged FEP, surface charged FEP, and beta particle irradiated FEP showed no such response.

For the luminescence experiments, samples of uncoated 25.4 μm FEP film were mounted on ring carriers. They were then charged at between 2×10^{-8} and 10×10^{-8} Amps per cm^2 using the electron beam system described in Chapter III. Charge densities were calculated at about 3×10^{-7} coul per cm^2. After about 30 minutes annealing in vacuum, the samples were removed and tested.

Thermally-Stimulated Luminescence. The simplest qualitative test for thermally-stimulated luminescence was visual observation. In a darkened room, a freshly charged sample was placed in a glass petri dish on a hot plate and observed. As the sample was heated, a faint glow became visible to dark-accustomed eyes. The glow appeared to have a slightly greenish tint, although the impression of color is questionable because the human eye is a poor detector of color at low light intensities.

A more quantitative analysis of thermally stimulated luminescence employed a Harshaw 2080 thermoluminescence analyzer. Portions of the charged FEP sample, 0.635 cm in diameter, were cut from a charged sample using a paper punch. The portions were mounted on the thermoluminescence analyzer's heating filament and covered with a glass cover slip to prevent curling. The portions were then heated to 270° C at 1° C per second. Luminescence was monitored using a photomultiplier tube, biased to 1100 volts, whose current output was recorded as a function of time. The result is a thermal luminescence spectrum indicating relative light output as a function of temperature.

Ion Stimulated Luminescence. Pulse luminescence, induced by energetic ions, was also investigated. The detection system consisted of a photomultiplier tube and an electronic system essentially identical to that used to measure the electrical response to energetic ions. An electron-beam charged FEP foil sample, mounted on a ring carrier, was covered with a uranium-coated copper disk and mounted on the window of an RCA 6342 photomultiplier tube. The tube was

biased to 1100 volts. Output from the tube went to an Ortec 113 charge sensitive preamplifier and then to the same linear amplifier-multichannel analyzer-recorder system used in the electronic response experiments. When a neutron flux was needed, the photomultiplier tube assembly was placed directly in front of the open door of the thermal neutron pile.

Results

Electron-beam charged FEP responds with photon emissions to both thermally stimulated discharge and discharge by energetic ions. Under certain conditions, the luminescence is visible to the naked eye. Further, the light response decays over a period of days.

Thermally Stimulated Luminescence. The controlled heating of portions of charged FEP samples produced a distinctive thermal luminescence spectrum. Two spectra are shown in Figure 6-1. One was taken from a sample only about 1 hour after charging. The other was taken about 24 hours later. The data were smoothed using a three-channel moving average. Note that there is a broad low-temperature peak at about 65° C, which cuts off fairly sharply at about 80° C. The data generating this peak contains some very large channel-to-channel variations. This would indicate pulsed light emissions, rather than a continuous, even glow. A high temperature peak is also present at about 170° C. There are significant differences between the spectrum from a freshly-charged electret and one stored at room temperature for 24 hours after charging. Note that there is an order of magnitude reduction in the low temperature peak for the aged sample. This change is accompanied by a significant increase in the high temperature peak.

Ion Stimulated Luminescence. Pulsed luminescence was observed when samples were irradiated by alpha particles or fission fragments. Freshly-charged electrets were particularly active but decayed over a period of hours. However, even freshly-charged samples did not produce one detectable photopulse per ion interaction. There was no luminescence detected from uncharged FEP, surface charged FEP, or beta particle irradiated FEP.

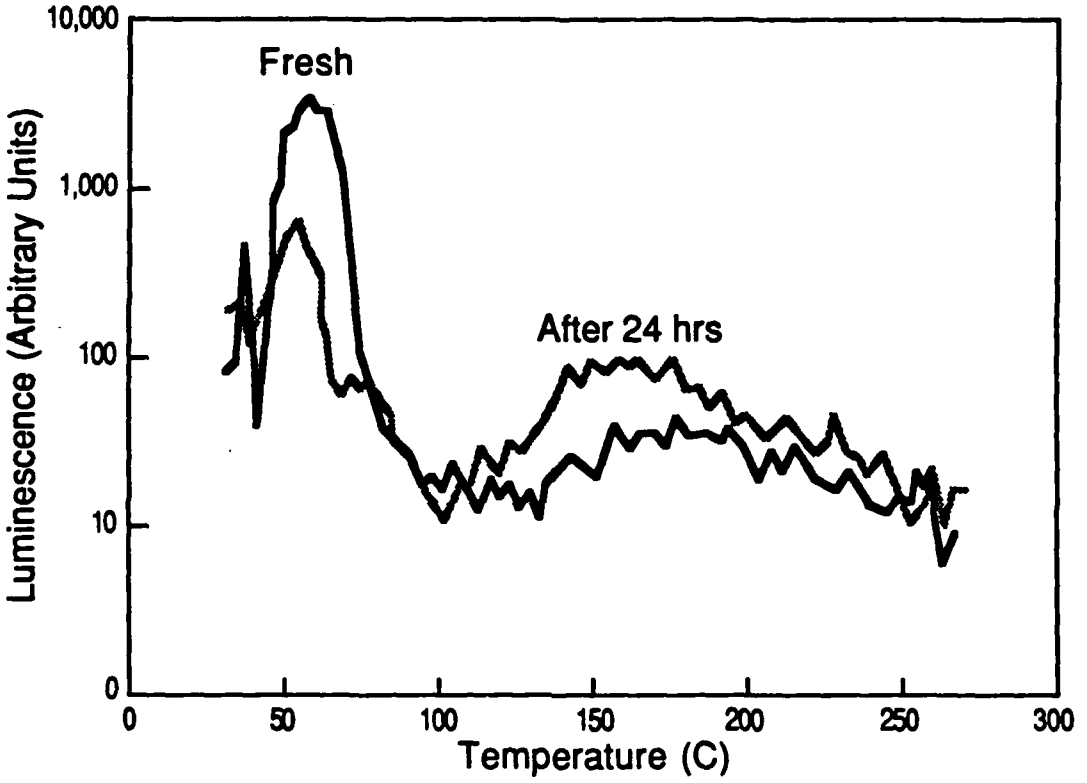

Figure 6-1. Thermoluminescence Spectra of Electron-beam Charged FEP

Pulsed luminescence was detected in electron-beam charged FEP electrets. Both spontaneous and ion induced pulses were observed. Figure 6-2 shows how the rate of light pulses changes over time. It is a record of the pulse rate over a 50 hour period under various conditions. Initially the sample was covered with a blank copper disk and emitted spontaneous pulses. These pulses decayed away over about 10 hours. After 20 hours the blank disk was replaced by a uranium-coated copper disk and the assembly placed in a neutron flux. The pulse rate increased sharply, then began to decay. After 1 more hour the neutron flux was removed, but no change in the pulse rate or the rate of decay was observed. At 25 hours the blank disk was reinstalled and the count rate fell, but not to the original background rate. Restoration of the uranium at 27 hours appeared to restore the higher count rate but the decay appeared to have continued in the absence of the uranium. At 45 hours the pulse rate had decayed to less than 10 counts per hour and the neutron flux was restored. The count rate then increased perceptibly.

Freshly charged FEP emits spontaneous photopulses at a rate which decays with a time constant of about 1 hour. The presence of the uranium stimulates additional photopulses, and this rate decays with a time constant of about 2 hours. The presence of the neutron flux appears to have no effect on either the count rate or its decay. Removal of the uranium reduces the pulse rate, but the decay appears to continue in the absence of the uranium. Finally, at very low count rates, the presence of neutron-induced fission events appears to increase the count rate perceptibly.

Discussion

The source of the luminescence from electron-beam charged FEP cannot be determined solely from the available data. However, the data does suggest that electron-hole recombination is a potential source and that trap-modulated hole transport is not the source. A frequency spectrum of the light would be a significant help in determining the exact source.

Photon emissions from electron-beam charged FEP appear to be closely tied to electrical discharge of the electret. The thermal luminescence spectrum

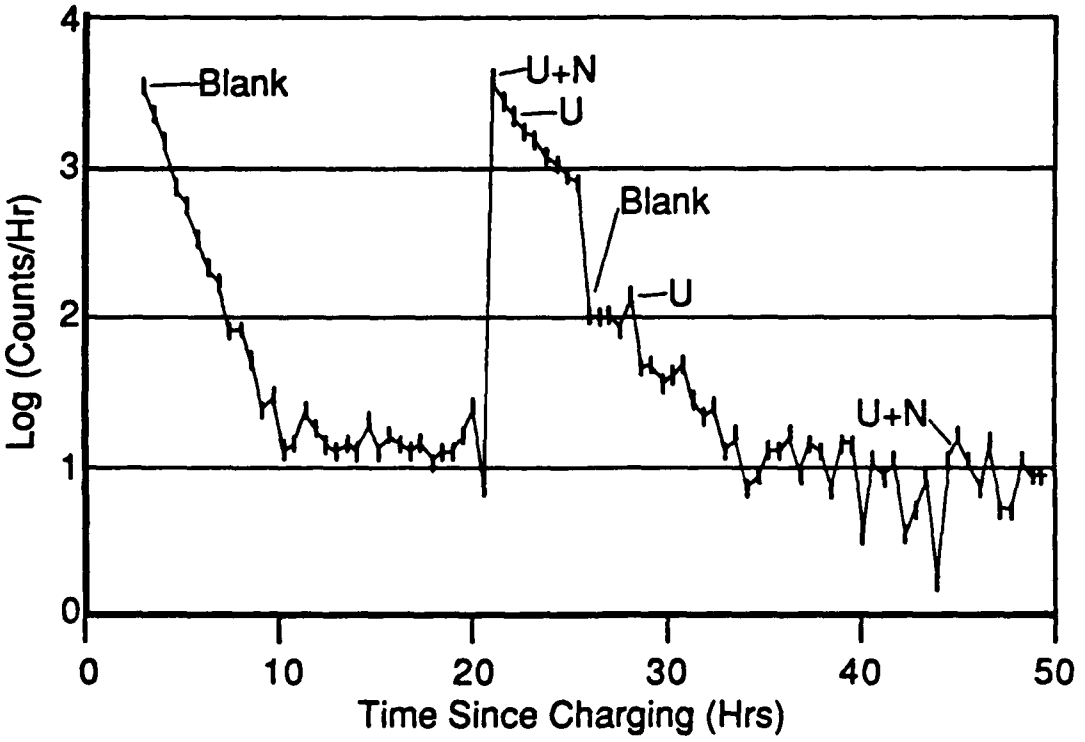

Figure 6-2. Photopulse Emission Rates in Electron-beam Charged FEP. U Indicates ^{235}U Present, N Indicates Neutron Flux Present

resembles the thermally stimulated current spectrum reported by other researchers.(11) Like electrical discharge, luminescence may be either spontaneous or induced by energetic ions. Analysis of the wavelengths of the possible photon sources suggests that electron recombination with holes is the likely source of the luminescence. The signal decay data supports this assertion.

The two peaks in the thermal luminescence spectrum correspond fairly closely to the two peaks observed in the thermally stimulated current spectrum.(29:3329) The differences between the light and current spectra may be due to the different heating rates, $1^{\circ}\ C$ per sec vice $1^{\circ}\ C$ per min. The similarity strongly suggests that the observed luminescence is associated with charge drift within the electret. Both processes suspected as the source of the luminescence, trapping and recombination, act on drifting charges.

Analysis of the trap and recombination energies suggests that only recombination is energetic enough to produce photons visible to the eye and to the photomultiplier tube used in the experiments. Particularly deep electron trapping may be marginally energetic enough to be observed, if no energy is lost to vibration of the molecular structure. Hole trapping does not involve sufficient energies to be observed.

The observation of spontaneous photon emissions and their fairly rapid decay also suggest that retrapping is the source of the phenomenon. The trapping rate is determined by the trap density while the recombination rate is determined by the hole density. The trap density in electron-beam charged FEP does not change under normal conditions while the hole density falls rapidly with aging. Because hole traps are shallow, hole mobility is an order of magnitude greater than electron mobility. Holes produced in the irradiated region by the electron beam migrate to the charge region and recombine. This process would produce spontaneous recombination that decays with time as the hole density decreases.

The observation of ion-induced photon emissions and their decay may also be accounted for by the recombination process. Ion interaction frees trapped charges in the charge region. They subsequently drift into the irradiated region and either recombine or become trapped. The hole density determines the recombination rate but the hole density continually decays. This would explain the increase in

luminescence with the onset of ion irradiation and the continued decay.

One aspect of the pulsed luminescence rate data not explained by a recombination process is an apparent elevation of the spontaneous pulse rate when the ion irradiation was discontinued. One would expect it to fall to or below the level reached before irradiation. If the ion irradiation were contributing holes, the pulse rate would not decay. This aspect of the data remains unexplained.

The data presented cannot confirm that recombination is the mechanism producing photon emissions from electron-beam charged FEP. A recombination theory does explain some aspects of the data but does not explain others. Additional data is needed, in particular a frequency spectrum of the light. A frequency spectrum would give the energy or energies of the process emitting the light. Unfortunately, because the signal is so faint and fleeting, such data may be difficult to obtain.

VII - Conclusions and Recommendations

This investigation into the interaction of energetic ions with electrets has established that detectable, and useful, signals of various types occur. Indirect interaction of the ions (interaction with air above the electret) yielded a signal that may have practical applications. In the case of direct interaction with the electret medium itself, the resulting electrical signal is much smaller than was originally expected. The luminescence signal from electron-beam charged FEP may prove particularly useful to the investigation of charge transport processes in dielectrics. Further research in all three areas is recommended.

Indirect Ion Interaction

When ions interact in an air space above an electret, the electrical signal results from the production of charge-carrier pairs in the air, followed by charge separation and collection by the electret's electric field. The mechanism is identical to that of the ion chamber used in radiation detection and dosimetry. Two potentially useful devices making use of this signal were tested; a thermal neutron detector and an environmental radon detector. Prototypes of both devices operated successfully. These devices should be investigated further with a view to producing practical radiation monitors.

The radon detector has already demonstrated its ability to measure environmental levels of radon. However, it was very sensitive to acoustic noise and it lost counting efficiency after several days of operation. Either problem would make the device impractical as a radon monitor. The inclusion of a moisture barrier at the air entry may help to stabilize the electret charge, and thus stabilize its counting efficiency. Acoustic damping or an acoustic signal anticoincidence system should eliminate its noise sensitivity. In general, the design of the detector is far from optimum and much improvement is possible. The potential of this detector as an environmental radon monitor is worthy of additional effort.

Fission Fragment Interaction

The direct interaction of energetic ions, especially fission fragments, with the electret medium itself also produces a detectable electric signal. However, the signal is much weaker and less frequent than predicted by the charge-carrier production model used for ion chambers. The charge intersection model was developed which may explain many of the observations. The model could not be verified by this research, principally because sufficient uniformity in the charge region of the electrets could not be achieved. Additional work in this area should focus on producing a verified model of the charge interaction process. A practical application must await a better understanding of the phenomenon.

Uniformity of charge density in an electret depends on a uniform distribution in the electron beam current used to charge the electret. A uniform distribution cannot be achieved by spreading the beam with focusing rings. The inherent nonuniformities in the emission filament are retained through the focusing process. Beam scanning by means of X-Y deflection lenses is the only method which has thus far achieved good spatial charge distribution in electrets.

The electron beam system used in this study lacked X-Y scanning capability and adding the capability would prove extremely difficult. A better approach would be to modify an electron microscope. The microscope already has an X-Y deflection system, an adjustable mounting stage, a high quality vacuum system and even imaging capability. The only modification needed would be to adjust the electron gun to reduce its output by about two orders of magnitude. This would probably require modification of the filament and the filament current controls. Once converted, the system would produce electron-beam charged electrets of excellent spatial charge distribution with good reproducibility.

Another major problem with identifying the source of the fission fragment signal was the lack of directional control of the fission fragments. I propose the construction of a fission fragment gun system to provide a collimated beam of energetic heavy ions outside the neutron pile. It would consist simply of an evacuated tube with a plating of ^{235}U at one end and a vacuum adaptor and gate valve at the other. The end containing uranium could be placed in the pile and an experimental device attached to the other end. When the valve was opened,

fission fragments would enter the experimental device. Although the fission fragment flux would be quite low, it would be strongly directional and there would be no interference from neutron interaction with the detection electronics. There would be a stream of alpha particles accompanying the fission fragments.

Luminescence from Electron-Beam Charged FEP

The luminescence resulting from the discharge of electron-beam charged FEP is a very poorly understood phenomena. Although a mechanism for producing the signal was suggested, there is little solid evidence to support it. The similarities between the thermal luminescence spectrum and the thermally stimulated current spectrum do strongly suggest that the luminescence is associated with charge drift. The energy available from electron and hole trapping processes appears to be insufficient to produce detectable emissions. Very little else is known.

The luminescence clearly warrants further investigation. The most useful data to be obtained would be a frequency spectrum of the photon emission. The frequency will indicate the energy associated with the phenomenon. If the spectrum extends into the infrared, even the photon emissions from trapping processes may be observable. A frequency spectrum would offer significant insight into the mechanisms of charge transport, trapping and recombination in FEP electrets.

The luminescence is both weak and transient, creating some problems in collecting a frequency spectrum. A qualitative view of the spectrum may be achievable using a diffraction grating and broad spectrum photographic film. Such a method would show up any sharply defined emission frequency and give the general pattern of the spectrum. A more quantitative method would use a scanning spectrophotometer. However, these systems are fairly slow relative to the life of the thermal emission. Repeated charging and thermal discharge of a single sample may be necessary to generate a useful spectrum.

The electron beam system used in these studies may prove useful in repeatedly charging and discharging an electret. It has an optical window through which a sample could be viewed immediately after charging. The spontaneous photon emissions could be recorded on a spectrophotometer to produce a spectrum. Recording the thermally stimulated luminescence would require a heating

element within the vacuum chamber. In either case, repeatedly charging and discharging the sample would eventually allow collection of a useful signal.

APPENDIX A

Average Signal Produced in a Small Cylindrical Medium

Let us assume a cylindrical medium of height T and radius R, with the ion source evenly distributed over the base, as shown in Figure A-1. Both T and R are less than the track length. We want the average charge, $\bar{Q}$, generated by a heavy ion interaction. We assume that both the stopping power, $\bar{S}$, and the average energy required to produce a charge carrier pair, W, are constant.

By Equation 4-1, the charge, Q, produced by an emission at the center of the source and emitted at angle θ from normal is:

$$Q = \frac{\bar{S}Te}{W\cos(\theta)} \; ; \; 0 \leq \theta \leq \theta_m \tag{A-1}$$

$$Q = \frac{\bar{S}Re}{W\sin(\theta)} \; ; \; \theta_m \leq \theta \leq \frac{\pi}{2} \tag{A-2}$$

where:

$$\theta_m = \tan^{-1}\left(\frac{R}{T}\right) \tag{A-3}$$

To find the average value of Q, we integrate all values of Q resulting from the distribution of possible ion tracks over 0 to $\pi/2$ and divide by all possible tracks:

$$\bar{Q} = \frac{\frac{\bar{S}eT}{W}\int_0^{\theta_m}\frac{\sin(\theta)}{\cos(\theta)}\,d\theta + \frac{\bar{S}eR}{W}\int_{\theta_m}^{\frac{\pi}{2}} d\theta}{\int_0^{\frac{\pi}{2}}\sin(\theta)\,d\theta}$$

$$\bar{Q} = \frac{\bar{S}e}{W}\left[T\int_0^{\theta_m}\cot(\theta)\,d\theta + R\left(\frac{\pi}{2} - \theta_m\right)\right]$$

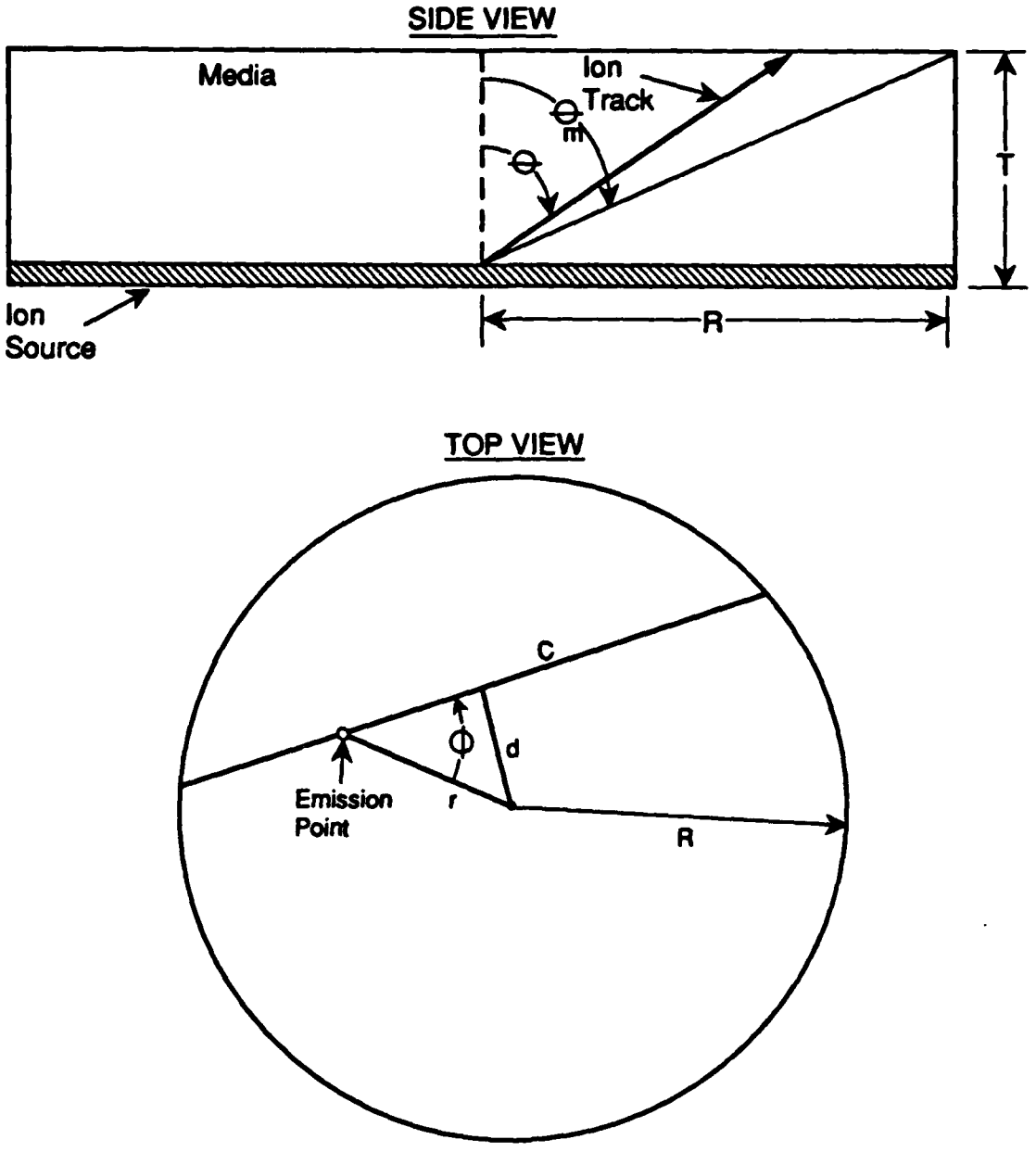

A-1. Diagram of Ion Interaction in a Small Volume Medium

$$\bar{Q} = \frac{\bar{S}e}{W}\left[-T\ ln(cos(\theta_m)) + R\left[\frac{\pi}{2} - \theta_m\right]\right]$$

$$\bar{Q} = \frac{\bar{S}e}{W}\left[T\ \ln\left[\frac{\sqrt{R^2+L^2}}{L}\right] + R\ \tan^{-1}\left[\frac{L}{R}\right]\right] \qquad \text{(A-4)}$$

The value of R is the radius of the cylinder for a particle emitted at the center. For off-center emissions, it is actually the distance to the edge of the cylinder in the direction the particle is traveling. We therefore need the expected distance to the edge of a disk from an arbitrary point within and moving in an arbitrarily chosen direction. Both position and direction of the emission are random but an average value is computable. We begin by using Figure A-1 and noting that chord C_h is the sum of the distances to the wall taken at point r in direction angle ϕ and $\phi+\pi$. This distance is:

$$C_h = 2\sqrt{R^2 - D^2} = 2\sqrt{R^2 - r^2\sin^2(\phi)} \qquad \text{(A-5)}$$

To determine the average, we integrate C_h over all points on the disk and from 0 to π angles. Normalization requires that we divide by all possible points and angles. Thus our mean distance, $\bar{R}$ is:

$$\bar{R} = \frac{\int_0^R 2\pi r\left[\int_0^\pi 2\sqrt{R^2 - r^2\sin^2(\phi)}\ d\phi\right]dr}{\int_0^R 2\pi r\left[\int_0^{2\pi} d\phi\right]dr} \qquad \text{(a-6)}$$

We may evaluate the denominator readily:

$$\bar{R} = \frac{\int_0^R 2\pi r\left[\int_0^\pi 2\sqrt{R^2 - r^2\sin^2(\phi)}\ d\phi\right]dr}{2\pi^2R^2} \qquad \text{(A-7)}$$

The integral on ϕ in the numerator has no general solution. However, it may be converted to a definite integral form that has an infinite series solution:

$$\bar{R} = \frac{8\pi R\int_0^R r\left[\int_0^{\frac{\pi}{2}}\left[1 - \left[\frac{r}{R}\right]^2\sin^2(\phi)\right]^{\frac{1}{2}} d\phi\right]dr}{2\pi^2R^2} \qquad \text{(A-8)}$$

We now let $p = r/R$ and change variables, dividing out terms:

$$\bar{R} = \frac{4R}{\pi} \int_0^1 p \left[\int_0^{\frac{\pi}{2}} \sqrt{1 - p^2 \sin^2(\phi)}\, d\phi \right] dp \qquad \text{(A-9)}$$

The integral on ϕ is substituted with an infinite series:

$$\bar{R} = \frac{4R}{\pi} \int_0^1 p \left[\frac{\pi}{2} \left[1 - \frac{1}{2 \cdot 2} p^2 - \frac{3 \cdot 3}{2 \cdot 2 \cdot 4 \cdot 4} \frac{p^4}{3} - \frac{3 \cdot 3 \cdot 5}{2 \cdot 2 \cdot 4 \cdot 4 \cdot 6 \cdot 6} \frac{p^6}{5} - \ldots \right] \right] dp \qquad \text{(A-10)}$$

This integral is a simple polynomial (although of infinitely many terms) with constant coefficients. It solves to:

$$\bar{R} = 2R \left[\frac{1}{2} - \frac{1}{2 \cdot 2 \cdot 4} - \frac{3}{2 \cdot 2 \cdot 4 \cdot 4 \cdot 6} - \frac{3 \cdot 3 \cdot 5}{2 \cdot 2 \cdot 4 \cdot 4 \cdot 6 \cdot 6 \cdot 8} - \ldots \right] \qquad \text{(A-11)}$$

We now note that the average distance to the wall divided by the radius is a constant, as might have been expected. Evaluating the first four terms of the series, we get:

$$\frac{\bar{R}}{R} = 1 - 0.125 - 0.015625 - 0.0048828 - \cdots \qquad \text{(A-12)}$$

The physical constraints of the problem require that $\bar{R}$ be greater than zero. Therefore, this series must converge to a value greater than zero. The remainder theorem requires that the sum of the unevaluated terms be greater than -0.0071 and less than zero. We may now state that:

$$\frac{\bar{R}}{R} = 0.85 \qquad \text{(A-13)}$$

with accuracy to two decimals. This is certainly adequate for radiation path length estimates. Additional accuracy may be gained by evaluating additional terms. Our final solution is:

$$\bar{Q} = \frac{\bar{S}e}{W} \left[T \ln \left(\frac{\sqrt{(0.85R)^2 + L^2}}{L} \right) + 0.85R \tan^{-1} \left(\frac{L}{0.85R} \right) \right] \qquad \text{(A-14)}$$

The separate determination of the averages in Equations A-4 and A-6 assumes that they are fully independent variables. This is not strictly true as θ_m is dependent on R. The result of the assumption is the introduction of second order errors in the estimate. These errors are expected to be smaller than those introduced by the assumptions of constant S and W. This estimate should be useful in determining the rate of generation of compensating charge in an irradiated air gap.

APPENDIX B

The Effective Charge Equation

When a charge moves within the plates of a shorted capacitor, it causes an effective charge to pass through the shorting wire. The size of the effective charge is determined by both the size of the internal charge and the distance it travels. The effective charge is the result of a combination of inductive and conductive currents within the capacitor. By considering both types of current, we may derive the relationship between the effective charge and the internal charge.

Consider a parallel plate capacitor of area A_c and thickness D, as shown in Figure B-1. Within the capacitor, a charge q moves distance s normal to the capacitor plates. We want to determine the effective charge Q_e seen at the capacitor plates. We first divide the capacitor into three capacitors of identical area and of thicknesses D_1, s, and D_3. They are connected in series and carry voltages V_1, V_2 and V_3. The capacitor series is shorted and the charge Q through the shorting wire may be measured. We temporarily short the center capacitor to let charge q pass between its plates. We now derive the relationship between q and Q.

The charge contributed by a conductive current is simply q. To determine the charge contributed by inductive currents, we note that, by definition:

$$Q = \int i \, dt \tag{B-1}$$

where i is current. The inductive current is:

$$i = C\frac{dV}{dt} \tag{B-2}$$

so the charge contribution is:

$$Q = C \, \Delta V \tag{B-3}$$

From Kirchhoff's Current Rule we know that the total current (the sum of the inductive and conductive currents) through each capacitor must be the same. The

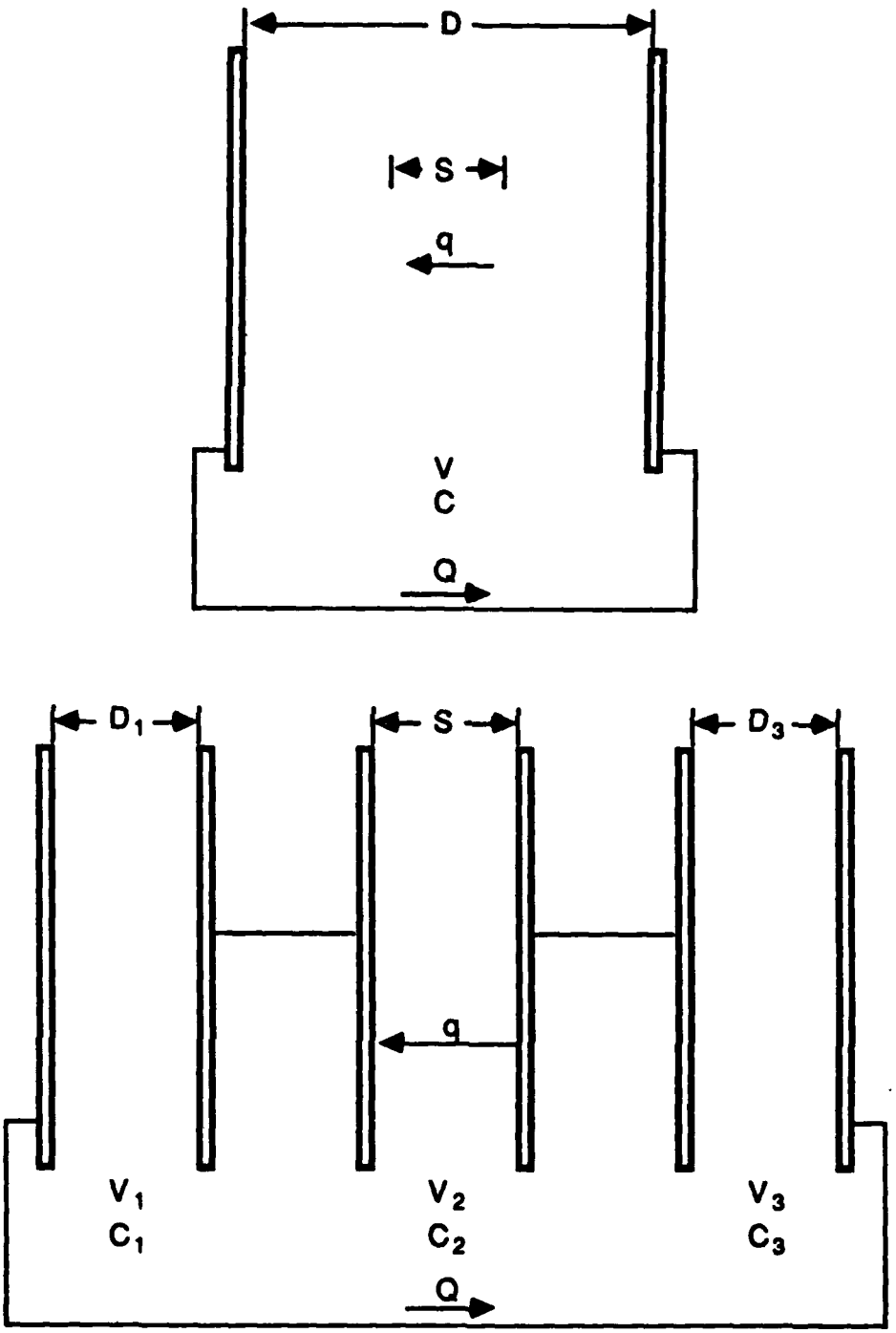

B-1. Diagram of Charge Transport in a Capacitor, V is Voltage, C is Capacitance

effective charge must also be the same. Thus, in each capacitor:

$$Q = C_1 \Delta V_1 \tag{B-4}$$

$$Q = C_2 \Delta V_2 + q \tag{B-5}$$

$$Q = C_3 \Delta V_3 \tag{B-6}$$

By Kirchhoff's Voltage Rule:

$$V_1 + V_2 + V_3 = 0 \tag{B-7}$$

so also the differences:

$$\Delta V_1 + \Delta V_2 + \Delta V_3 = 0 \tag{B-8}$$

Therefore:

$$\frac{Q}{C_1} + \frac{Q}{C_2} - \frac{q}{C_2} + \frac{Q}{C_3} = 0 \tag{B-9}$$

$$Q \left[\frac{1}{C_1} + \frac{1}{C_2} + \frac{1}{C_3} \right] = \frac{q}{C_2} \tag{B-10}$$

By the rule of series capacitors:

$$\frac{1}{C} = \frac{1}{C_1} + \frac{1}{C_2} + \frac{1}{C_3} \tag{B-11}$$

so:

$$\frac{Q}{C} = \frac{q}{C_2} \tag{B-12}$$

$$Q = \frac{C}{C_2} q \tag{B-13}$$

For parallel plate capacitors:

$$C = \frac{k \epsilon_0 A_c}{D} \tag{B-14}$$

Thus, for capacitors of identical area and dielectric constant, k, the capacitance is inversely proportional to the thickness. Therefore:

$$\frac{C}{C_2} = \frac{s}{D} \tag{B-15}$$

so:

$$Q = \frac{s}{D} q \qquad \text{(B-16)}$$

We now see that the effective charge detected at the electrodes of a parallel plate capacitor is proportional to the charge transported inside the capacitor. The proportionality constant is the ratio of the distance traveled by the charge to the electrode spacing.

APPENDIX C

The Charge Intersection Model

The method by which a fission fragment induces discharge in an electron-beam charged electret is not fully understood. The charge intersection model is a proposed mechanism for charge release and transport. Although not yet verified by the experiments, it does produce results remarkably similar to the experimental data.

In the charge intersection model, the fission fragment induces discharge by producing a conductive path from the surface into the charge region. The resulting local upset of the field within the charge region frees trapped electrons to be conducted along the fission fragment track. Figure C-1 shows the process. A fission event in the layer of fissionable material ejects one of its fragments through the front conductive surface and into the electret. Behind the fragment is a track of ionized and excited material of much enhanced conductivity. Since the fission fragment completes its journey in only a few nanoseconds, the conductive path effectively 'materializes' within the electret.

The conductive path from the front surface to the charge region upsets the normally one-dimensional electric field within the electret. Since the electric potential of the track is the same as the front surface, a strong radial field about the track is created. Within a certain radius of the track, this field exceeds the breakdown strength of the dielectric material. Trapped electrons within this radius are released to flow to the conductive track and then along the track. The net result is as though the fission fragment had a cross section which intersects and collects trapped electrons from the charge layer.

Calculating the charge collected by the fission track requires estimates of the radius of the intersection phenomena and the direction and distance the freed electrons travel. Let us initially assume that trapped charges of volumetric charge density $\rho(x)$ reside in an electret of thickness s. Electrodes are present at both

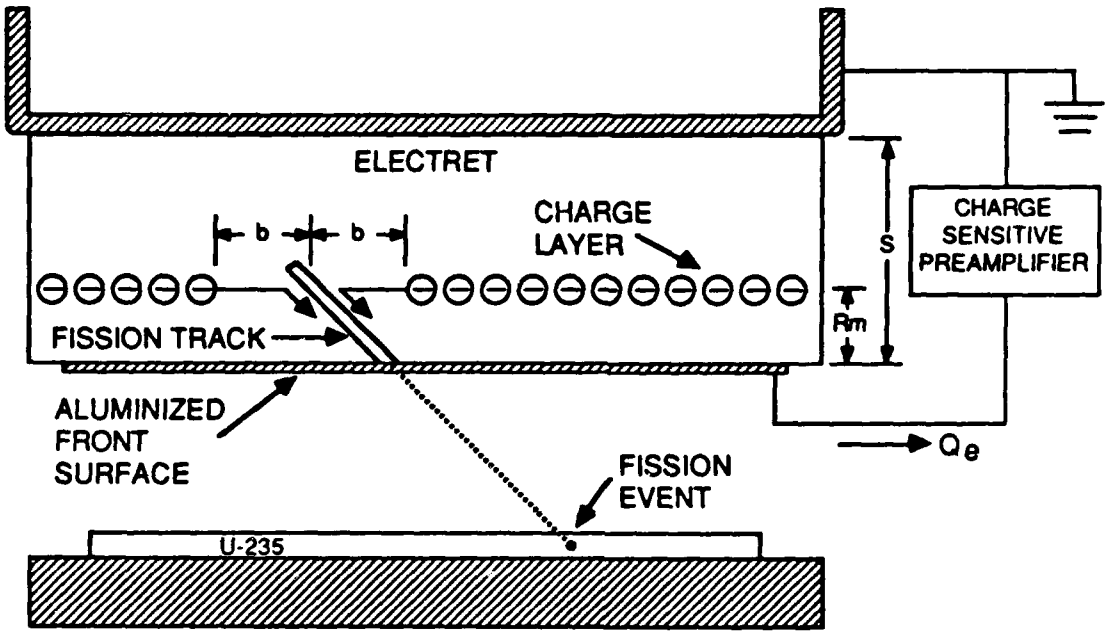

C-1. Diagram of the Charge Intersection Model

surfaces and shorted. Using Equations 2-6 and 2-7, we can determine the electric field, $E(r)$, at any point r between the front electrode and the charge layer:

$$E(r) = \frac{1}{s\,\epsilon_0 k}\left[\int_0^r \rho(x)\,(s-x)\,dx + \int_r^s \rho(x)\,x\,dx\right] \tag{C-1}$$

If we assume that the charge layer is thin, the area charge density, σ, may be used:

$$\sigma = \int_0^s \rho(x)\,dx \tag{C-2}$$

The thin layer is assumed to reside at depth R_m from the front surface. Using the thin layer assumption we get the electric field, $E(r)$:

$$E(r) = \frac{\sigma}{\epsilon_0 k}\left(1 - \frac{R_m}{s}\right);\ 0 < r < R_m \tag{C-3}$$

$$E(r) = \frac{\sigma}{\epsilon_0 k}\left(\frac{R_m}{s}\right);\ R_m < r < s \tag{C-4}$$

Note that for the thin charge layer, the electric fields on either side are constant. The field may be integrated to give the electric potential between the front surface and point r, thus:

$$V(r) = \int_0^r E(x)\,dx \tag{C-5}$$

or, for the thin charge layer:

$$V(R_m) = \frac{\sigma\,R_m}{\epsilon_0 k}\left(1 - \frac{R_m}{s}\right) \tag{C-6}$$

We now assume that the fission fragment track is at the same potential as the front surface and generates a cylindrically symmetric field. The electric field, E, at a point x between concentric cylinders having applied voltage, V, is:

$$E(x) = \frac{V}{x\,\ln\left(\frac{b}{a}\right)} \tag{C-7}$$

where a is the radius of the inner cylinder and b is the radius of the outer

cylinder. We now assume that the outer radius is the at the edge of the undisturbed charge layer, that is the radius at which the field becomes less than E_b, the breakdown field strength of the dielectric. The equation for this radius is:

$$b \ln\left(\frac{b}{a}\right) = \frac{V(r)}{E_b} \tag{C-8}$$

For a thin charge layer:

$$b \ln\left(\frac{b}{a}\right) = \frac{\sigma R_m}{\epsilon_0 k E_b}\left(1 - \frac{R_m}{s}\right) \tag{C-9}$$

Trapped electrons within this radius are drawn to the track. The total charge intersected by the fission track is therefore:

$$Q(r) = \int_0^r \pi b^2 \rho(x)\, dx \tag{C-10}$$

where $\rho(x)$ is the volumetric charge density. For a thin charge layer:

$$Q = \pi b^2 \sigma \tag{C-11}$$

Once in the fission fragment track, the electrons will be conducted either to the front surface or to the end of the track, depending on the direction of the electric field at that point. The point inside the electret at which the electric field reverses, R_0 will always reside within the charge layer. We must, therefore, relax the thin layer approximation to determine what portion of the charge will move to the front surface. If the charge is uniformly distributed within the charge layer, $E(r)$ is linear within the charge region and constant on either side. The portion of the charge density at $r < R_0$ and transported to the front surface, σ_f, and the charge flowing in the other direction, σ_b follow from:

$$\frac{\sigma_f}{\sigma_b} = \frac{E(0)}{E(s)} = \frac{(s - R_m)}{R_m} \tag{C-12}$$

$$\sigma_f + \sigma_b = \sigma \tag{C-13}$$

$$\sigma_f = \sigma \frac{(s - R_m)}{s} \tag{C-14}$$

$$\sigma_b = \sigma \frac{R_m}{s} \tag{C-15}$$

Finally we need to determine the effective charge, Q_e, (that seen at the electrodes) resulting from the movement of the freed electrons. As shown in Appendix B, for charge Q moving from point P_1 to point P_2 the effective charge, Q_e, is:

$$Q_e = Q \frac{P_2 - P_1}{s} \tag{C-16}$$

We can now determine Q_e resulting from a fission fragment track penetrating to r, where $r \geq R_m$:

$$Q_e(r) = \frac{\pi b^2}{s} \left[\sigma_f R_m - \sigma_b (r - R_m)\right]$$

$$Q_e(r) = \frac{\pi b^2 \sigma R_m}{s} \left[1 - \frac{r}{s}\right] \tag{C-17}$$

By the assumptions of the model, if $r < R_m$ then $Q_e = 0$. Note that charge released beyond R_0 travels to the end of the track and is subtracted from Q_e. If we discount the slowly varying logarithmic term in Equation C-8, we see that b is a function of σ. Thus $Q_e(r)$ is a function of σ^3. Charge density is the most critical factor in achieving a useful fission event signal.

Equation C-17 offers the advantage of being a calculable first order approximation. But the assumption of a thin charge layer is very poor. A distributed charge layer is more realistic. However, even very simple (and arbitrary) charge distributions create enormous problems in obtaining closed form solutions to the integrals in Equations C-1, C-5, and C-10. A numerical solution is required. Using Equations C-10 and C-16, the equation for the effective charge becomes:

$$Q_e(r) = \pi \int_0^{R_0} \frac{x b^2 \rho(x)}{s} dx - \pi \int_{R_0}^{r} \frac{(s - x) b^2 \rho(x)}{s} dx \tag{C-18}$$

with Equation C-8 defining b and Equation C-5 defining $V(r)$.

Appendix E contains a Pascal program which evaluates this system of equations for various charge densities, mean depths and distributions. The charge distribution used for the numerical evaluation is defined by σ, R_m, and a width value, W. For both sawtooth and square distributions, W is the extent of the charge distribution, i.e. the charge is distributed from $R_m - W$ to $R_m + W$. The program was validated by comparing its output with Equation C-17 for

charge distributions approximating a thin layer. As expected, the program results were very slightly lower, reflecting the effect of the approximation.

APPENDIX D

Ion Stopping Power Calculations

Stopping power is the linear rate at which an ion loses its kinetic energy in a medium. Its units are energy per unit length. The energy loss occurs principally through electronic interaction between the positively charged ion and the valence electrons of the medium. The amount of interaction (and thus the stopping power) is a complex function of the apparent charge of the ion, the velocity of the ion, and the composition of the medium.

There is no completely satisfactory theoretical method for determining the stopping power of any ion at any velocity in any medium. There is, however, a set of semi-empirical calculations which provide a reasonably good value for stopping power over a wide range of ions, ion velocities and media.(22) The algorithm begins with an empirical equation which is a fit to the stopping power of a proton in an elemental medium. It uses three tabulated parameters for the characteristics of the medium; the mean ionization energy, the number of external electrons, and a low-energy friction coefficient. The stopping power of the heavy ion is then determined by an empirical function relating heavy ion stopping power to that of the proton. A detailed discussion of the entire algorithm is contained in the reference.

The Pascal program below implements this algorithm to determine the energy deposition and track length of heavy ions in a medium. It tracks the position and energy loss of the ion as it passes through a given medium, repeatedly recalculating the stopping power to correspond to the ion's current energy. For a compound medium the program uses the Bragg-Kleeman rule. It sums the stopping powers for each element in the compound at that element's atomic number density. The variables used in the program, and their units, are identified in comment statements. Other comments tell specifically what each procedure and function do.

The program was validated by first comparing its results with those contained in the reference. No variance was seen. The results were then compared with reported stopping powers for various heavy ions in aluminum.(19:53) Table D-1 shows a comparison of the stopping powers for ions in aluminum. The calculated values were found to be quite accurate except for medium weight and heavy ions at relatively low energies.

Table D-1: Stopping Power of Various Ions in Aluminum
{ Stopping Power in MeV $(Mg\text{-}cm^2)^{-1}$ }

Ion	Ion Energy (MeV)	Calculated Stopping Power	Reference Stopping Power(19:53)	Percent Difference
Hydrogen	1.0	0.033	0.035	-6
	0.1	0.163	0.20	-19
	0.01	0.491	0.45	9
Chlorine	35.0	0.030	0.029	3
	3.5	0.058	0.060	-3
	0.35	0.036	0.030	20
Iodine	127.0	0.018	0.018	0
	12.7	0.018	0.020	-10
	1.27	0.0088	0.060	47
Fermium	257.0	0.011	0.010	10
	25.7	0.0086	0.009	-4
	2.57	0.0038	0.002	90

PASCAL PROGRAM TO CALCULATE ION STOPPING POWER

```
program ffeloss;
{ determines the fission fragment stopping power in a }
{ given material with modifications, the program can be }
{ used to estimate the stopping power of any ion in any  }
{ material }


uses printer;

const maxele = 5;  { max number of elements }
      delt = 1.00e-14 ;  { time step, sec }
      fissev = 168.0e6 ;  { ev per fission event }
      jperev = 1.60219e-19 ;
            { conversion factor, joules per ev }
      kgperamu = 1.66e-27 ;
            { conversion factor, kg per amu }
      pi = 3.14159;
      e = 1.602e-19 ;
            {  charge of an electron, Coulombs }
      ih = 13.598 ;
            { ionization potential of hydrogen, ev }
      e0 = 8.854e-12 ;
            { permitivity of free space, coul2/j/m }
      m0 = 9.11e-31 ;  { mass of electrons, kg }
      v0 = 2.189e6 ;  { Bohr velocity, m/sec }
      avogadro = 6.02e26 ;
            { avogadro's number, molecules/kgmole }

var numele : integer;  { number of elements considered }
    n : real;
```

```
    { molecular number density of media, molecules/m3 }
  nm : array[1..maxele] of integer;
       { number of element atoms in media molecule }
  zm : array[1..maxele] of real;
       { atomic number of media }

  zp0 : real; { atomic number of particle }
  mp : real; { mass of ff, amu }
  ep : real; { energy of particle, ev }
  zp : real; { charge number of particle }
  vp : real; { velocity of particle, m/sec }
  xp : real; { position of particle, m }
  i : integer;
  xout,eplast,xplast : real;
  outp : text;

function pwr(val,exponent: real): real;
{ returns val to the power of exponent }

begin
 if val <= 0 then
 begin
  pwr := 0.0;
  writeln('exponent of negative value');
 end
 else pwr := exp(exponent * ln(val));
end; { pwr }

function ion(v,z:real):real;
{ returns the ionization of the particle at velocity v }
{ from Material Characterization using Ion Beams, pg }

begin
```

```
 if v > 2.0 * v0 then
       ion := z * ( 1.0 -
           (1.035-0.4*exp(-0.16*z)) *
           exp(-0.879*v/v0/pwr(z,0.65)) )
 else if v < pwr(z,0.66666)*v0 then
       ion := pwr(z,0.33333) * v / v0
 else   ion := z * (1.0 - exp(-v/v0/pwr(z,0.6666)))

end; { ion }

function dedx(zpf,vpf,nmf,zmf: real): real;
{ returns stopping power from Montenegro et al., }
{ Physics Letters, 92A, 8 Nov 82, 195 }
{ units are ev/m }

const z2s : array[3..92] of real =
(3.0,  4.0,  3.0,  4.0,  5.0,  6.0,  7.0,  8.0,
 9.0, 10.0, 11.0, 10.0,  5.0,  6.0,  7.0,  8.0,
 9.0, 10.0, 11.0, 12.0, 13.0, 14.0, 15.0, 16.0,
17.0, 18.0, 19.0, 18.0, 19.0, 20.0, 15.0, 16.0,
17.0, 18.0, 19.0, 10.0, 11.0, 12.0, 13.0, 14.0,
15.0, 16.0, 17.0, 18.0, 19.0, 20.0, 21.0, 20.0,
21.0, 22.0, 21.0, 18.0, 19.0, 20.0, 21.0, 22.0,
23.0, 24.0, 25.0, 16.0, 17.0, 18.0, 19.0, 20.0,
21.0, 22.0, 23.0, 24.0, 25.0, 26.0, 27.0, 28.0,
29.0, 30.0, 31.0, 32.0, 33.0, 34.0, 33.0, 20.0,
21.0, 22.0, 23.0, 24.0, 19.0, 20.0, 21.0, 22.0,
23.0, 24.0);
{ number of external electrons }

    k : array[3..92] of real =
( 7.050,11.232,12.361,13.145,14.759,13.250,10.417, 9.748,
 12.700,18.946,20.754,20.734,16.148,17.222,25.216,28.633,
```

```
25.736,27.584,25.985,24.292,22.383,19.900,17.332,17.582,
15.688,17.752,18.466,21.034,25.186,27.749,26.595,29.348,
28.034,32.031,28.449,31.671,32.011,33.645,34.484,32.101,
33.969,30.517,29.598,26.170,28.094,29.048,31.127,32.026,
37.472,34.869,38.596,41.124,36.408,39.465,40.175,37.417,
36.428,35.463,34.524,33.615,32.730,33.670,31.037,27.564,
26.075,25.336,24.612,23.917,24.447,25.121,23.672,22.853,
25.980,25.331,24.706,22.363,24.262,21.524,23.597,26.575,
29.758,30.767,30.997,30.882,34.719,37.502,38.216,38.521,
37.007,36.423   );
{ Low energy coefficient, ev cm2 / atom  }

    iavg : array[3..92] of real =
( 47.0,  63.0,  75.0,  79.0,  86.0,  99.0, 118.8, 135.0,
  141.0, 149.0, 162.0, 159.0, 168.9, 179.2, 170.3, 180.0,
  189.4, 195.0, 215.0, 228.0, 237.0, 257.0, 275.0, 284.0,
  304.0, 314.0, 330.0, 323.0, 335.4, 323.0, 354.7, 343.4,
  339.3, 347.0, 349.7, 353.3, 365.0, 382.0, 391.3, 393.0,
  416.2, 428.6, 436.4, 456.0, 470.0, 466.0, 479.0, 511.8,
  491.9, 491.3, 452.4, 459.0, 484.8, 485.5, 493.8, 512.7,
  520.2, 540.0, 537.0, 545.9, 547.5, 567.0, 577.2, 578.0,
  612.2, 583.3, 629.2, 637.0, 655.1, 662.9, 682.0, 695.0,
  713.6, 726.6, 743.7, 760.0, 742.0, 768.4, 764.8, 761.0,
  762.9, 765.0, 761.7, 733.1, 762.3, 760.1, 767.9, 776.4,
  807.0, 808.0   );
{  mean ionization energy, ev }

var a,b,c,d,e,f,u,sqru,sp0,beta : real;
   g,sp,alpha,zhiszps,shi,de : real;

begin
  a := 9.5616 * zmf;
  b := 4.0 * ih / iavg[round(zmf)];
```

```
 c := a * b;
 d := k[round(zmf)]/c + b/2.0 + z2s[round(zmf)]/9.0/zmf;
 e := 3.0*sqr(b)*d / ( pwr(zmf,1.4)*b*sqr(d) +
        sqr(b) + sqr(d) );
 f := c * e * sqr(e)/d ;
 u := vpf/v0;
 sqru := sqr(u);
 sp0 := k[round(zmf)]*u*exp(-u) + a/sqru*ln(1.0 + b*sqru) -
      c/( 1.0 + d*sqru ) + f*sqr(sqru)/pwr((1.0 +
      e*sqru),3);
 beta := a / 9.5616 / zmf;
 g := 2.0*beta/3.0/c;
 sp := sp0 - beta * pwr(g*sqru,1.5) / 6.0 / sqr(b) /
       sqr(sqr(1.0 + g*sqru));
 alpha := pwr(zpf,-0.66666);
 zhiszps := ( 1.0 - exp(-alpha*u) -
       alpha*u/6.0*exp(-2.0*alpha*u) ) /
       ( 1.0 - exp(-u) - u/6.0*exp(-2.0*u) );
 shi := sqr(zpf)*sqr(zhiszps)*sp*1e-15;   { ev-cm2/atom }
{ (**)writeln(' Stopping power = ', shi:12 );    }
 de := shi * 1e-4 * nmf;
{ writeln(' dedx = ',de:12);   }
 dedx := de;
end; { dedx }


procedure update ;
{ updates the characteristics of the ff in each material }

var i : integer;
   xmove : real;
   eloss : real;
```

```
begin
  zp := zp0 ;
  xmove := vp * delt ;
  eloss := 0.0;
  for i := 1 to numele do
      eloss := eloss + dedx(zp,vp,n*nm[i],zm[i]) * xmove ;
{  writeln(' eloss = ',eloss:12);       }
  ep := ep - eloss;
  vp := sqrt( 2.0 * ep * jperev / mp / kgperamu ) ;
  xp := xp + vp * delt ;
end;  { update }

procedure initialize;
{ initialize the variables }

var i : integer;
    density,mwm : real;

begin
  numele := 2;
  density := 2.10e3; { density of media, kg/m3 }
  mwm := 250.0;  { molecular weight of media, amu }
  nm[1] := 10; { fluorine }
  nm[2] := 5; { carbon }
  zm[1] := 9.0;
  zm[2] := 6.0;
  n := density * avogadro / mwm ;
  zp0 := int(mp / 254.0 * 92.0);
           { atomic number of particle }
  ep := fissev * (1.0 - mp/257.0);
  vp := sqrt( 2.0 * ep * jperev / mp / kgperamu ) ;
  xp := 0.0;
  zp := zp0;
```

```
end; { initialize }

begin
 assign(outp,'a:dedx90.dat');
 rewrite(outp);
 writeln(lst,
   ' Position(Microns)      Stopping Power(Mev/micron)');
 begin
  mp := 90.0;    { atomic mass of particle }
  initialize;
  xout := 0.0;
  eplast := ep;
  xplast := 0.0;
  repeat
   writeln(vp:12,'  ',ep:12,'  ',xp:12);
   update;
   if xp >= xout then
   begin
    writeln(outp,xp*1e6:12:6,'    ',
        (eplast - ep)/(xp - xplast)*1e-12:12:4);
    writeln(lst,xp*1e6:12:6,'                ',
      (eplast - ep)/(xp - xplast)*1e-12:12:4);
    eplast := ep;
    xplast := xp;
    xout := xout + 1.0e-6;
   end; { if-xp }
  until ion(vp,zp0) < 0.10;
 end; { for-i }
 close(outp);
end.
```

APPENDIX E

Calculation of the Charge Intersection Model

The charge intersection model described in Appendix C has a closed form solution if a thin charge layer is assumed. For more realistic charge distributions, the integrals used to describe the electric fields and the electric potentials within the electret require a numerical solution. Also, the distribution in depth of penetration of fission fragments is an empirical representation requiring a numerical treatment. For these reasons, the distribution in the fission event signal predicted by the charge intersection model must be determined by numerical approximation.

The program first does a Simpson's rule integration on the charge density distribution to determine the electric fields within the electret. It then does a Simpson's rule integration on the electric fields to determine the electric potentials in the electret. It then has the values needed to integrate Equation C-18 using Equation C-8. Note that Equation C-8 is not explicit. The value of the charge collection radius is determined by a Newton-Raphson approximation. The result of integrating Equation C-18 is the charge collected as a function of the ion depth of penetration. The program then multiplies this function by the (numerically approximated) distribution in the fission fragment depth of penetration to produce the percent of fission fragments producing a signal of a given charge.

An important parameter required by the program is the charge density distribution. The charge density distribution is difficult to determine experimentally. The mean depth of the charge may be determined from the electron beam energy using Figure 2-2. The total charge may be determined using Equation 2-3. The distribution must be approximated by some function. The equations for both square distributions and sawtooth distributions are included in the code, with one set of equations commented out. Both may be represented by a single value, the full width of the charge density at half maximum. The sawtooth distribution produces a signal charge distribution about 20 percent higher than the square

distribution but with few structural differences. The sawtooth distribution was used for analysis of the charge intersection model.

The program also needs the radius of the conductive ion track. Obviously there is no clearly defined boundary to the ion track so this value must be estimated. Fortunately the value is in a logarithmic term which makes it less influential. Photographs of spontaneous discharge tracks in FEP show that their radius is about 10^{-5} cm.(2:5149) This is the value used in the analysis of the charge intersection model.

The program was validated by approximating a thin film charge distribution and comparing its results to those of Equation C-17. For the following input values:

$\sigma = 1 \times 10^{-7} coul/cm^2$

$R_m = 8 \times 10^{-4} cm$

$W = 1 \times 10^{-4} cm$

$s = 25.4 \times 10^{-4} cm$

$r = 8 \times 10^{-4} cm$

the equation gives 3.47×10^{-16} coul while the program gives 2.7×10^{-16} coul. The slightly higher value from the equation indicates that a sharply defined charge layer yields a somewhat stronger signal than a distributed layer. This is as predicted by the model.

PASCAL PROGRAM TO CALCULATE THE CHARGE DISTRIBUTION FROM FISSION FRAGMENT INTERACTION WITH ELECTRON-BEAM CHARGED FEP USING THE CHARGE INTERSECTION MODEL

```
program chargedist;
{ ion path charge collection in an electret by }
{ charge intersection }


const  s = 25.4e-4 ;
         { electret thickness, cm }
       eb = 2e6 ;
         { breakdown field strength of FEP, V/cm }
       tradius = 0.1e-4;
         { fission fragment track radius, cm }
       k = 2.2 ;
         { dielectric ratio of material }
       e0 = 8.854e-14 ;
         { dielectric permitivity of free space, farads/cm }
       q0 = 1.602e-19 ;
         { charge of an electron, coulombs }
       numarray = 200;
         { number of elements in interpolate routines }
       numch = 100 ;
       { number of charge intervals in charge distribution }
       maxch = -0.5e-15 ;
         { maximum charge in charge distribution }
       numdepths = 25 ;
         { number of depths calculated  }

var field,volt : array[0..numarray] of real;
         { field and volt interpolation arrays }
```

```
  chrg : array[1..6,1..numdepths]of real;
      { the output array, coul }
  rm : real ;
      { center of charge region, cm }
  w : real ;
      { half width of charge region, cm }
  sigma : real ;
      { total area charge density, coul/cm2 }
  chdist : array[1..6,1..numch] of real;
      { the charge distribution array }
  i,j : integer;
  txt,txt1,txt2 : text;



function chargeden(rc:real):real;
{ returns the value of the charge density at point rc )
{ insert the charge density function }

begin

{ square distribution }
{ if (rc >= rm-w) and (rc <= rm+w) then
     chargeden := sigma/2/w
     else chargeden := 0.0;     }


{ sawtooth distribution }
 if (rc > rm - w) and (rc < rm) then
     chargeden := sigma/sqr(w)*(w-rm+rc)
     else if (rc >= rm) and (rc < rm + w)
        then chargeden := sigma/sqr(w)*(rm+w-rc)
```

```
        else chargeden := 0.0;

end; { chargeden }


{ numerical integration of electric field formula }


function givefield(re:real):real;
{ integrates under function from 0 to s for electric }
{ field at r }

function simpfn(rs,pt : real):real;
{ insert the function to be integrated }

begin
  if pt = rs then simpfn := 0.0
     else if pt > rs then
        simpfn := chargeden(pt)*(pt - s)/s/e0/k
     else simpfn := chargeden(pt)*(pt)/s/e0/k;
end; { simpfn }

const n = 200 ;  { number of intervals, must be even }

var i : integer;
   simp,sumvar,interval,curval : real;

begin
  interval := (s)/n;
  sumvar := simpfn(re,0) + simpfn(re,s) +
      4.0*simpfn(re,s - interval);
  for i := 1 to ((n div 2) - 1) do
  begin
```

```
    curval := interval*2.0*i;
    sumvar := sumvar + 4.0 * simpfn(re,curval - interval);
    sumvar := sumvar + 2.0 * simpfn(re,curval);
  end;
  simp := sumvar * interval/3.0;
  givefield := simp;
end; { givefield }

function efield(r : real): real;
{  returns potential at r, using interpolation }

var inp : integer;
    fract : real;

begin
  inp := trunc(r/s*numarray);
  fract := frac(r/s*numarray);
  if inp >= numarray then efield := field[numarray]
      else  efield := field[inp] +
                fract*(field[inp+1]-field[inp]);
end;  { efield }


function givevolts(rv : real):real;
{ returns voltage at r wrt surface electrodes }

function simpfn(rs : real):real;
{ insert the function to be integrated }

begin
  simpfn := efield(rs);
end; { simpfn }
```

```
const n = 200 ;  { number of intervals, must be even }

var i : integer;
    simp,sumvar,interval,curval : real;

begin
  interval := (rv)/n;
  sumvar := simpfn(0) + simpfn(rv) +
        4.0*simpfn(rv - interval);
  for i := 1 to ((n div 2) - 1) do
  begin
    curval := interval*2.0*i;
    sumvar := sumvar + 4.0 * simpfn(curval - interval);
    sumvar := sumvar + 2.0 * simpfn(curval);
  end;
  simp := sumvar * interval/3.0;
{  (**)writeln('Volts at ',re:14,' is ',simp:14,' V.'); }
  givevolts := simp;
end; { givevolts }

function volts(r: real): real;
{ returns voltage at r WRT surface electrodes, }
{ uses interpolation }

var inp : integer;
    fract : real;

begin
  inp := trunc(r/s*numarray);
  fract := frac(r/s*numarray);
  if inp >= numarray then volts := volt[numarray]
      else  volts := volt[inp] + fract*(volt[inp+1] -
              volt[inp]);
```

```
end; { volts }

procedure setarray;
{ set up field and volts arrays }

var i : integer;
   d : real;

begin
 for i := 0 to numarray do
 begin
   d := i * s /numarray;
   field[i] := givefield(d);
 end; { for-i }
 for i := 0 to numarray do
 begin
   d := i * s /numarray;
   volt[i] := givevolts(d);
   (**)writeln(i:4,' volts: ',volt[i]:11,
          ' field: ',field[i]:11);
 end; { for-i }
end; { setarray }


{ numerical integration of charge collection formula }


function getb(p:real):real;
{ solves for the radius of effect at point p }
{ b*ln(b/tradius) = volts(p)/eb }
{ uses Newton-Raphson: newx = x - f(x)/f'(x) }

const mindiff = 1e-7;
```

```
    { acceptable difference for successive approximation }

var b,newb,v : real;

begin
  v := volts(p);
  newb := 1e-4;
  repeat
    b := newb;
    newb := b - (b*ln(b/tradius) - v/eb)/(1.0 +
         ln(b/tradius));
{    (**)writeln(b:14,' ',newb:14);          }
  until ( abs(b-newb) < mindiff );
  getb := newb;
end;  { getb }


{ Determine the charge collected }


function charge(ai,bi:real):real;
{ the charge collected along a path from a to b }

function simpfn(pt : real):real;
{ insert the function to be integrated }

var brad: real ; { radius of charge collection }
    ep : real ;  { end point to which charge travels }
    si : real ;

begin
  brad := getb(pt);
  if efield(pt) > 0.0 then ep := ai else ep := bi;
```

```
    { which end the charge goes to }
  si := sqr(brad) * pi * chargeden(pt) * (pt - ep)/s;
{  (**)writeln(ai:11,'  ',pt:11,'  ',bi:11,'  ',si:14); }
  simpfn := si;
end; { simpfn }

const n = 2000;  { number of intervals, must be even }

var i : integer;
    simp,sumvar,interval,curval : real;

begin
  interval := (bi - ai)/n;
  sumvar := simpfn(ai) + simpfn(bi) +
        4.0*simpfn(bi - interval);
  for i := 1 to ((n div 2) - 1) do
  begin
    curval := ai + interval*2.0*i;
    sumvar := sumvar + 4.0 * simpfn(curval - interval);
    sumvar := sumvar + 2.0 * simpfn(curval);
  end;
  simp := sumvar * interval/3.0;
  charge := simp;
end; { charge }


procedure chargeout;
{ calculates and outputs the charge resulting from ff }
{ penetration in FEP }

var i,j : integer;
    test : real;
```

```
begin   sigma := -1e-7;
 for i := 1 to 6 do
 begin
  rm := (13-i)*1e-4;
  w :=  (1+i)*1e-4;
  setarray;
  for j := 1 to numdepths do
  begin
   test := j*1e-4;
   chrg[i,j] := charge(0.0,test);
   (**)writeln(i:4,'  ',j:4,'  ',chrg[i,j]:14);
  end; { for-j }
 end;  { for-i }
 assign(txt,'charge.dat');
 rewrite(txt);
 writeln(txt,
     'Charge collection. Rm = ',rm:6:4,' W = ,w:6:4 ');
 for j := 1 to numdepths do
 begin
  for i := 1 to 6 do write(txt,chrg[i,j]:11,'  ');
  writeln(txt);
 end;  { for-j }
 close(txt);
end;  {  chargeout }



{ determine the charge distribution from fission fragments }



function depthfr(depth:real):real;
{ returns the fraction per cm of fission fragments that }
```

```
{ stop at depth }

const fr : array [1..50] of real =
 ( 0.124667, 0.072,    0.060667, 0.072667, 0.062667
 , 0.068667, 0.065333, 0.067333, 0.07 ,    0.069333
 , 0.061333, 0.067333, 0.071333, 0.065333, 0.066
 , 0.068667, 0.067333, 0.067333, 0.065333, 0.064667
 , 0.066667, 0.068667, 0.068,    0.063333, 0.062667
 , 0.040667, 0.034,    0.029333, 0.029333, 0.026667
 , 0.028,    0.025333, 0.024667, 0.018667, 0.007333
 , 0.007333, 0.001333, 0.0 ,     0.0 ,     0.0
 , 0.0 ,     0.0 ,     0.0 ,     0.0 ,     0.0
 , 0.0 ,     0.0 ,     0.0 ,     0.0 ,     0.0 );
{  The distribution per um of fission fragments stopping }
{   in 25 um FEP }

var inp : integer;
    fract : real;

begin
  inp := trunc(depth*2.0e4) ;
  fract := frac(depth*2.0e4) ;
  if (inp>0) and (inp<50) then depthfr := ( fr[inp] +
          fract*(fr[inp+1]-fr[inp]) ) * 1.0e4
      else depthfr := 0.0;
end;  { depthfr }

function chdepth(n:integer; depth: real):real;
{  returns the charge released by a ff stopping at depth }
{  uses column n from array chrg[] generated by chargeout }

var inp : integer;
    fract : real;
```

```
begin
 inp := trunc(depth/1e-4) ;
 fract := frac(depth/1e-4) ;
 if (inp>0) and (inp<numdepths) then chdepth :=
       chrg[n,inp] + fract*(chrg[n,inp+1]-chrg[n,inp])
     else chdepth := 0.0;
end; { chdepth }

procedure findchrg(n:integer);
{ determines the charge distribution from fission }
{ events in FEP }

const  num = 2000 ; { number of depths tested }

var i,j,inp : integer;
   width,d,ch : real;

begin
 for i := 1 to numch do chdist[n,i] := 0;
 width := 25.0e-4/num;
 for i := 1 to num do
 begin
   d := i*width;
   ch := chdepth(n,d);
   inp := trunc(ch/maxch*numch);
   (**)writeln(ch:11,'  ',inp:3);
   if inp < 1 then inp := 1;
   if inp > numch then inp := numch;
   chdist[n,inp] := chdist[n,inp] + depthfr(d)*width;
 end; { for-i }
end; { findchrg }

procedure readchrg;
```

```
{ read in the charge collection array }

var i, j : integer;
    strng : string[80];
    ch : char;

begin
  assign(txt1,'charge.dat');
  reset(txt1);
  readln(txt1,strng);
  for i := 1 to numdepths do
  begin
    for j := 1 to 6 do
    begin
      read(txt1,chrg[j,i]);
      (**)writeln(j:4,i:4,'  ',chrg[j,i]:12);
    end; { for-j }
    readln(txt1,strng);
  end; { for-i }
  close(txt1);
end; { readchrg }

procedure writchrg;
{ write the charge distribution array }

var i, j : integer;

begin
  assign(txt2,'chdist.dat');
  rewrite(txt2);
  for i := 1 to numch do
  begin
    for j := 1 to 6 do
```

```
    begin
      write(txt2,chdist[j,i]:11,', ');
    end; { for-j }
    writeln(txt2);
  end; { for-i }
  close(txt2);
end; { writchrg }



begin { main program }
  chargeout;     { use to create charge.dat if necessary }
{  readchrg; }  { use to read charge.dat if necessary }
  for i := 1 to 6 do findchrg(i);
  writchrg;
end.
```

APPENDIX F

Acronym, Unit and Symbol Definitions

Symbol	Definition
A	Activity of source
A_c	Area of capacitor
A_b	Area covered by the electron beam
B	Boron
b	Constant used in DRIC equation
b	Radius of charge collection in derivation
c	Speed of light
C	Degrees centigrade
C	Capacitance of capacitor
C_1	Capacitance of capacitor
C_2	Capacitance of capacitor
C_3	Capacitance of capacitor
C_h	Chord length across medium
cm	Centimeters
coul	Coulombs
D	Distance between electrodes
D_1	Thickness of capacitor
D_2	Thickness of capacitor
DRIC	Delayed radiation induced conductivity
e	Charge of an electron
E	Energy of photon
$E(r)$	Electric field at point r
E_1	Electric field in e-beam charged electret
E_2	Electric field in e-beam charged electret

Symbol	Definition
E_e	Electric field in e-beam charged electret
E_α	Energy of alpha particle
E_b	Electric field in e-beam charged electret
E_f	Energy of fission fragment
E_i	Energy of ion
E_{total}	Total kinetic energy of fission
eV	Electron volt
F	Fluorine
F	Neutron flux
FEP	Polyfluoroethylene propylene, Teflon
FET	Field effect transistor
G	Conductivity
G_0	Conductivity at termination of irradiation
h	Planck's constant
H	Half life
He	Helium
hr	Hours
i	Current
i_b	Electron beam current
k	Dielectric coefficient
k_1	Dielectric coefficient
k_2	Dielectric coefficient
keV	Kilo electron volt
kV	Kilovolts
L	Ion track length
Li	Lithium
MeV	Million electron volts
M_{ff}	Mass of fission fragment
mil	10^{-3} inches
min	Minutes

Symbol	Definition
M_{total}	Total mass of fissionable atom
N	Number of source atoms
nm	Nanometers
N_n	Number of ion events
p	Change variable in derivation
PET	Polyethylene terephthalate, Mylar
q	Charge moving in capacitor
Q	Charge collected
$\overline{Q}$	Average charge collected
Q_e	Effective charge collected
Q_s	Total effective surface charge
r	Charge layer depth
R	Distance traveled by charge
R	radius of medium
rads	Unit of radiation dose
RIC	Radiation induced conductivity
R_m	Mean depth of charge layer
S	Stopping power
s	Thickness of electret
s_1	Distance between electret and electrode
s_2	Distance between electret and electrode
$\overline{S}$	Average stopping power
sec	Seconds
SFC	Split faraday cup
s_k	Term used in electret field equations
T	Height of medium
T	Temperature
t	time
t_c	Charging time
TFE	Polytetrafluoroethylene, Teflon

Symbol	Definition
Th	Thorium
t_n	Time required to neutralize electret charge
Torr	Torricelli
TSC	Thermally stimulated current
U	Uranium
um	Micrometers, microns
V	Surface potential of electret
$V(r)$	Electric potential at point r
V_1	Voltage on capacitor in derivation
V_2	Voltage on capacitor in derivation
V_3	Voltage on capacitor in derivation
W	Average energy to produce a charge carrier pair
W	Charge depth distribution full width at half maximum
δ	Exponent used in RIC equation
$\delta(x)$	Volumetric charge density
ΔV	Change in voltage of capacitor
ΔE	Energy difference
ϵ_0	Dielectric constant
λ	Wavelength of photon
ϕ	Radiation dose rate, rads/sec
π	pi, 3.14159.....
ρ	Volumetric charge density
σ	Charge density
σ_f	Neutron absorption cross section
$\hat{\sigma}$	Effective surface charge density
$\hat{\sigma}_0$	Initial surface charge density
τ	Time decay constant for charge density
θ	Angle from surface normal
θ_m	Angle from surface normal to corner of medium

Bibliography

1. Anderson, E. W., L. L. Blyler Jr., G. E. Johnson and G. L. Link "Electret Stability in the Presence of Ions," **Electrets - Charge Storage and Transport in Dielectrics** edited by M. M. Perlman, The Electrochemical Society, 1973.
2. Balmain, K. G., and C. R. Dubois, "Surface Discharges in Teflon, Mylar and Kapton," **IEEE Transactions on Nuclear Science NS-26:** 5146-5151, (December 1979).
3. Bauser, H. and W. Ronge "The Electret Ionization Chamber: A Dosimeter for Long-term Personnel Monitoring", **Health Physics, 34:** 97-102, (January 1987).
4. Campos, L. L., A. A. Suarez and S. Mascarenhas "A New Electret Dosimeter for Fast Neutrons," **Health Physics, 43:** 731-733, (November 1982).
5. Chudleigh, P. W. "Charging of Polymer Foils using Liquid Contacts," **Applied Physics Letters, 21:** 547-548, (1 December 1972).
6. Fjeld, R. A. and T. M. Owens "The Effects of Particle Charge on Penetration in an Electret Filter," Unpublished Paper, 1987.
7. Gross, B., G. M. Sessler, H. von Seggern and J. E. West "Hole Transit in Teflon Films," **Applied Physics Letters, 34:** 555-557, (1 May 1979).
8. Gross, B., G. M. Sessler and J. E. West "Charge Dynamics for Electron-irradiated Polymer-foil Electrets," **Journal of Applied Physics, 45:** 2841-2851, (July 1974).
9. Gross, B., G. M. Sessler and J. E. West "Heat Sealing of Teflon Electrets by Annealing," **Journal of Applied Physics, 46:** 4674-4677, (November 1975).
10. Gross, B., G. M. Sessler and J. E. West "Radiation Hardening and Pressure-actuated Charge Release of Electron-irradiated Teflon Electrets," **Applied Physics Letters, 24:** 351-353, (April 1974).

11. Gross, B., G. M. Sessler, and J. E. West "TSC Studies of Carrier Trapping in Electron- and Gamma-irradiated Teflon," **Journal of Applied Physics, 47:** 968-975, (March 1976).

12. Gross, B., J. E. West, H. von Seggern and D. Berkley "Generalized Box Model for Electron Irradiated Teflon Foils," **1980 Annual Report: Conference on Electrical Insulation and Dielectric Phenomena,** National Academy of Sciences,1980.

13. Gross, B., J. E. West, H. von Seggern and D. Berkley, "Time-dependant Radiation-induced Conductivity in Electron-irradiated Teflon Foils," **Journal of Applied Physics, 51:** 4875-4881, (September 1980) .

14. Hilczer, B. and J. Malecki **Electrets.** New York: Elsevier, 1986.

15. Hirsch, J. and E. H. Martin "Electron-induced Conduction in Plastics. II. Bulk Excitation in Polystyrene and Other Insulating Plastics," **Journal of Applied Physics, 43:** 1008-1015, (March 1972).

16. Ikeya M., and T. Miki "Electret Dosimeter Utilizing Gas Multiplication," **Health Physics, 39:** 797-799, (November 1980).

17. Kahn, A., and C. R. Phillips "Electrets for Passive Radon Daughter Dosimetry," **Health Physics, 46:** 141-149, (January 1984).

18 Kirsh, Y. and R. Chen "Radiation Effects in Polarized Electrets - Applications to Radiation Dosimetry", **Radiation Effects, 83:** 161-183, (1984).

19. Knoll, G. F. **Radiation Detection and Measurement.** New York: John Wiley and Sons, 1979.

20. Kotrappa, P., J. C. Dempsey, J. R. Hickey and L. R. Stieff "An Electret Passive Environmental Rn-222 Monitor Based on Ionization Measurement," **Health Physics, 54:** 47-56, (January 1988).

21. Martin, E. H., and J. Hirsch "Electron-induced Conduction in Plastics. I. Determination of Carrier Mobility," **Journal of Applied Physics, 43:** 1001-1007, (March 1972).

22. Montenegro, E. C., S. A. Cruz and C. Vargas-Aburto "A Universal Equation for the Electronic Stopping of Ions in Solids," **Physics Letters, 92A:** 195-202, (8 November 1982).

23. Moreno, R. A. and B. Gross "Measurement of Potential Buildup and Decay, Surface Charge Density, and Charging Currents of Corona-charged Polymer Foil Electrets," **Journal of Applied Physics, 47:** 3397-3402, (August 1976).

24. Sawa, G., D. C. Lee and M. Ieda "Discharge Current from Corona Charged Polyethylene," **Japanese Journal of Applied Physics, 14:** 643-649, (May 1975).

25. Sessler, G. M. "Physical Principles of Electrets," **Topics in Applied Physics - Electrets** (Second Edition) edited by G. M. Sessler. New York: Springer-Verlag, 1987.

26. Sessler, G. M. and J. E. West "Charging of Polymer Foils with Monoenergetic Low-Energy Electron Beams," **Applied Physics Letters, 17:12** 507-509, (15 December 1970).

27. Sessler, G. M. and J. E. West "Electrets Formed by Low-energy Electron Injection," **Journal of Electrostatics, 1:** 111-123, (1975).

28. Sessler, G. M. and J. E. West, "Foil-electret Transducers: A Review," **Electrets, Charge Storage and Transport in Dielectrics,** edited by M. M. Perlman, Dielectrics and Insulation Division, The Electrochemical Society, 1973.

29. Sessler, G. M. and J. E. West "Population and Temperature Shift of TSC Peaks of Electron-beam-charged Teflon FEP," **Journal of Applied Physics, 50:** 3328-3330, (May 1979).

30. Sessler, G. M., and J. E. West "Production of High Quasipermanent Charge Densities on Polymer Foils by Application of Breakdown Fields," **Journal of Applied Physics, 43:** 922-926, (March 1972).

31. Sessler, G. M. and J. E. West, "Research in Polymer Electrets," **Second International Conference on Electrophotography,** Society of Photographic Scientists and Engineers, 1974.

32. Sessler, G. M. and J. E. West, "Trap-modulated Mobility of Electrons and Holes in Teflon FEP," **Journal of Applied Physics, 47:** 3480-3484, (August 1976).

33. **Teflon Film.** Product Bulletin E-67603, Polymer Products Department, E. I. du Pont de Nemours and Co., Wilmington, DE.

34. Thomas, E. W. "The Physics of Ion Implantation", **Ion Plating and Implantation, Application to Materials,** edited by R. F. Hochman, American Society of Metals, 1986.

35. West, J. E. "Non-destructive Charge Release from High Volume Resistivity Polymers," **Charge Storage, Charge Transport and Electrostatics with their Applications,** edited by Y. Wada, M. M. Perlman and H. Kokado. New York: Elsevier, 1979.

36. West, J. E., Personal interview. A T and T Bell Laboratories. 3 September 1988.

VITA

Major Stephen R. Berggren was born [redacted] He graduated from Waggener High School in 1967 and obtained a B.S. in Chemical Engineering from Rose-Hulman Institute of Technology in 1971. Following graduation, he began his military career by enlisting in the USAF and serving as a munitions maintenance technician in the Far East. In 1975, he received his commission and served in several assignments as a munitions maintenance officer working with ICBM re-entry vehicles and strategic bomber weapon release systems. In 1982, he received an M.S. in Nuclear Engineering from the Air Force Institute of Technology. Subsequently, he served as an engineering officer with the Air Force Technical Applications Center. In 1985, he entered the doctoral program in Nuclear Engineering at the Air Force Institute of Technology.

[redacted]

UNCLASSIFIED
SECURITY CLASSIFICATION OF THIS PAGE

REPORT DOCUMENTATION PAGE

Form Approved
OMB No. 0704-0188

1a. REPORT SECURITY CLASSIFICATION UNCLASSIFIED	1b. RESTRICTIVE MARKINGS
2a. SECURITY CLASSIFICATION AUTHORITY	3. DISTRIBUTION/AVAILABILITY OF REPORT Approved for public release; distribution unlimited.
2b. DECLASSIFICATION/DOWNGRADING SCHEDULE	
4. PERFORMING ORGANIZATION REPORT NUMBER(S) AFIT/DS/ENP/88-1	5. MONITORING ORGANIZATION REPORT NUMBER(S)
6a. NAME OF PERFORMING ORGANIZATION School of Engineering 6b. OFFICE SYMBOL (If applicable) AFIT/ENG	7a. NAME OF MONITORING ORGANIZATION
6c. ADDRESS (City, State, and ZIP Code) Air Force Institute of Technology Wright-Patterson AFB OH 45433-6583	7b. ADDRESS (City, State, and ZIP Code)
8a. NAME OF FUNDING/SPONSORING ORGANIZATION 8b. OFFICE SYMBOL (If applicable)	9. PROCUREMENT INSTRUMENT IDENTIFICATION NUMBER
8c. ADDRESS (City, State, and ZIP Code)	10. SOURCE OF FUNDING NUMBERS PROGRAM ELEMENT NO. / PROJECT NO. / TASK NO. / WORK UNIT ACCESSION NO.

11. TITLE (Include Security Classification)

See Box 19

12. PERSONAL AUTHOR(S)
Stephen R. Berggren, B.S., M.S., Major, USAF

13a. TYPE OF REPORT	13b. TIME COVERED	14. DATE OF REPORT (Year, Month, Day)	15. PAGE COUNT
PhD Dissertation	FROM _____ TO _____	988 September	144

16. SUPPLEMENTARY NOTATION

17. COSATI CODES			18. SUBJECT TERMS (Continue on reverse if necessary and identify by block number)
FIELD	GROUP	SUB-GROUP	
20	03		Electrets, Uranium, Fission Fragments, Ions
20	07		

19. ABSTRACT (Continue on reverse if necessary and identify by block number)

Title: THE PULSE RESPONSE OF ELECTRETS TO ENERGETIC IONS

Dissertation Chairman: George John
Professor of Nuclear Engineering

Approved for Release in accordance with AFR 190-1
27 Dec. 1988

20. DISTRIBUTION/AVAILABILITY OF ABSTRACT ☒ UNCLASSIFIED/UNLIMITED ☐ SAME AS RPT. ☐ DTIC USERS	21. ABSTRACT SECURITY CLASSIFICATION UNCLASSIFIED
22a. NAME OF RESPONSIBLE INDIVIDUAL George John	22b. TELEPHONE (Include Area Code) (513) 255-5187 22c. OFFICE SYMBOL AFIT/ENP

DD Form 1473, JUN 86 *Previous editions are obsolete.*

ABSTRACT

The purpose of this study was to investigate how electrets respond to energetic ion irradiation. When an energetic ion interacts with an electret, a dielectric material containing a quasi-permanent electrostatic polarity, both electrical signals and luminescence signals result. The energetic ions used in the study were alpha particles and fission fragments. The electrets used were corona-charged and electron-beam charged polyfluoroethylene propylene. Both direct interaction (with the electret material itself) and indirect interaction (with the air above the electret) were studied.

The electret's pulse electrical response was measured at surface and near-surface electrodes using a charge-sensitive amplification system and a multi-channel analyzer. Alpha particles were found to produce an electrical pulse response by indirect interaction. In a 0.2 cm air space, alpha particles produce a signal of about 10^{-15} coulombs. Fission fragments produce an electrical response by both indirect and direct interaction. The indirect interaction signal is about 10^{-14} coulombs while the direct interaction signal is barely above background noise at 10^{-16} coulombs. Further, the direct response occurs only in freshly electron-beam charged electrets and decays away over several hours. A model for the interaction of ions with electron-beam charged electrets is proposed which explains many of the characteristics of the direct interaction signal.

The pulse luminescence response of electrets was measured using a photomultiplier-amplifier-multi-channel analyzer system. Luminescence was found to occur from the direct interaction of both alpha particles and fission fragments with electron-beam charged electrets. This response also decays away over several hours. The mechanism generating the luminescence was not determined but the data suggest that electron-hole re-combination is responsible.

Because the direct response to energetic ions was found to be transient, it may not be useful in radiation detection. The pulse response to the indirect interaction of alpha particles is useful. An environmental radon monitor and a thermal neutron detector using this phenomenon were successfully tested.